

IDŐJÁRÁS

QUARTERLY JOURNAL
OF THE HUNGARIAN METEOROLOGICAL SERVICE

CONTENTS

Regular papers

André Simon, Ákos Horváth and Jozef Vivoda: Case study and numerical simulations of the November 19, 2004 severe windstorm in Central Europe 91

István Matyasovszky: Developing an optimal system of circulation pattern types for downscaling purposes 125

Miklós Drucza and Ferenc Ács: Relationship between soil texture and near surface climate in Hungary 135

György Babolcsai and Tamás Hirsch: Characteristics and synoptic classification of heavy snowfall events in Budapest for the period 1953–2003. Part II 155

Short communications

Nándor Fodor: Estimating global radiation using the meteorological input data of crop models 175

Jadwiga Woyciechowska and Rafał Bąkowski: Comparison of values of the chosen meteorological fields measured at the aerological stations and the values taken from NCEP/NCAR Reanalysis 183

News 191

<http://www.met.hu/Journal-Idojaras.php>

IDŐJÁRÁS

Quarterly Journal of the Hungarian Meteorological Service

Editor-in-Chief
LÁSZLÓ BOZÓ

Executive Editor
MARGIT ANTAL

EDITORIAL BOARD

- | | |
|---|---|
| AMBRÓZY, P. (Budapest, Hungary) | MÉSZÁROS, E. (Veszprém, Hungary) |
| ANTAL, E. (Budapest, Hungary) | MIKA, J. (Budapest, Hungary) |
| BARTHOLY, J. (Budapest, Hungary) | MERSICH, I. (Budapest, Hungary) |
| BATCHVAROVA, E. (Sofia, Bulgaria) | MÖLLER, D. (Berlin, Germany) |
| BRIMBLECOMBE, P. (Norwich, U.K.) | NEUWIRTH, F. (Vienna, Austria) |
| CZELNAI, R. (Dörgicse, Hungary) | PAP, J.M. (Greenbelt, MD, U.S.A.) |
| DÉVÉNYI, D. (Boulder, U.S.A.) | PINTO, J. (R. Triangle Park, NC, U.S.A.) |
| DUNKEL, Z. (Budapest, Hungary) | PRÁGER, T. (Budapest, Hungary) |
| FISHER, B. (Reading, U.K.) | PROBÁLD, F. (Budapest, Hungary) |
| GELEYN, J.-Fr. (Toulouse, France) | RADNÓTI, G. (Budapest, Hungary) |
| GERESDI, I. (Pécs, Hungary) | S. BURÁNSZKY, M. (Budapest, Hungary) |
| GÖTZ, G. (Budapest, Hungary) | SZALAI, S. (Budapest, Hungary) |
| HANTEL, M. (Vienna, Austria) | SZEIDL, L. (Pécs, Hungary) |
| HASZPRA, L. (Budapest, Hungary) | TAR, K. (Debrecen, Hungary) |
| HORÁNYI, A. (Budapest, Hungary) | TÁNCZER, T. (Budapest, Hungary) |
| HORVÁTH, Á. (Siófok, Hungary) | TOTH, Z. (Camp Springs, U.S.A.) |
| HORVÁTH, L. (Budapest, Hungary) | VALI, G. (Laramie, WY, U.S.A.) |
| HUNKÁR, M. (Keszthely, Hungary) | VARGA-HASZONITS, Z. (Moson-
magyaróvár, Hungary) |
| † KONDRATYEV, K.Ya. (St. Petersburg,
Russia) | WEIDINGER, T. (Budapest, Hungary) |
| MAJOR, G. (Budapest, Hungary) | |

*Editorial Office: P.O. Box 39, H-1675 Budapest, Hungary or
Gillice tér 39, H-1181 Budapest, Hungary
E-mail: bozo.l@met.hu or antal.e@met.hu
Fax: (36-1) 346-4809*

Subscription by

*mail: IDŐJÁRÁS, P.O. Box 39, H-1675 Budapest, Hungary;
E-mail: bozo.l@met.hu or antal.e@met.hu; Fax: (36-1) 346-4809*

IDŐJÁRÁS

Quarterly Journal of the Hungarian Meteorological Service
Vol. 110, No. 2, April–June 2006, pp. 91–123

Case study and numerical simulations of the November 19, 2004 severe windstorm in Central Europe

André Simon^{1*}, Ákos Horváth² and Jozef Vivoda¹

¹*Slovak Hydrometeorological Institute, Jeséniova 17, 833 15 Bratislava, Slovakia*

²*Hungarian Meteorological Service, Storm Warning Observatory
Vitorlás u. 17, H-8600 Siófok, Hungary*

E-mails: Andre.Simon@shmu.sk; Horvath.A@met.hu; Jozef.Vivoda@shmu.sk

(Manuscript received in final form April 18, 2006)

Abstract—The study analyses the synoptic weather situation and mesoscale impacts of the November 19, 2004 windstorm, which affected several countries of central Europe. Particular attention was paid to the windstorm at the High and Low Tatra regions in Slovakia, where the event showed several attributes of downslope windstorm. This was investigated by using the ALADIN and MM5 numerical models with high horizontal resolution. Effects of the hydrostatic and non-hydrostatic dynamics were compared, as well as the method of the so called dynamical adaptation. It is concluded that downslope windstorms similar to the November 19 case can be forecasted by numerical models of 2.5 km resolution with higher precision than by using the current operational models. Nested version of the MM5 model at 1.0 km indicated possibility of simulation of microscale effects as orographically induced jets. It is shown that computationally effective hydrostatic models based on dynamical adaptation approach can be sufficient in forecasting extreme non-convective wind, similar to the evaluated event. Nevertheless, the results are strongly dependent on the physical parameterization of the model (turbulence, orographic drag, etc.). Hence, future versions of both hydrostatic and non-hydrostatic numerical models should be carefully examined and tested to keep the performance of forecasting severe downslope windstorms.

Key-words: numerical model, high resolution, downslope windstorm, High Tatras

1. Introduction

Forecasting of rapid cyclogenesis and mesoscale weather phenomena belongs to the main objectives of modern synoptic meteorology and numerical weather prediction. Both aspects were present in the case of the November 19, 2004

* Corresponding author

windstorm that affected several countries in central Europe. The main reason of severe weather was a rapidly developing and fast propagating macrosynoptic scale cyclone that was well predicted by several global and limited area numerical models used in the operational service at Slovak Hydrometeorological Institute (SHMÚ) and Hungarian Meteorological Service (HMS). The passage of the cyclone caused conditions favorable for mesoscale enhancement of the wind, above all at mountain areas. Some of these events can be appointed to occurrence of downslope windstorm and became particular object of this study.

Downslope windstorm is defined as very strong, usually gusty, and occasionally violent wind that blows down the lee slope of a mountain range, often reaching its peak strength near the foot of mountains and weakening rapidly farther away from the mountains (*Glossary of Meteorology*, 2000). This kind of flow appears at many mountainous regions all around the world (*Lane et al.*, 2000; *Sandvik*, 2001; *Tutiš*, 2002; *Águstsson and Ólafsson*, 2005) and can be sometimes associated with considerable damages (*Gaberšek*, 2003; *Meyers et al.*, 2003; *Vigh*, 2005; *Klaić and Belušić*, 2005) and also with potential hazard to aviation (*Kaplan et al.*, 2003; *Doyle et al.*, 2006). Several synoptic-dynamical studies were given about events from Dalmatian coast of Croatia called “bora” (*Klemp and Durran*, 1987; *Picek and Tutiš*, 1996; *Jurčec and Brzović*, 1995). Occurrence of severe downslope wind is also very frequent at eastern slopes of central Colorado Rocky Mountains in the vicinity of Boulder (*Lilly*, 1978).

The study of the flow structure at lee side of the mountains usually requires high density of surface observations and balloon, airplane, or LIDAR observations (*Vergeiner and Lilly*, 1970; *Gohm and Mayr*, 2005a, b), which are not always available. Operational forecasting and better understanding of the flow associated to downslope windstorms demands numerical simulations with models of resolution much higher than it was used at SHMÚ and HMS on November 19, 2004 (*Dierking*, 1998; *Vosper*, 2003; *Zhang et al.*, 2005).

For above mentioned reasons, high resolution numerical models were used to study the wind field in the area of the High and Low Tatras, where the November 19, 2004 windstorm caused particularly large devastation to the forest. Both hydrostatic and non-hydrostatic versions of the ALADIN model were tested at SHMÚ, and the non-hydrostatic Penn State and UCAR MM5 model was evaluated at HMS.

The main motivation of the research using the ALADIN model was to see, how much a 2.5 km high resolution hydrostatic model can improve the operational forecast of the windstorm. The use of hydrostatic approximation and hydrostatic dynamics at 2.5 km horizontal resolution can be still plausible by simulation of non-convective flows, although features related to gravity waves reflection and propagation (trapped lee waves, potential flow) are

already misinterpreted at this resolution (*Kasahara and Qian, 2000; Laprise and Peltier, 1989b; Nance and Durran, 1987a, b; Smith, 2002*). The length of large amplitude mountain waves predicted by hydraulic theory is usually bigger than 10 km. Waves of these dimensions and features, as hydraulic jumps, are usually reproduced by hydrostatic models (*Klemp and Lilly, 1978*). On the other hand, flow at the lee side of the mountains produces significant vertical accelerations and vertical downward and upward velocities in orders of units or even tens of m/s observed by glider pilots (*Zejda, 1986*) or during field experiments (*Grubišić and Lewis, 2004*). In these areas one may expect presence of not negligible non-hydrostatic pressure perturbations and pressure perturbation forces.

Hence, another objective was to see, whether the non-hydrostatic approach produces forecasts of different quality. The purpose of the MM5 experimental run was to obtain a wind field at 1 km resolution, which could show microscale effects as rotors (*Kuettner and Hertenstein, 2002; Doyle and Durran, 2002*) or wind strengthening by mountain passes, called gap wind (*Colle and Mass, 1998a, b, 2000; Pan and Smith, 1999*). Another point of the research was the effectiveness of several computational approaches including the dynamical adaptation of the ALADIN model (*Žagar and Rakovec, 1999*) and nesting technique of MM5. Beside that, sensitivity on different packages of physical parameterizations was tested on operational model versions of the ALADIN SHMÚ model. It was the first occasion both for SHMÚ and HMS, that a windstorm was studied in such extent, using high resolution numerical models.

The paper is divided in 10 Sections. The next Section gives a brief description of the macro-synoptic situation. Section 3 is related to meso-synoptic conditions for mountain wave generation. Sections 4 and 5 inform about the impact of the windstorm in central Europe with more details about the event at the High Tatras. Section 6 is an overview of research methods and brief description of used versions of numerical models. Section 7 presents forecasts of the model operationally used on November 19, 2004. Sections 8 and 9 show the main results of the high resolution runs of the ALADIN and MM5 models, respectively. Conclusions and consequences for operational forecasting are given by Section 10.

2. Synoptic situation

A day before the event, on November 18, 06:00 UTC, it was already possible to recognize the development of shallow cyclones in a widespread trough of low pressure, with axis westerly from Ireland. The weather in central Europe was influenced by deep cyclone centred over the southern part of Scandinavian

Peninsula and Baltic Sea (the sea level pressure dropped below 980 hPa in the middle of this low). In the upper troposphere, a jet stream was spread from Northern Atlantic with axis over the Northern Sea, Denmark, and Poland with northwesterly wind of speed exceeding 80 m/s along the axis at the 300 hPa height according to ECMWF analysis. At the same time, at both 850 and 500 hPa levels, a strong southward directed temperature gradient formed that could be detected over big part of northern Europe (*Fig. 1*). A strong westerly flow was present over Europe containing several patterns of mesosynoptic scale perturbations.

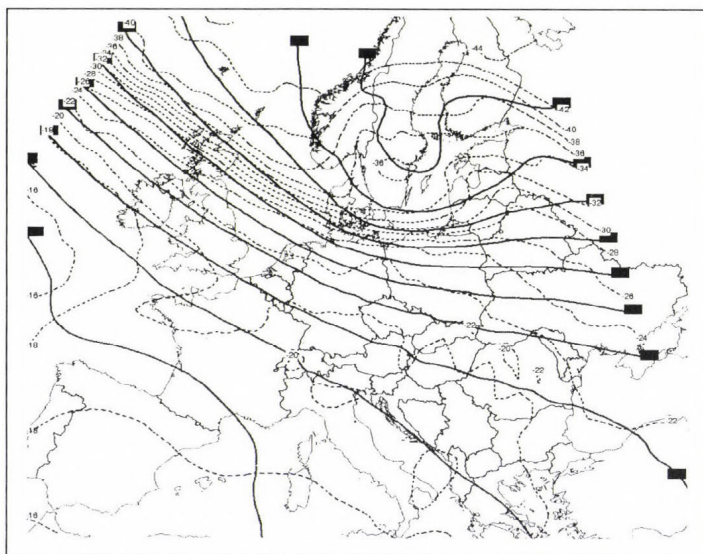


Fig. 1. Geopotential height (m) and temperature ($^{\circ}\text{C}$) at 500 hPa from the 6-hour forecast of the ECMWF model, valid for November 18, 2004, 06:00 UTC. Note the well expressed baroclinic zone over Scotland, Northern Sea, Denmark, and the Baltic Sea region.

On November 19, 00:00 UTC, there was already a deep surface trough and frontal zone over Northern Germany and France. The upper air trough with axis over Scandinavia, the Northern Sea, and the British Isles deepened as well, and the axis of the jet stream moved southward. This caused change of the flow direction over northwestern Europe from westerly to northwesterly. Consequently, intense advection of cold air started, which can be demonstrated on changes of potential vorticity (PV) field at upper tropospheric levels. Ertel's potential vorticity on isentropic surfaces is

$$PV = -g(\zeta + f) \frac{\partial \theta}{\partial p}, \quad (1)$$

where g is the acceleration of gravity, ζ is relative vorticity, f is the Coriolis parameter, θ represents potential temperature, and p is the atmospheric pressure (see, e.g., the textbook of *Bluestein*, 1993). The potential vorticity is usually expressed in Potential Vorticity Units ($1 \text{ PVU} = 1 \times 10^{-6} \text{ m}^2 \text{ s}^{-1} \text{ K kg}^{-1}$). Maximum values of potential vorticity (more than 10 PVU) occur usually in the stratosphere due to high static stability of the stratospherical air. Hence, considerable increase of potential vorticity can be found above the tropopause, which is usually considered at the level with potential vorticity of 1.5 PVU. Regions with negative potential vorticity indicate presence of dry symmetric instability (*Bennets and Hoskins*, 1979). The mean distribution of potential vorticity at isentropic levels is zonal, however, meridional advection of cold/warm air creates disturbances (anomalies) at upper tropospheric levels (315–330 K). Cold, polar air-masses are characterized by low altitudes of tropopause and the 1.5 PVU level (4–8 km), whereas in warm, mid-latitude airmasses the tropopause is reached higher (8–12 km). Exchange of the air mass is often manifested by sudden drop of the 1.5 PVU height. For practical use, maps of the 1.5 PVU surface heights are plotted to follow the displacement of air-masses and formation of upper air potential vorticity anomalies (*Morgan and Nielsen-Gammon*, 1998).

In the evaluated case the cold air advection was marked by drop of the 1.5 PVU height over the Northern Sea. Hence, upper air anomaly of potential vorticity was created, and it was spreading from the area of Northern Sea southeastwards (*Fig. 2a*). Approach of the positive upper air potential vorticity anomaly to surface baroclinic zone in environment of strong vertical wind shear created ideal conditions for baroclinic instability (*Hoskins et al.*, 1985). After November 19, 00:00 UTC it is possible to observe an isolated but shallow cyclone (996 hPa deep) over the central part of Germany, which deepened very fast during the next hours and propagated westwards. At 06:00 UTC the centre of the cyclone is already over the borders of Germany, Poland, and Czech Republic. In the vertical cross Section through the cyclone, it is possible to see well expressed anomaly of potential vorticity at low and middle tropospheric levels (*Fig. 2b*). Such anomalies are consequences of diabatic heating associated with latent heat released by precipitation or related to effects of friction (*Davis and Emanuel*, 1991; *Romero et al.*, 2002; *Arreola et al.*, 2003 and *Adamson et al.*, 2006). This, in turn, supports baroclinic instability, development of upward vertical motions, and deepening of the cyclone. At 12:00 UTC the cyclone moved over the southeastern part of Poland, at 18:00 UTC it was situated over Ukraine and Belarus (*Fig. 3*).

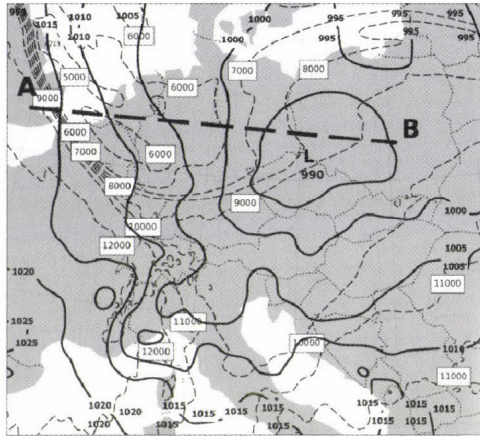


Fig. 2a. Height of the 1.5 PVU level (m) showed by dashed lines and mean sea level pressure (hPa) by solid lines from the 6-hour forecast of the ALADIN SHMÚ model, valid for November 19, 2004, 06:00 UTC. The thick dashed AB line marks the direction of the cross-section in Fig. 2b.

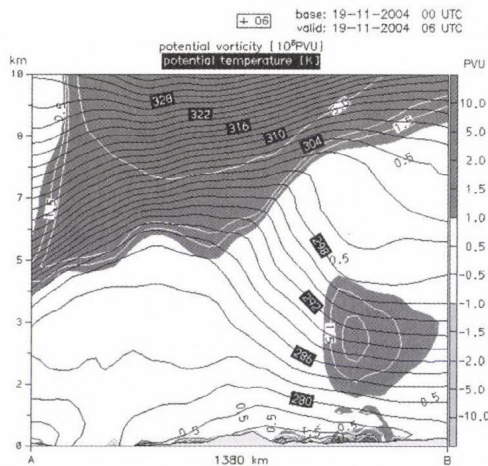


Fig. 2b. Vertical cross section through the field of potential vorticity (white isolines and grey scale) and potential temperature (black isolines), valid for November 19, 2004, 06:00 UTC. The potential vorticity field is shown in Potential Vorticity Units ($1 \text{ PVU} = 1 \times 10^{-6} \text{ m}^2 \text{ s}^{-1} \text{ K kg}^{-1}$, right axis). Dark grey filled areas show values of potential vorticity higher than 1 PVU (values in the troposphere are usually lower than 1 PVU). Light grey filled areas (with potential vorticity smaller than 0 PVU) are associated with the presence of dry symmetric instability.

Note the upper air potential vorticity anomaly at left (west) side of the cross-section (the anomaly is visible as the drop of the 1.5 PVU height). This anomaly interacts with isolated low-level potential vorticity anomaly on the right (east) side of the cross-section (with maximum value of potential vorticity exceeding 2.0 PVU). Thus, strong vertical motions are created at mid-troposphere in the part between the anomalies (indicated by the tilt of the potential temperature isolines).

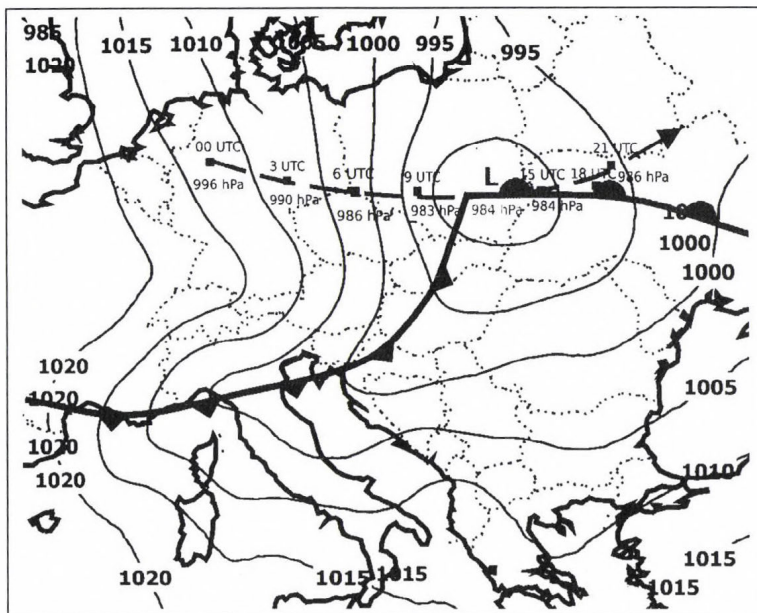


Fig. 3. Analysis of the mean sea level pressure (in hPa) and fronts, valid for November 19, 2004, 12:00 UTC. The dashed line shows the track of the November 19 cyclone with positions of its centre and value of the lowest mean sea level pressure from SYNOP observations from November 19, 2004, 00:00 UTC until November 19, 2004, 21:00 UTC with 3-hour frequency.

The passage of this cyclone in the central part of Europe was accompanied by strong cold air advection and fast changes of pressure. At 09:00 UTC, when the cold front of the cyclone reached the borders of Germany and Czech Republic, 12 hPa/3h rise of pressure were reported over Germany and 5–8 hPa/3h drops of pressure in the Czech Republic. The passage of the cold front according to high pressure gradients and strong flow both in upper and lower parts of the troposphere was fast — it reached the northwestern borders of the Slovak Republic at 11:00 UTC, at 13:00 UTC the line of the front crossed the High Tatra region, Budapest, and Balaton, after 16:00 UTC the front left the territory of Hungary and the Slovak Republic. The passage of the front was associated with wind gusts reaching 20–30 m/s at many places and with turn of the wind direction from southwesterly to westerly and northwesterly, respectively. Thunderstorms occurred at frontal line — already in the morning hours in the south of Germany and west of Austria, later, between 11:00 and 15:00 UTC, several thunderstorm clouds formed in the northwest and central parts of Hungary.

3. Mesoscale conditions for mountain wave generation

The mechanism of downslope windstorms is very closely related to generation of mountain waves. First explanation of this mechanism was given by nonlinear hydraulic theory, in which the airflow over a mountain was compared to fluid flowing over an obstacle (Long, 1953, 1954). The properties of the upstream flow can be characterized by Froude number (F_r). Different definitions and purposes of using the Froude number can be found in textbooks and scientific papers (Smith, 1980; Durran, 1986). In this paper the Froude number is considered as fraction of the kinetic energy of the upstream air parcels and potential energy needed to overcome the obstacle.

$$F_r = \frac{U}{NH}, \quad (2)$$

where N is the Brunt Väisälä frequency, U is the wind speed, H represents the height of the obstacle (Bluestein, 1993). The Froude number defined by Eq. (2) describes the ability of the air to flow over obstacles and to generate mountain waves. It can be used also as a measure of linearity of the flow regime described by certain systems of dynamic equations (Smith, 1980).

The air has a tendency to go around the obstacle by weak upstream flow or high static stability ($F_r \ll 1$). Such airflow is called subcritical. However, as the airspeed increases (or static stability decreases), a part of the air mass starts to flow over the obstacle, while generating waves at the lee side of the mountain (Smolarkiewicz and Rotunno, 1989; Stull, 2003). If the kinetic energy of the upstream air parcels overlaps the potential energy needed to overcome the obstacle ($F_r > 1$), the flow is called supercritical and generates stationary wave of large amplitude at the lee side of the mountain. As a consequence, strong winds start to blow downhill, at the downslope part of the wave, because potential energy of the air parcels is converted into kinetic energy during the entire time when the parcels are traversing the mountain. On the other hand, surface winds calm down quickly below the upslope part of the wave, where the supercritical flow undergoes a turbulent transition (called hydraulic jump) to the subcritical environment (Holton, 1992). A hypothetical example of idealized hydraulic flow across the High Tatra Mountains is given by Fig. 4a.

A linear theory was based on generation of vertically propagating internal gravity waves (Klemp and Lilly, 1975). Klemp and Lilly showed that amplification of surface winds is related to the reflection of some parts of the upward propagating wind energy due to the presence of middle tropospheric level inversion. These conditions are favorable for generation of trapped lee waves (Fig. 4b).

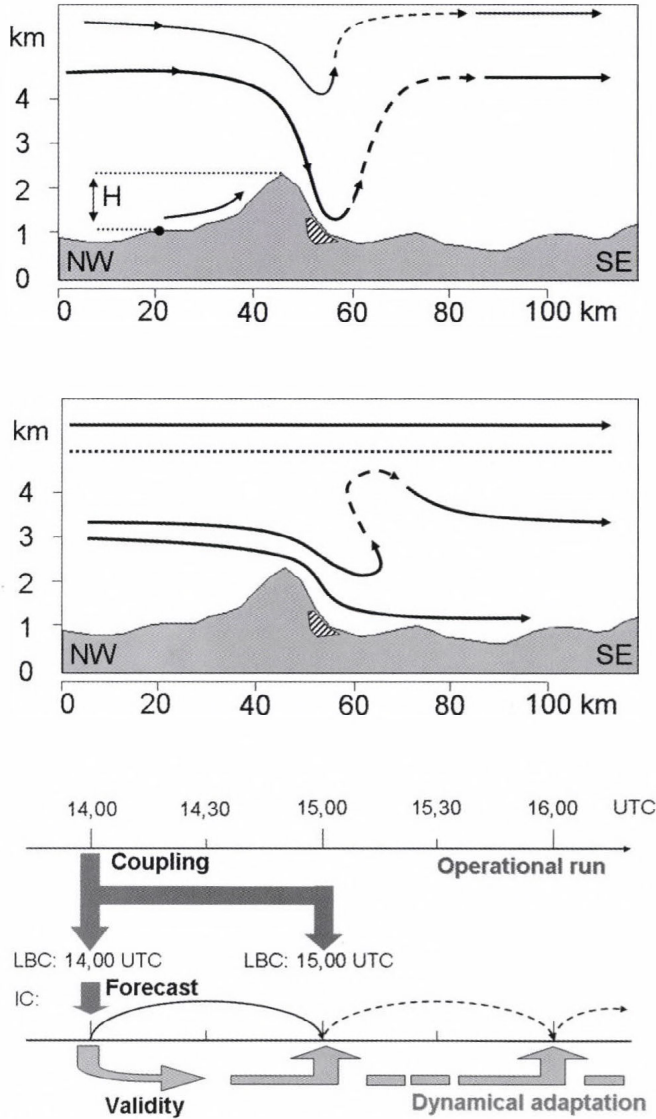


Fig. 4. Schemes of three possible mechanisms of downslope windstorm occurring at the High Tatras on November 19, 2004: (a) creation of a large mountain wave according to nonlinear hydraulic theory, (b) development of trapped lee waves related to reflection of internal gravity waves, (c) breaking of mountain waves and reversal of the flow. The northwest-southeast cross-section is applied to the relief of the High Tatras. Solid lines are streamlines; the dashed part denotes the upslope part of the wave (hydraulic jump). The symbol H means the height of the mountain over terrain at the upstream reference point (selected for calculation of the Froude number in Section 3). The thick dotted line represents the area of the temperature inversion in (b) and the so called critical level with flow reversal in (c). The hatched area at the lee slope of the mountain marks the location of the most intense damage observed at the High Tatras.

Third theory was presented in papers of *Clark and Peltier (1977)* and *Peltier and Clark (1979)*. According to their research, based on numerical simulations, downslope windstorm is related to mountain wave breaking and reversal of the cross-mountain wind (*Fig. 4c*). In that case the energy of the upward propagating wave remains trapped below a certain critical layer (where the flow component across the mountain drops to zero and reverses sign), thus producing significant increase in the wave amplitude. *Durran (1986)* attempted to create a unifying concept of downslope windstorms based on nonlinear transition from upstream gravity wave structures to supercritical flow along the lee side of the mountain. He showed that wave breaking may be explained by hydraulic theory. It was confirmed that this phenomenon can be important for amplification of the surface wind, although it is not an ultimate condition for the onset of downslope windstorm.

Increase in computer power and development of numerical weather prediction techniques allowed the simulation of mountain waves on realistic case studies with high resolution numerical models (*Satomura and Bougeault, 1994; Belušić and Klaić, 2003; Kraljević and Tudor, 2005*) and recently even operational forecasting of downslope windstorms (*Ivatek-Šahdan and Tudor, 2004*). Results achieved in case studies generally accept all above listed possibilities of mountain waves generation and amplification, showing features as hydraulic jump, trapped lee waves, or lee flow reversals, which were simulated earlier in idealized experiments or described analytically.

Aerological observations in the vicinity of the November 19 cyclone at 12:00 UTC show, that the thermal stratification was stable and the air was relatively moist before the passage of the cold front (at aerological stations Poprad Gánovce and Budapest Lőrinc). There was a remarkable wind shear in the low and middle troposphere, while the wind speed increased from 5 m/s at the ground until 30 m/s at the 700 hPa altitude. At or just behind the line of the cold front, the stratification became potentially unstable at lowest 1600 meters, but the estimated energy of instability was rather small (61 J/K measured at the aerological station Prostějov in the Czech Republic). The area of instability (or small stability) was capped by shallow and not very significant layer of temperature inversion. Aerological observations on November 20, 00:00 UTC showed considerable drop of the temperature due to strong cold air advection at the rear side of the cyclone (e.g., the temperature at the 850 hPa level at Poprad Gánovce decreased from 0.5 to -8.8 degrees of Celsius within 12 hours) and presence of dry air in the entire profile of the troposphere.

There are no aerological observations that would be representative for the conditions at the windward side of the High Tatra Mountains during the windstorm. Hence, the properties of the air mass flowing over the crest of Tatras were assessed from ALADIN model forecast (*Fig. 5*). The static

stability represented by the Brunt-Vaisala frequency was very low at lowest 700–800 meters above ground, and together with high wind shear it gave conditions favorable for turbulence (small Richardson numbers). The Brunt-Vaisala frequency significantly increased between the altitudes of 1500 and 2400 meters above sea level (just below the tops of the High Tatra Mountains). The Froude number (F_r) was evaluated with Brunt Vaisala frequency (N) and wind speed (U) averaged over the variable depth H that represented the height of the obstacle above terrain.

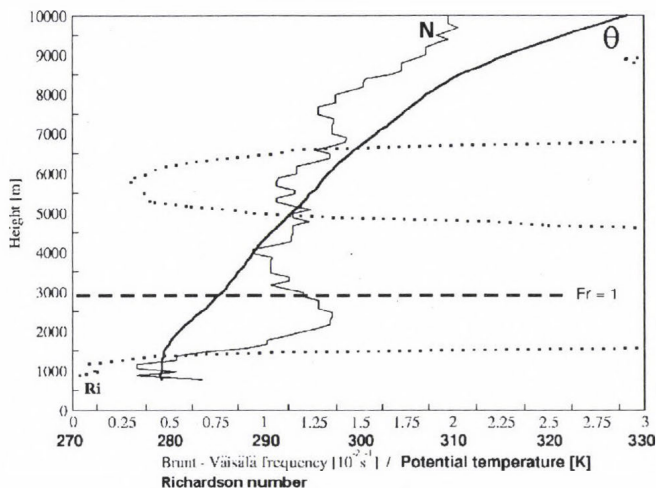


Fig. 5. Vertical profile of several parameters derived from the forecast of the ALADIN HS model, valid for November 19, 2004, 15:00 UTC and for the point over Zakopane (in Poland, at windward side of the High Tatras). Thin solid line denotes the Brunt Vaisala frequency N (upper horizontal scale); thick solid line denotes the course of the potential temperature θ (bottom horizontal scale). Dotted line shows the course of the Richardson number Ri (upper horizontal scale). The vertical axis indicates the height above sea level (in meters). Dashed line marks the height, where the dimensionless Froude number (given by mean static stability and mean wind speed of the layer below) attains unity. For obstacles below this height, the flow can be considered as supercritical and overcoming the obstacle.

The Froude number profile was decreasing with height according to the increase of the mean static stability and increase of the height of the obstacle. However, by corresponding wind speed and stratification of the atmosphere, the air parcels would be able to rise along the slopes of the mountains even to the heights of 3000 m above the sea level. Such conditions are generally favorable for creating of mountain waves of large amplitudes at the lee side of the mountains and for the onset of downslope windstorms (Poulos *et al.*, 2000).

4. Impact of the windstorm in Central Europe

The majority of the information related to the storm impact in Central Europe comes from SYNOP reports. Smaller number of reports originate from climatological and automatic stations (Czech Republic, Slovakia, and Hungary) or from wind measurements provided by non-meteorological institutions (High Tatras National Park — TANAP). Occasionally, it was possible to get additional information concerning damage observations (e.g., from meteorological institutes, forestry departments, and the state department of nature protection of the Slovak Republic — ŠOPSR). An overview of wind maxima and damage observations is given by *Table 1*. Below we concentrate on the impact of the windstorm in Slovakia and Hungary, where more detailed information were available to the authors.

Table 1. Overview of wind gusts reported by synoptic (S) and climatological (C) stations in Central Europe. Abbreviations D, A, CZ, P, SK, HU, and UA are related to Germany, Austria, Czech Republic, Poland, Slovak Republic, Hungary, and Ukraine. Data in the fourth column, represented by synoptic stations, are the time of the hourly reported maximum wind gusts as in SYNOP report. By certain synoptic and climatological stations these are the exact times of the occurrence in UTC time

Station	Altitude (m)	Wind gust (m/s)	Time (UTC)	Damage observation
Wendelstein, D (S)	1835	50	7:00	D: not available
Grosser Arber, D (S)	1446	44	8:00	
Alpinzentrum, D (S)	2310	45	10:00	
Linz Hoersching, A (S)	298	30	9:00	A: reported near
Wiener Neustadt, A (S)	280	34	15:00	Salzburg
Kocelovice, CZ (S,C)	519	32	08:50	CZ: near Brno,
Dukovany, CZ (S)	400	34	12:00	1 casualty
Raciborz, P (S)	206	31	12:00	P: not available
Nowy Sacz, P (S)	292	31	18:00	
Poprad letisko, SK (S,C)	694	34	13:21	SK: northern
Stará Lesná, SK (C)	810	45	16:28	Slovakia,
Skalnaté Pleso, SK (C)	1778	54	17:54	2 casualties
Siófok, HU (S)	108	29	12:30	HU: reported in
Balatonfüred, HU (S)	108	31.1	13:00	middle Hungary
Kab hegy, HU (S)	600	38.7	11:50	
Plaj,UA	1300	40	not available	not available

The majority of the stations in Slovakia measured the maximum wind speed during or shortly after the passage of the cold front between 11:00 and 16:00 UTC. Several observations of wind gusts with speed higher than 30 m/s come from northern Slovakia (Poprad, Liesek, Telgárt) or from southwest Slovakia (Piešťany, Nitra). The intensity and severity of the wind was

decreasing towards southeast. Heavy damages in the forest occurred in several mountain regions of the northern and central parts of Slovakia, e.g., in regions of Orava, Kysuce, High and Low Tatras, or in the regions of Muránska Planina and Poľana (web site of ŠOPSR department — www.sopsr.sk). Two casualties were reported during the event at the High and Low Tatras, where the wind reached the most severe intensity. Gusty wind exceeding 40 m/s and 10 minute average wind speed higher than 24 m/s were recorded at the top of the Tatra Mountains between 14:00 and 21:00 UTC (synoptic stations Lomnický Štít and Chopok). Strengthening of the wind at the southern (lee) slopes and foots of the High Tatras was observed after the passage of the cold front and reached the maximum intensity between 15:00 and 19:00 UTC, during the advection of cold air at the rear side of the November 19 cyclone (records of the meteorological stations Stará Lesná and Skalnaté Pleso belonging to Geophysical Institute of Slovak Academy of Sciences).

The cold front arrived to northwestern Hungary at 11:00 UTC. At first the station at Mosonmagyaróvár registered the turn of the wind from southwesterly to westerly and northwesterly direction. After 12:00 UTC the front propagating by mean speed of 20 m/s reached the area of lake Balaton, where in Siófok 29 m/s, at Balatonfüred 31.1 m/s peak wind gusts were measured, and at the highest point of the Bakony Mountains (Kab hegy), 38.7 m/s was recorded by the automatic station. Thunderstorms formed on the edge of the cold front and moved southwesterly, approximately parallel to the line Komárom–Budapest. Some funnel clouds and hails (area of Budapest) were observed. Due to the thunderstorms, the distribution of the wind gusts became more chaotic. Nevertheless, the highest magnitudes of the wind speed were measured either in the central and right part of the Danube basin, or in mountain regions. In the eastern part of Hungary the impact of the windstorm was considerably weaker.

5. Impact of the windstorm at the High Tatras

The forest at High Tatras was reported to be destroyed on area of 120 km² in a belt of 40–50 km long and 2–5 km wide at the altitudes between 750 and 1200 m (*WWF position paper*, 2004, materials of ŠOP SR, and personal communication with Stanislav Celer from ŠOP SR). In the past, at least 17 major windstorms were referenced for the High Tatras between the years 1898 and 2000 (*Koreň*, 2005; *Luczy*, 2005). Wind of severe intensity (the mean hourly wind speed exceeding 21 m/s) is not unique at high altitudes of the High and Low Tatras, where it occurs with 5‰ frequency (what means two-three days in a year in average). Orographical strengthening and high gustiness

of the wind are frequently observed at the lee sides of mountain passes. Climatological studies for years 1951–1960 showed, that at some places (e.g., Skalnaté Pleso, 1778 m above sea level) daily maxima of wind gusts overlapping the speed of 105 km/h (29.2 m/s) can have an occurrence frequency of 20% (Otruba, 1964; Otruba and Wiszniewski, 1974). Rarer are cases, when the windstorm reaches the altitudes of forest between 700 and 1200 meters, as it happened during the event of November 19, 2004. Windstorms in the years 1915, 1919, 1941 (Konček, 1944), 1964 (Rak, 1967), and 1981 (Koreň, 2005) had large destructive consequences (although smaller in comparison with the 2004 case). Wind blowing from northern direction and accelerating along the slopes of the Tatras was considered as a possible reason for these extreme events.

The start of the November 19 windstorm at the High Tatras according to observations (Stará Lesná station) can be placed after 14:20 UTC. It was marked by sudden increase of both average wind speed and speed of the wind gusts, and by turn of the wind from westerly to northwesterly direction. The north and northwestern flanks of the mountains were windward and the south and southeastern flanks leeward according to the mean low and middle tropospheric flow. The gusty character of the wind is underlined by the big difference between the hourly mean wind speed (almost 20 m/s) and maximum measured wind gusts (45 m/s at Stará Lesná at 16:28 UTC and 54 m/s at Skalnaté Pleso at 17:54 UTC). Wind gusts were accompanied by fast oscillations of the atmospheric pressure of order 3 hPa. The speed of the wind gusts in the Poprad Valley remained mostly below 30 m/s during the windstorm at the High Tatras (station Poprad airport and station Poprad Gánovce). The wind speed was even continuously decreasing between 15:00 and 17:00 UTC, because the Poprad Valley region was not directly affected by the windstorm. The end of the event at the High and Low Tatras can be situated to 21:00 UTC, although at lower altitudes the speed of the wind gusts was below 30 m/s already after 17:30 UTC (station Stará Lesná). After 21:00 UTC the speed of the gusts decreased below 30 m/s everywhere, and the wind has lost its severity.

6. Numerical weather prediction tools

Horizontal resolution of the limited area hydrostatic model ALADIN, which run operationally at SHMÚ on November 19, 2004, was 9 km, and the model used 37 vertical levels. The driving model was the global model ARP GE with 3-hour coupling frequency. The model was initialized with digital filter (see more details about ALADIN in Radnóti *et al.*, 1995; Horányi *et al.*, 1996; Gerard, 2000; Derková, 2005). After the event, the test with 2.5 km

horizontal resolution was carried out with the hydrostatic version of the model (further denoted as ALADIN HS). It used the physical parameterization from the reference operational model version with convection parameterization switched off. The ALADIN HS run was based at November 19, 2004, 00:00 UTC and was integrated for 36 hours. The initial and boundary conditions for ALADIN HS were taken from the operational run with 1 hour coupling frequency.

The second experimental run used the non-hydrostatic ALADIN dynamics (further ALADIN NH) and several packages of physical parameterization of the ALADIN model. The dynamics of the model is using the two time levels semi-Lagrangian advection with iterative centered implicit scheme and mass based terrain following coordinate (*Laprise, 1992; Bubnová et al., 1995; Bénard et al., 2004, 2005*). In the case of the ALADIN NH run, the integraton period and the coupling strategy were the same as in the ALADIN HS experiment.

Another test was performed with the so-called dynamical adaptation approach at 2.5 km horizontal resolution. It was expected, that even the simplified and computationally effective hydrostatic simulation at short time ranges will keep a good representation of interaction of atmospheric flow with the terrain. The main difference against the ALADIN HS run was in the length of the integration and way of the treatment of boundary and initial conditions. The dynamical adaptation run for 30 minutes and 60 minutes, respectively, using 15 vertical levels only, adjacent to the model surface. The model integration was provided with 1 hour frequency starting from initial conditions provided by operational model. The 30-minute integration with time constant coupling is time inconsistent, because its final output is approximated as the state of the atmosphere at the beginning of the integration (*Fig. 6a*). The 60-minute integration is time consistent, hence, providing better estimates for minimal and maximal values in the given period (*Fig. 6b*).

The operational service at the Hungarian Meteorological Service was using the ECMWF global model, which was the source of several macrosynoptic analyses and forecasts applied in the study of the synoptic situation described in Section 2. Further, outputs of the ALADIN/HU model at 6.5 km and MM5 model forecasts at 4 km horizontal resolution were available. For the November 19 case study, a nested grid version of the MM5 model at 1 km resolution was created, which covered the area of the High Tatras and received initial and boundary conditions from MM5 run at larger domain with 3 km resolution, which received its boundary conditions from ECMWF deterministic model. The MM5 model did not use cumulus parameterization. Both domains applied ETA PBL scheme (*Janjic, 1990*) and Reisner graupel moisture schemes (*Reisner et al., 1998*). The ETA PBL scheme is a detailed PBL method, which calculates turbulent kinetic energy

and vertical fluxes with an implicit diffusion scheme. The Reisner graupel method is based on mixed-phase scheme, where snow, ice, water, water vapor, and graupel are also calculated. The model used 26 vertical sigma levels; the upper pressure level was 100 hPa.

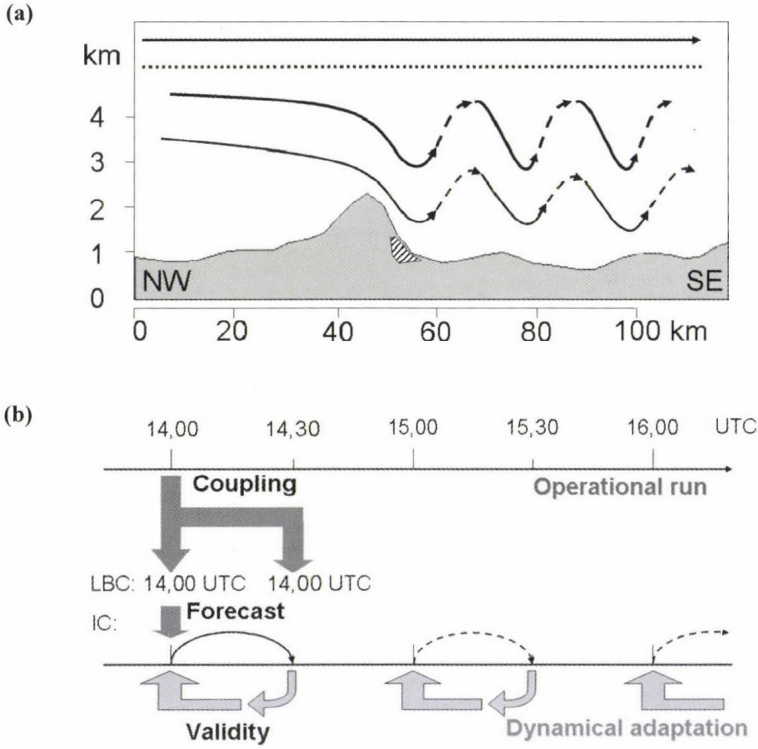


Fig. 6. Scheme of the dynamical adaptation procedure for: (a) time inconsistent and (b) time consistent approaches. LBC are Lateral Boundary Conditions, which are constant in time in (a). IC is abbreviation for Initial Condition. The scheme of coupling (dark grey arrows) is figured out only for the 14:00 UTC integration (solid line), the following integrations are depicted only schematically (by dashed lines). Light grey arrows point at the validity of the 30-minute forecast in (a) and of the 1 hour integration in (b).

7. Tests with the ALADIN model at 9 km resolution

Synoptic scale forecasts of the November 19, 2004 cyclone development, mean sea level pressure and wind distribution were provided by models ECMWF, operational ARPEGE/ALADIN, and MM5 with very high precision. High speed instantaneous winds and wind gusts exceeding 30 m/s were

forecasted on large territory by the ALADIN model more than 36 hours in advance (by the November 18, 2004, 00:00 UTC run). The reference ALADIN SHMÚ run in this study was based on November 19, 2004, 00:00 UTC, and it forecasted peak wind gusts of 40 m/s with maximum situated in the region of the High Tatras. Time course of the values forecasted and interpolated to the locality of Lomnický štít (2633 m above sea level) were compared with records of the meteorological station (*Fig. 7*). The start of the event was predicted with small time shift (1 hour) for the operational run, but the overall tendency fitted the observations very well. The horizontal distribution of the wind field was less precise –the magnitude of the wind was overestimated in the Poprad valley and underestimated in certain regions, e.g., in the Low Tatras (*Fig. 8*). These results gave forecasters a good possibility to estimate severe wind occurrence. However, at 9 km resolution it was not possible to sufficiently localize the position of the event. The cross Sections of vertical velocity and potential temperature (*Fig. 9*) show a moderate effect of downslope wind at southeastern flank of the High Tatras. It is associated with upward motions at windward side and downward motions at the lee side of the mountains.

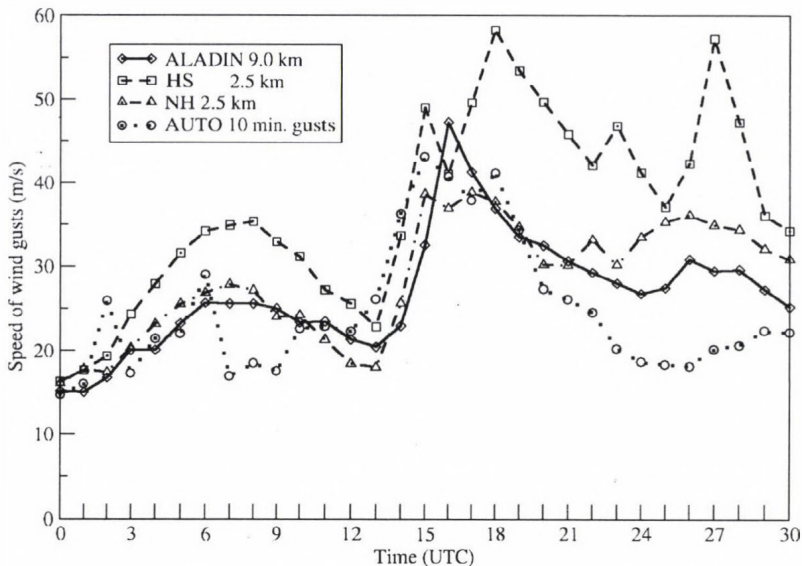


Fig. 7. Time evolution of the ALADIN model forecast of wind gusts from operational run (solid line) and experimental run HS (dashed line) for the Lomnický štít station (2633 m above sea level). Dash-dotted line (with triangles) shows the forecast of the ALADIN NH non-hydrostatic run at 2.5 km resolution. Dotted line (with circles) is the speed of maximum wind gust recorded for the previous 10 minutes by the automatic station.

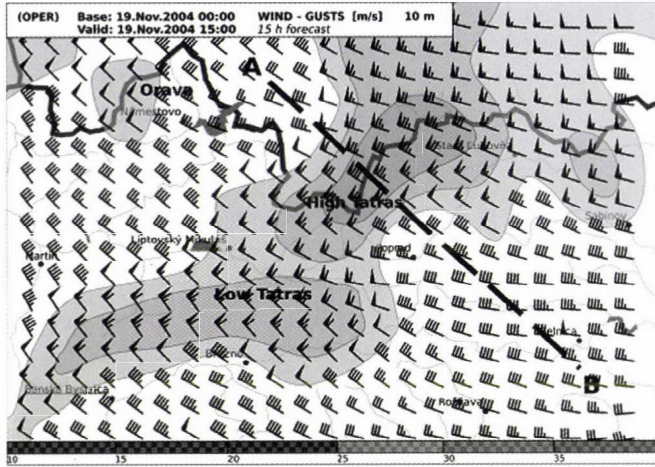


Fig. 8. Operational forecast of the ALADIN SHMÚ model of the wind gust field at the 10 m height over the model surface (wind barbs) and of the wind gust magnitude (grey scale), based on November 19, 2004, 00:00 UTC and valid for November 19, 2004, 15:00 UTC (m/s). The AB line denotes the direction of the cross-section in Figs. 9 and 12.

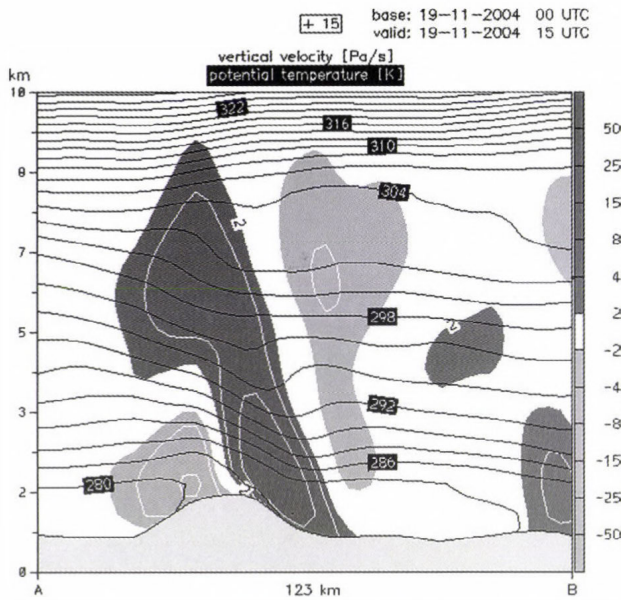


Fig. 9. Vertical cross section through the field of potential temperature (black lines) and vertical velocity in Pa/s (grey scale and white lines) as derived from the forecast of the ALADIN SHMÚ model, based on November 19, 2004, 00:00 UTC and valid for November 19, 2004, 15:00 UTC. The direction of the AB cross section is from north-west to south-east (marked in Fig. 8).

Tests were provided with newer versions of the ALADIN model with different physical parameterization setup (Geleyn, 2004). This contains the Xu-Randall cloudiness scheme (Xu and Randall, 1996), an improved radiation scheme (Geleyn *et al.*, 2005), and gustiness parameterization (Belluš, 2002). The parameterization of turbulent fluxes (Louis *et al.*, 1982) and the critical Richardson number (Geleyn, 2001) was tuned with respect to situations with stable stratifications and temperature inversions (allowing less turbulent transport of momentum and heat in the stably stratified planetary boundary layer). The distribution of the wind gust field showed decrease of the wind speed at the region of the Low Tatras and higher wind speed in the regions of Orava and southwestern Slovakia (Simon and Vivoda, 2005). However, the physical mechanism of the parameterization influence on the forecast of the November 19, 2004 windstorm is probably very complex, and the exact origin of the major changes in wind field remained unknown even after several tests with above mentioned setup.

The operational ALADIN model uses the envelope orography, where additional mass is added to model orography to represent variations in the subgrid scale (Wallace *et al.*, 1983). Model runs without the envelope failed in forecasting of the November 19, 2004 windstorm. Therefore, the presence of the envelope in the model with 9 km horizontal resolution is probably still important, despite of some systematic negative effects (e.g., exaggeration of precipitation at windward side of the mountains). Sensitivity of the ALADIN model results on the representation of the sub-grid scale orography was confirmed also for severe bora cases in Croatia (Drvar *et al.*, 2005).

8. Tests with the ALADIN model at 2.5 km resolution

8.1 Hydrostatic high resolution experiment (ALADIN HS)

Resolution of the horizontal grid is very important in the numerical simulation of small scale events. In the operational model configuration at 9 km resolution, the area of the High Tatras is represented only by few grid points. Hence, models with higher resolution should describe better the spatial distribution of the wind and should localize the wind speed maxima with higher precision. Outputs of the hydrostatic run at 2.5 km fulfilled these expectations. The distribution of the wind gust field (Fig. 10) coincides with the stationary observations and information from damage survey better than the operational run with lower resolution. Maximum predicted wind gust at southeastern flank of the High Tatras was 50 m/s, which was observed at some locations (e.g., Skalnaté Pleso). The wind distribution for Poprad valley and

the second maximum of wind speed located at the southern slopes of the Low Tatras seem to be realistic as well. Forecasts of the high resolution model show very interesting features in the field of mean sea level pressure and wind at the 10 m height (*Fig. 11*). A mesoscale cyclone forms on the lee side of the High Tatras, and a ridge of high pressure appears on the windward side. This configuration creates significant pressure gradient on the southern slopes of the mountains. The wind in this region is cross-isobaric, hence, the forcing is characterized by strong pressure drag, which is typical for downslope windstorms (*Tutiš and Picek, 1991; Picek and Tutiš, 1995*).

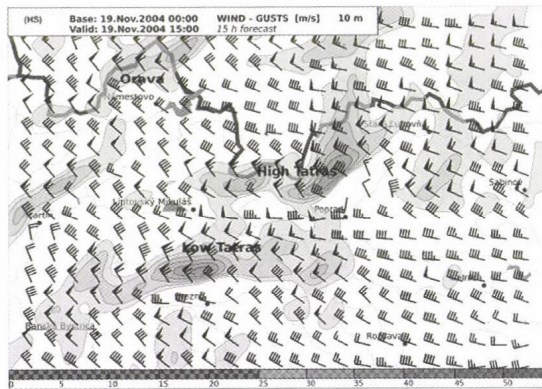


Fig. 10. The same as in *Fig. 8* except for the experimental model HS.

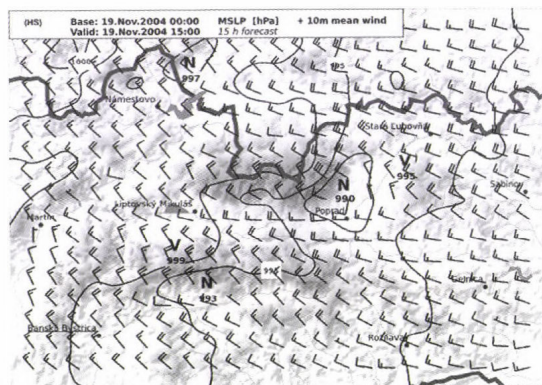


Fig. 11. Forecast of the wind field at the 10 m height over the model surface (wind barbs) and of the mean sea level pressure in hPa (thin black line). The background shows the orography in the region of the High Tatras (centre of the figure) and Low Tatras (southerly from the High Tatras). Border with Poland is marked by thick grey line. Note the mesocyclone at the south-eastern flank of the High Tatras (990 hPa in the centre of the low).

However, estimated values are much in excess of usual vertical wind speed in non-convective environment (in order of 0.1–1 Pa/s), and it is similar to the so called hydraulic jump effect (see, e.g., *Holton, 1992* and *Stull, 2003*) occurring by strong flow over an obstacle.

8.2 Non-hydrostatic experiment (ALADIN NH)

Non-hydrostatic simulation of the November 19 windstorm showed qualitatively similar results to the ALADIN HS experiment (*Fig. 12b*). Small differences between the two runs are visible in the shape, tilt, and position of the generated mountain wave. In the case of the ALADIN NH model, the wave is more symmetric; its axis is almost vertical and shifted little bit downstream against the hydrostatic output. The maximum predicted wind gusts were not as high as in the hydrostatic integration (45 m/s at southeastern flank of the High Tatras; *Fig. 13*).

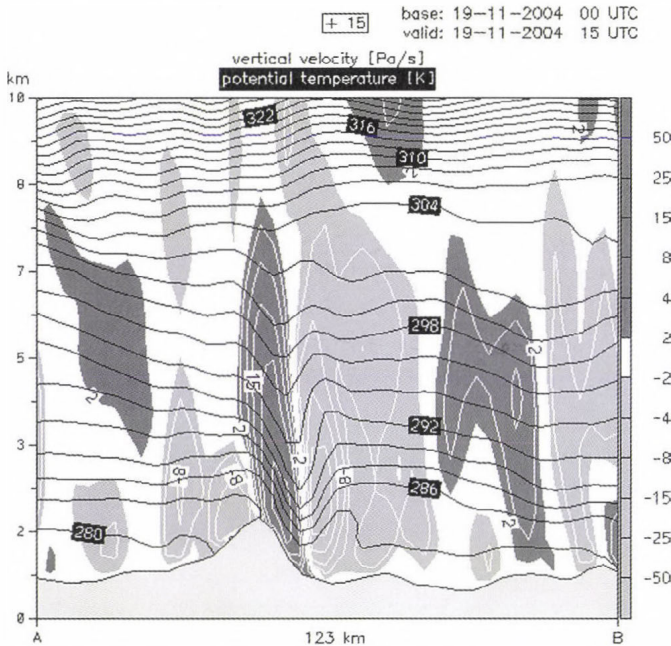


Fig. 12b. The same as in *Fig. 12a* except for the non-hydrostatic model.

Test with newer setup of physical parameterization (similar to the one referenced in Section 7) showed almost three hours delay of the windstorm onset comparing to the reference operational run. This led to differences in

the wind field distribution of the 15-hour forecast and to weaker wind gusts (maximum speed of 35 m/s). The forecast valid for 18:00 UTC already showed results similar to 2.5 km hydrostatic run and wind gusts up to 50 m/s. However, the high resolution ALADIN HS and ALADIN NH runs with physical parameterization of the reference ALADIN SHMÚ operational model corresponded much better with the observations. The possibility of the time shift of the windstorm forecast due to physical parameterization seems to be a very interesting feature, although the model physics and model dynamics interaction in this case is not yet understood.

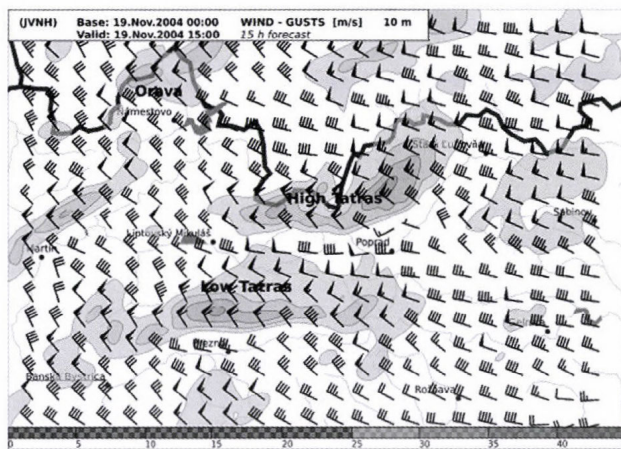


Fig. 13. The same as in Fig. 8 except for the non-hydrostatic model.

8.3 Dynamical adaptation with the ALADIN model at resolution 2.5 km

The dynamical adaptation forecasted the strongest wind gusts (58 m/s) from all high resolution runs (Fig. 14). The distribution of this parameter equals to the output of the ALADIN HS experiment. Despite of the time inconsistency, the dynamical adaptation using 30-minute integration valid at 15:00 UTC described the situation better than the time consistent version with one hour integration valid for the same time. In the latter case, the start of the windstorm was predicted with one hour delay. This experience suggests that the dynamical adaptation is very dependent on the initial and boundary conditions obtained from the reference run. One hour integration using dynamical adaptation is probably not sufficient for the onset of the downslope windstorm, if proper mesosynoptic conditions were not established in the initial input file taken from the reference run.

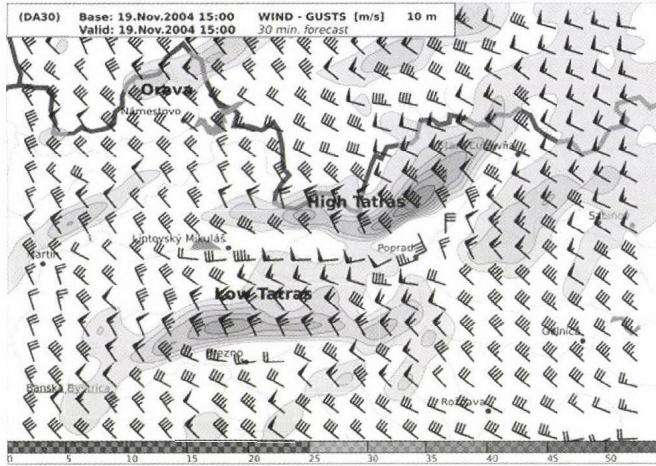


Fig. 14. The same as in Fig. 8 except for the time inconsistent dynamical adaptation.

9. Tests with the MM5 model at 1 km resolution

The start of the windstorm was forecasted by the fine scale MM5 model at 15:00 UTC, and it appeared as turn of the wind direction from westerly to northwesterly direction and as increase of the instantaneous wind speed at the 10 and 20 m height above terrain, at the top of the mountains. The downslope character of the wind is distinct at 16:00 UTC, where local maxima of the wind speed higher than 25 m/s can be found both at mountain crests and southeastern foots of the mountains at the 900 m altitude (Fig. 15). Between these two maxima, there is a belt of lower wind speed between altitudes 1100 and 1600 m, which corresponds to the information about the character of the damage in this part of the High Tatras (personal communication with Milan Koreň from TANAP organization). Projection of very high 10 m wind values is situated at the 1400 m altitude, in the axis of the valley, at the central part of the High Tatras (bottom left). Amplification of the wind in the valley can be seen also at the 20 m height above the model surface. It indicates that the flow could be amplified or suppressed due to microscale orographic conditions. However, the damage to the forest at the central part of the High Tatras was less severe and its distribution was rather chaotic, so it is difficult to verify the validity of the model result without reliable observations. Nevertheless, the main impact of the wind was observed at the southeastern part of the High Tatras, where the creation of gap winds in valleys was either impossible or it had only minor influence on the total damage. The 10 and 20 m wind in the MM5 simulation gets again weaker after 17:00 UTC. A lee cyclone occurs in

the MM5 field of mean sea level pressure at 14:00 UTC (*Fig. 16*). The depth of the cyclone (990 hPa), its position and its dimensions are almost identical with the outputs of the hydrostatic and non-hydrostatic ALADIN runs. It is noticeable, that the pressure gradient (and pressure drag) increased in time as the cold advection from northwest was getting stronger, but the low level flow was still blocked by the ridge of the Tatra Mountains.

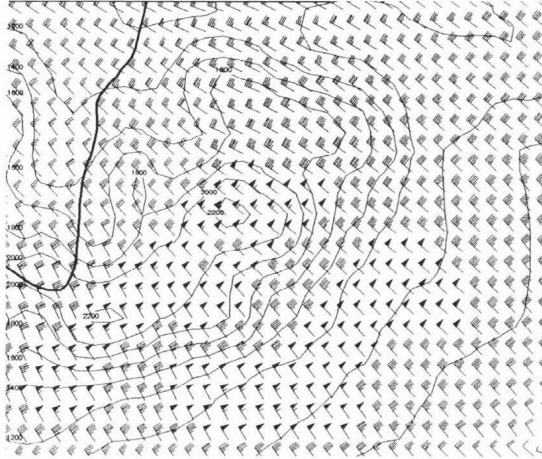


Fig. 15. Forecast of the wind field at the 20 m height over model surface with the nested version of MM5 at 1.0 km resolution for the area of the High Tatras valid for November 19, 2004, 16:00 UTC. Thin solid lines denote the model orography (m).

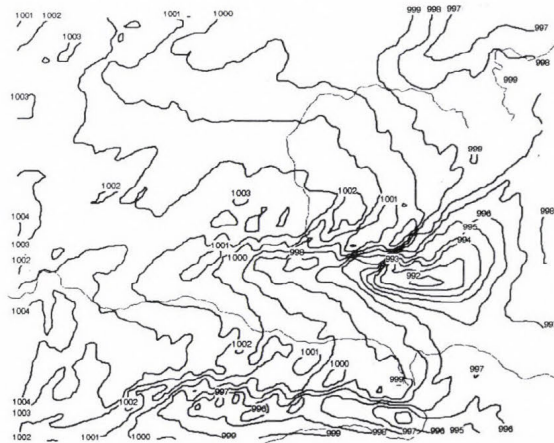


Fig. 16. Forecast of the mean sea level pressure field (hPa) via the nested version of MM5 at 1.0 km resolution for the area of the High Tatras valid for November 19, 2004, 16:00 UTC. Note the presence of the lee cyclone at the southeastern flank of the High Tatras, similarly to Fig. 11.

Finally, vertical cross-sections were provided in the northwest – southeast direction, nearly identical to those used by the ALADIN high resolution runs but valid to 16:00 UTC. The cross-section through the field of the potential temperature and meridional wind component shows undoubtedly an effect of severe downslope wind (*Fig. 17*). An isolated maximum of the wind speed of 35 m/s is situated over the southeastern slopes of the High Tatras at altitudes between 800 and 900 hPa. The cross-section through the field of vertical velocities shows a well expressed hydraulic jump with local minimum -9 m/s in the downslope and maximum 4 m/s in the upslope part of the wave (*Fig. 18*).

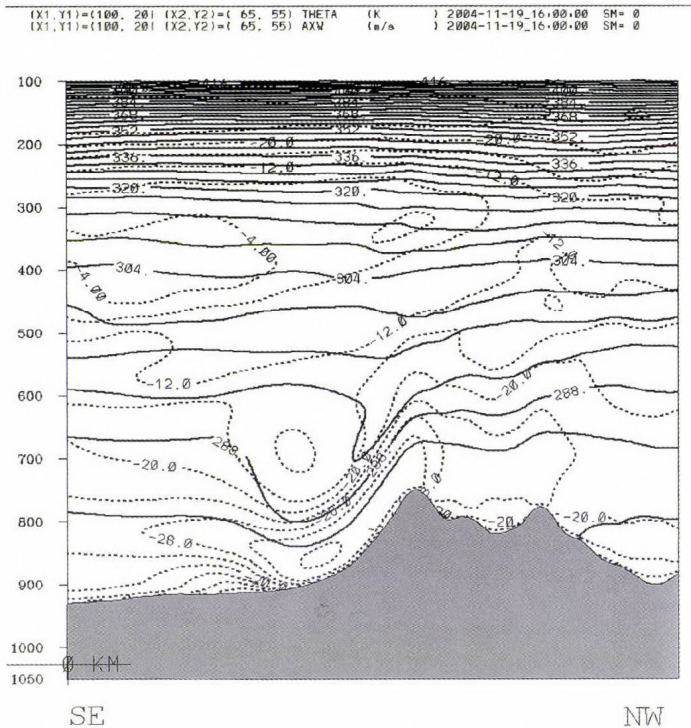
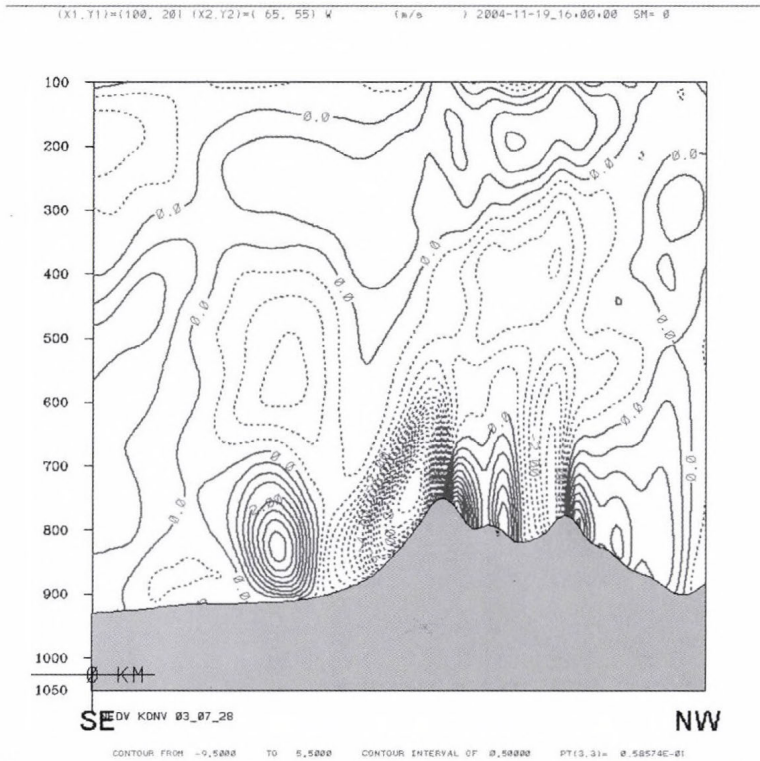


Fig. 17. Vertical cross section through the field of potential temperature (in K, solid lines) and the zonal component of wind (m/s, dotted lines) from the nested MM5 model forecast, valid for November 19, 2004, 16:00 UTC. The sense of the cross section is from northwest (right) to southeast (left), similarly to the AB line denoted by Fig. 8.

However, the fields are different from the results of the ALADIN high resolution simulations. The wave in the potential temperature field is less deep and it is significantly tilted north-westward, which indicates reversal of the flow

in the upslope part of the wave similarly to the situation depicted in Fig. 4c. Differences between the ALADIN and MM5 simulations are visible also in the field of vertical velocities. Strong upward motions in the upslope part of the wave are bounded by the 700 hPa level in the MM5 run, while in the ALADIN outputs these are observed until the tropopause and their maximum are situated at higher altitudes. According to the field of wind speed, the effect of downslope windstorm is much stronger by the MM5 than by the non-hydrostatic ALADIN simulation at 2.5 km resolution.



(overturning) of the lee wave. It creates statically unstable areas and can be considered as a signature of mountain wave breaking, which typically occurs in simulations of intense downslope wind. This phenomenon is supposed to be responsible for amplification of the intensity of downslope windstorm, because the energy of the flow is reflected from the overturned layer and remains trapped in the layer between the ground and reversed flow (*Peltier and Clark, 1979; Laprise and Peltier, 1989a*).

10. Conclusion

Results of the study presented in this paper imply several consequences for future development and operational suite of numerical weather prediction. It was shown, that models with sufficiently high resolution are able to forecast extreme mesoscale event as the November 19, 2004 windstorm at the High and Low Tatras. Further, hydrostatic approximation seems to be sufficient to simulate substantial effects of intense downslope winds. It turned out, that the dynamical adaptation of the ALADIN model already provides satisfying outputs and better horizontal distribution of the wind field at 2.5 km resolution, in comparison to the reference run at lower resolution. This is important for the operational suite, because the dynamical adaptation is computationally more effective than conventional integration of the model with full number of vertical levels.

Similarity of the hydrostatic and non-hydrostatic solutions in general is not as much surprising, because the horizontal length of the simulated mountain wave (about 30 km) is big enough to be explicitly resolved by hydrostatic dynamics, and the influence of the moist convection is minor during the event. On the other hand, strong vertical motions in the downslope and upslope part of the wave lead to not negligible non-hydrostatic pressure departures, which cannot be simulated by a hydrostatic model. Hence, further increase of the resolution by hydrostatic models would probably not give better forecast of the event. Although the structure of the potential temperature and vertical velocity fields roughly agree with the concept of the downslope windstorm as described by *Smith (1985)* and *Durran (1986)*, the hydrostatic approximation tends to exaggerate the effect of the mountain waves breaking (*Laprise and Peltier, 1989b*). Realistic simulations of the downslope windstorm at resolutions smaller than 2.5 km most probably require models with non-hydrostatic dynamics. This tendency is indicated also by the outputs of the ALADIN non-hydrostatic model.

Integration of the MM5 model at 1 km resolution gave even more detailed wind distribution close to the surface, which seems to agree with the observed

impact of the windstorm at the most affected southeastern slopes of the High Tatras. Further it shows, that at resolution 1 km and less, it would be already possible to simulate some effects of the microscale, which are given by particularities of the local orography (e.g., orientation of the valleys and peaks). However, verification of such effects is currently very problematic and it would need higher density of meteorological observations and, additionally, very detailed information from the damage survey (e.g., comparison with aerial photographs).

Results of the high resolution runs are dependent on the performance of the model giving the initial and boundary conditions. It was shown, that the success of the ALADIN reference run was linked with optimal setup of physical parameterization used by the operational model version on November 19, 2004. Different schemes of horizontal diffusion or the parameterization of turbulence might have considerable influence on both low and high resolution simulations. Hence, the case of November 19, 2004 should be used to test the future versions of the model dynamics and physics to keep the performance of forecasting windstorms of these types.

From the forecasters point of view, it is important that all model forecasts with high resolution showed typical features of a downslope windstorm (e.g., the hydraulic jump). Forecasters in Slovakia and Hungary do not have many experiences with extreme events similar to the November 19, 2004 windstorm, because downslope wind of this intensity occurs rarely in these countries. The density of available surface observations is also not sufficient to get complete information from scales less than 10 km in horizontal. Hence, forecasters are forced to accept and rely on the model results, which is easier if the dynamical reasons of the windstorm are better understood.

It can be concluded, that high resolution models are necessary to provide early warnings on extreme weather events with sufficient precision. Because of computational limitations, models with hydrostatic dynamics will be still used in the near future (particularly at large domains and by resolutions bigger than 2.5 km). However, realistic simulations of windstorms in general, will require further development of non-hydrostatic models.

References

- Adamson, D.S., Belcher, S.E., Hoskins, B.J., and Plant, R.S., 2006: Boundary layer friction in mid-latitude cyclones. Q. J. Roy. Meteor. Soc. 614, 101-124.*
- Ágústsson, H. and Ólafsson, H., 2005: The Freysnes windstorm. The 28th International Conference on Alpine Meteorology. Croatian Meteorol. J. 40, 517-520.*
- Arreola, J.L., Homar, V., Romero, R., Ramis, C., and Alonso, S., 2003: Multiscale numerical study of the 10-12 November 2001 strong cyclogenesis event in the western Mediterranean.*

- Proc. of the Plinius Conference on Mediterranean Storms IV*. European Geophysical Society, Alcodia (Spain), 2-4 October 2002, 5 pp.
- Belluš, M., 2002: Enhancement of the momentum and heat fluxes in ARPEGE/ALADIN by the gustiness parameterization. *ALADIN Internal Report*, 18 pp.
- Belušić, D., Klaić, Z.B., 2004: Estimation of bora wind gusts using a limited area model. *Tellus A* 56, 296.
- Bénard, P., Laprise, R., Vivoda, J., and Smolíková, P., 2004: Stability of leap-frog constant-coefficients semi-implicit schemes for the fully elastic system of Euler equations. Flat-terrain case. *Mon. Weather Rev.* 132, 1306-1318.
- Bénard, P., Mašek, J., Smolíková, P., 2005: Stability of leap-frog constant-coefficients semi-implicit schemes for the fully elastic system of Euler equations: Case with orography. *Mon. Weather Rev.* 133, 1065-1075.
- Bennets, D.A. and Hoskins, B.J., 1979: Conditional symmetric instability - a possible explanation for frontal rainbands. *Q. J. Roy. Meteor. Soc.* 105, 945-962.
- Bluestein, H.B., 1993: *Synoptic-Dynamic Meteorology in Midlatitudes, Vol. 2: Observations and Theory of Weather Systems*. Oxford University Press, 594 pp.
- Bubnová, R., Hello, G., Benard, P., and Geleyn, J.-F., 1995: Integration of the fully elastic equations cast in the hydrostatic pressure terrain-following coordinate in the framework of the ARP G /ALADIN NWP system. *Mon. Weather Rev.* 123, 515-535.
- Clark, T.L. and Peltier, W.R., 1977: On the evolution and stability of finite-amplitude mountain waves. *J. Atmos. Sci.* 34, 1715-1730.
- Colle, B.A. and Mass, C.F., 1998a: Windstorms along the western side of the Washington Cascade Mountains. Part I: A high resolution observational and modelling study of the 12 February 1995 event. *Mon. Weather Rev.* 126, 28-52.
- Colle, B.A. and Mass, C.F., 1998b: Windstorms along the western side of the Washington Cascade Mountains. Part II: Characteristics of past events and three-dimensional idealized simulations. *Mon. Weather Rev.*, 126, 53-71.
- Colle, B.A. and Mass, C.F., 2000: High-resolution observations and numerical simulations of Easterly Gap Flow through the Strait of Juan de Fuca on 9-10 December 1995. *Mon. Weather Rev.* 128, 2398-2422.
- Davis, C.A. and Emanuel, K.A., 1991: Potential vorticity diagnostics of cyclogenesis. *Mon. Weather Rev.* 119, 1929-1953.
- Derková, M., 2005: Numerical weather prediction activities at the Slovak Hydrometeorological Institute. *Meteorological Journal* 8, 53-64.
- Dierking, C.F., 1998: Effects of a mountain wave windstorm at the surface. *Weather Forecast.* 13, 606-616.
- Doyle, J.D. and Durran, D.R., 2002: The dynamics of mountain-wave-induced-rotors. *J. Atmos. Sci.* 59, 186-201.
- Doyle, J.D., Bond, N.A., and Jiang, Q., 2006: Observations and high-resolution simulations of a severe turbulence and downslope windstorm event. *AMS 12th Conference on Aviation Range and Aerospace Meteorology*. 28-30 January 2006, abstract.
- Drvar, D., Stiperski, I., Tudor, M., and Tutiš, V., 2005: ALADIN/HR: Testing the New Sub-Grid Scale Orography Representation on Bura Cases. The 28th International Conference on Alpine Meteorology. *Croatian Meteorological Journal* 40, 304-307.
- Durran, D.R., 1986: Another look at downslope windstorms. Part I: The development of analogs to supercritical flow in infinitely deep continuously stratified fluid. *J. Atmos. Sci.* 43, 2527-2543.
- Gaberšek, S., 2003: A downslope windstorm in NW Slovenia on 16 November 2002, *ICAM/MAP2003 Conference*. Brig, Switzerland, 19- 23 May 2003, abstract.
- Geleyn, J.-F., 2001: A summary of the latest changes in the parameterization of turbulent fluxes and PBL processes. *ALADIN Newsletter* 20, 84-88.
- Geleyn, J.-F., 2004: Some details about ALADIN physics in cycle 28T1. *ALADIN Newsletter* 26, 71-74.

- Geleyn, J.-F., Fournier, R., Hello, G., and Pristov, N., 2005: A new 'bracketing' technique for a flexible and economical computation of thermal radiative fluxes, on the basis of the Net Exchange Rate (NER) formalism. *WGNE blue book, 2005 Edition*, 4-07.
- Gerard, L., 2000: *Physical Parameterization in ARP G -ALADIN*. Internal ARP G /ALADIN documentation, 111 pp.
- Glossary of Meteorology* (ed.: T.S. Glickmann), 2000: AMS, Boston, Massachusetts, USA, 855 pp.
- Gohm, A. and Mayr, G.J., 2005a: On the bora breakthrough near a mountain gap. The 28th International Conference on Alpine Meteorology. *Croatian Meteorol. J.* 40, 217-220.
- Gohm, A. and Mayr, G.J., 2005b: Numerical and observational case-study of a deep Adriatic bora. *Q. J. Roy. Meteor. Soc.* 131, 1363-1392.
- Grubišić, V. and Lewis, J.M., 2004: Sierra Wave Project revisited 50 years later. *B. Am. Meteorol. Soc.* 85, 1127-1142.
- Holton, J.R., 1992: *An Introduction to Dynamic Meteorology*. Third edition. Academic Press, 282-287.
- Horányi, A., Ihász, I., and Radnóti, G., 1996: ARP G -ALADIN: A numerical weather prediction model for Central Europe with the participation of the Hungarian Meteorological Service. *Időjárás* 100, 277-301.
- Hoskins, B.J., McIntyre, M.E., and Robertson, A.W., 1985: On the use and significance of isentropic potential vorticity maps. *Q. J. Roy. Meteor. Soc.* 111, 877-946.
- Ivatek-Šahdan, S. and Tudor, M., 2004: Use of high-resolution dynamical adaptation in operational suite and research impact studies. *Meteorol. Z.* 13, 99-10.
- Janjic, Z.I., 1990: The step-mountain coordinate: Physical package. *Mon. Weather Rev.* 118, 1429-1443.
- Jurčec, V. and Brzović, N., 1995: The Adriatic bora: special case studies. *Geofizika* 12, 15-32.
- Kaplan, M.L., Huffman, A.W., Lux, K.M., Cetola, J.D., Charney, J.J., Riordan, A.J., Lin, Y.L., and Waight III, K. T., 2003: *Characterizing the Severe Turbulence Environments Associated With Commercial Aviation Accidents. Part II: Hydrostatic Mesobeta Scale Numerical Simulations of Supergradient Wind Flow and Streamwise Ageostrophic Frontogenesis*. Langley Research Center, Hampton, Virginia. NASA/CR-2003-212138 Report, 45 pp.
- Kasahara, A. and Qian, J.H., 2000: Normal modes of a Global Nonhydrostatic Atmospheric Model. *Mon. Weather Rev.* 128, 3357-3375.
- Klaić, Z.B. and Belušić, D., 2005: Severe Adriatic Bura event from 14 to 15 November 2004. The 28th International Conference on Alpine Meteorology. *Croatian Meteorol. J.* 40, 300-303.
- Klemp, J.B. and Durran, D.R., 1987: Numerical modelling of bora winds. *Meteorol. Atmos. Phys.* 36, 215-227.
- Klemp, J.B. and Lilly, D.K., 1975: The dynamics of wave-induced downslope winds. *J. Atmos. Sci.* 32, 320-339.
- Klemp, J.B. and Lilly, D.K., 1978: Numerical simulation of hydrostatic mountain waves. *J. Atmos. Sci.* 35, 78-107.
- Konček, M., 1944: Meteorological circumstances of catastrophic windstorm in Slovakia during autumn of 1941 (in Slovak). *Prírodovedecká fakulta Slovenskej university, Bratislava*, 44 pp.
- Koreň, M., 2005: Wind calamity of 19 November 2004 – new points of view and consequences (in Slovak). *Vysoké Tatry special issue* 15, 6-28.
- Kraljević, L. and Tudor, M., 2005: High resolution simulation of a severe bura event – an intercomparison of two models. Presentation, *15th ALADIN Workshop*. Bratislava June 6-10 2005 (<http://www.cnrm.meteo.fr/aladin/meetings/Wk2005/program.html>).
- Kuettner, J. and Hertenstein, R.F., 2002: Observations of mountain-induced rotors and related hypotheses: A review. *AMS Tenth Conference on Mountain Meteorology*. Park City Utah, 17-21 June 2002, 326-329.
- Lane, T.P., Reeder, M.J., Morton, B.R., and Clark, T.L., 2000: Observations and numerical modelling of mountain waves over the Southern Alps of New Zealand. *Q. J. Roy. Meteor. Soc.* 126, 2765-2788.

- Laprise, R. and Peltier, W.R., 1989a: The structure and energetics of transient eddies in a numerical simulation of breaking mountain waves. *J. Atmos. Sci.* 46, 565-585.
- Laprise, R. and Peltier, W.R., 1989b: On the structural characteristics of steady finite-amplitude mountain waves over Bell-Shaped topography. *J. Atmos. Sci.* 46, 586-595.
- Laprise, R., 1992: The Euler equations of motion with hydrostatic pressure as an independent variable. *Mon. Weather Rev.* 120, 197-207.
- Lilly, D.K., 1978: A severe downslope windstorm and aircraft turbulence event induced by a mountain wave. *J. Atmos. Sci.* 35, 59-77.
- Long, R.R., 1953: Some aspects of the flow of stratified fluids: I. A theoretical investigation. *Tellus* 5, 42-58.
- Long, R.R., 1954: Some aspects of the flow of stratified fluids: II. Experiments with a two fluid system. *Tellus* 6, 97-115.
- Louis, J.F., Tiedke, M., and Geleyn, J.-F., 1982: A short history of the operational PBL parameterization at ECMWF. *Workshop on Planetary Boundary Layer Parameterization*. ECMWF, 25-27 Nov 1981, 59-80.
- Luczy, G., 2005: Weather situations and calamities in Tatras, in Slovak. *Vysoké Tatry* 3, 14.
- Meyers, M.P., Snook, J.S., Wesley, D.A., and Poulos, G.S., 2003: A Rocky Mountain storm. Part II: The forest blowdown over the west slope of the Northern Colorado Mountains—observations, analysis, and modeling. *Weather Forecast.* 18, 662-674.
- Morgan, M.C. and Nielsen-Gammon, J.W., 1998: Using tropopause maps to Diagnose midlatitude weather systems. *Mon. Weather Rev.* 126, 2555-2579.
- Nance, L.B. and Durran, D.R., 1997: A modelling study of nonstationary trapped mountain lee waves. Part I: Mean-flow variability. *J. Atmos. Sci.* 54, 2275-2291.
- Nance, L.B. and Durran, D.R., 1998: A modelling study of nonstationary trapped mountain lee waves. Part II: Nonlinearity. *J. Atmos. Sci.* 55, 1429-1445.
- Otruba, J., 1964: Wind conditions in Slovakia (in Slovak). SAV, Bratislava, 130-134.
- Otruba, J. and Wiszniewski, W., 1974: Climate of Tatras (in Slovak). In *Klíma Tatier* (ed.: M. Konček). Veda, Bratislava, 328-339.
- Pan, F. and Smith, R.B., 1999: Gap winds and wakes: SAR observations and numerical simulations. *J. Atmos. Sci.* 56, 905-923.
- Peltier, W.R. and Clark, T.L., 1979: The evolution and stability of finite-amplitude mountain waves. Part II: Surface drag and severe downslope windstorms. *J. Atmos. Sci.* 36, 1498-1529.
- Picek, B.I. and Tutiš, V., 1995: Mesoscale Bora flow and mountain pressure drag. *Meteorol. Z.* 4, 119-128.
- Picek, B.I. and Tutiš, V., 1996: A case study of a severe Adriatic bora on 28 December 1992. *Tellus* 48A, 357-367.
- Poulos, G.S., Bossert, J.E., McKee, T.B., and Pielke, R.A., 2000: The interaction of katabatic flow and mountain waves. Part I: Observations and idealized simulations. *J. Atmos. Sci.* 57, 1919-1936.
- Radnóti, G., Ajjaji, R., Bubnová, R., Caian, M., Cordoneanu, E., 1995: The spectral limited area model Arp g -Aladin. In *PWPR Report Series n.7 - WMO TD n. 699*, 111-118.
- Rak, J., 1967: The gale in the Tatra region - in November, 1964 (in Slovak). *Sborník prác o Tatranskom národnom parku* 10, 49-64.
- Reisner, J., Rasmussen, R.J., and Brintjes, R.T., 1998: Explicit forecasting of supercooled liquid water in winter storm using the MM5 mesoscale model. *Q. J. Roy. Meteor. Soc.* 24B, 1071-1107.
- Romero, R., Homar, V., Ramis, C., and Alonso, S., 2002: Baroclinic and diabatic regulation of the 10-12 November 2001 superstorm in the Balearics. *European Conference on Severe Storms 2002*. Prague, Czech Republic, 26-30 August 2002, presentation and abstract.
- Sandvik, A.D., 2001: Case study of a downslope windstorm 16 January 2000. *Workshop on Fine-Scale Meteorological Modelling*. 17-18 September 2001 at Finse.
- Satomura, T. and Bougeault, P., 1994: Numerical simulation of lee wave events over the Pyrenees. *J. Meteorol. Soc. Japan* 72, 173-195.

- Simon, A. and Vivoda, J., 2005: Downslope windstorm in High Tatras 19 November 2004. Presentation, *15th ALADIN Workshop*. Bratislava, June 6-10 2005, (<http://www.cnrm-meteo.fr/aladin/meetings/Wk2005/program.html>).
- Smith, C., 2002: Stability analysis and precision aspects of the boundary condition formulation in the non-hydrostatic dynamics and exploration of the alternatives for discrete formulation of the vertical acceleration equation both in Eulerian and semi-Lagrangian time marching schemes. *ALATNET Newsletter 4*, (http://www.cnrm-meteo.fr/aladin/newsletters/news21/PhDs_6.html).
- Smith, R.B., 1980: Linear theory of stratified hydrostatic flow past an isolated mountain. *Tellus 32*, 348-364.
- Smith, R.B., 1985: On severe downslope winds. *J. Atmos. Sci.* 42, 2597-2603.
- Smolarkiewicz, P.K. and Rotunno, R., 1989: Low Froude number flow past three-dimensional obstacles. Part I: Baroclinically generated lee vortices. *J. Atmos. Sci.* 46, 1154-1164.
- Stull, R.B., 2003: *An Introduction to Boundary Layer Meteorology*. Kluwer Academic Publishers, 601-609.
- Tutiš, V., 2002: Violent Adriatic windstorms. *Proc. of the 4th EGS Plinius Conference*. Mallorca, Spain, October 2002.
- Tutiš, V. and Píček, I.B., 1991: Pressure drag on the Dinaric Alps during the ALPEX SOP. *Meteorol. Atmos. Phys.* 47, 73-81.
- Vergeiner, I. and Lilly, D.K., 1970: The dynamic structure of lee wave flow as obtained from balloon and airplane observations. *Mon. Weather Rev.* 98, 220-232.
- Vigh, J., 2005: *Downslope Windstorms and Rotors*. Department of Atmospheric Science, Colorado State University, presentation, (<http://euler.atmos.colostate.edu/~vigh/papers>).
- Vosper, S., 2003: Development and testing of a high resolution mountainwave forecasting system. *Meteorol. Appl.* 10, 75-86.
- Wallace, J., Tibaldi, S. and Simmons, A.J., 1983: Reduction of systematic forecast errors in the ECMWF model through the introduction of an envelope orography. *Q. J. Roy. Meteor. Soc.* 109, 683-717.
- WWF position paper, 2004: *Storm in Tatras National Park (Slovakia)*. Web page of WWF organisation (<http://assets.panda.org/downloads/wwfpositiontatrastorm.pdf>).
- Xu, K.-M. and Randall, D.A., 1996: A Semi-empirical cloudiness parametrization for use in climate models. *J. Atmos. Sci.* 53, 3084-3102.
- Žagar, M. and Rakovec, J., 1999: Small-scale surface wind prediction using dynamic adaptation. *Tellus 51*, 489-504.
- Zejda, V., 1986: Where the variometer shows 20 m per second (in Czech). *Letectví a Kosmonautika* 33, 193-194.
- Zhang, Y., Chen, Y.-L., and Kodama, K., 2005: Validation of the coupled NCEP mesoscale spectral model and an advanced land surface model over the Hawaiian Islands. Part II: A high wind event. *Weather Forecast.* 20, 873-895.

IDŐJÁRÁS

*Quarterly Journal of the Hungarian Meteorological Service
Vol. 110, No. 2, April–June 2006, pp. 125–134*

Developing an optimal system of circulation pattern types for downscaling purposes

István Matyasovszky

*Department of Meteorology, Eötvös Loránd University,
P.O. Box 32, H-1518 Budapest, Hungary, E-mail: matya@ludens.elte.hu*

(Manuscript received in final form May 29, 2006)

Abstract—A methodology to develop an optimal system of circulation pattern (CP) types is proposed for downscaling purposes. The success of downscaling depends on how strongly the stochastic behavior of a climate element can be related to CP types. Therefore, an optimal system of CP types has as much information on the specific climate element as possible. The problem includes also the choice of the number of CP types. The procedure proposed is applied to normally distributed daily mean temperatures and daily precipitation amounts having intermittence. In this latter case, CP types may be different for sequences of dry and wet days and for precipitation amounts on wet days.

Key-words: downscaling, circulation pattern, classification, temperature, precipitation

1. Introduction

In order to simulate climates under increasing concentration of atmospheric greenhouse gases, coupled atmosphere–ocean general circulation models (GCMs) are used. A standard method to assess the change of climate is to run such a model under the present atmospheric content of greenhouse gases (control run), and then run it again corresponding to a scenario of future content of greenhouse gases (changed climate). However, due to the relatively low horizontal resolution (a few hundred kilometres) and relatively simple parameterizations (atmosphere–surface feedbacks, radiative processes, cloud and precipitation forming, etc.) of these models, the results for small areas are considerably uncertain. There is a need, therefore, to “downscale” the large-scale output of GCMs to smaller scales.

Generally, two main types of downscaling approaches are used (*Giorgi and Mearns, 1991*). The first type of downscaling methods includes meso-scale numerical modeling. Meso-scale models use GCM outputs as initial and boundary conditions. This technique requires substantial effort in terms of modeling and computer programming, and no satisfactory long simulation is available to assess extremes. These difficulties, among others, may motivate the use of the second approach called stochastic downscaling. Stochastic downscaling methods have two key elements. The first element includes large-scale circulation of the atmosphere and the second element represents a linkage between local surface variables and large-scale circulation. The linkage is expressed by a stochastic model using an observational data series. Then, this model may be utilized with GCM outputs characterizing atmospheric circulation.

Stochastic downscaling has several specific versions. One of them is based on classification of the large-scale atmospheric circulation pattern (CP). Having a system of CP types, the stochastic behavior of a local climate element is described via stochastic properties conditioned on these types. A stochastic property Ψ of a local climate element is written as

$$\Psi = \sum_{j=1}^J r_j \Psi_j, \quad (1)$$

where Ψ_j is the property conditioned on the j th CP type and r_j is the probability of the occurrence of the j th CP type. The property in question under changed climate is then estimated by Eq. (1) with relative frequencies of CP types corresponding to GCM outputs under changed climate. In the simplest case, Ψ is expected value, but may include other parameters characterizing the stochastic behavior of a climate element. In a general case Ψ may be the probability distribution or density function. The literature of application of the concept is very broad, first attempts were reported by *Bardossy and Plate (1992)*, *Wilson et al. (1992)*, *Hughes et al. (1993)*.

A basic question concerning the application of the methodology based on CP types is how strongly the stochastic behavior of a climate element can be related to CP types. The stronger this relationship, the larger the estimated local response to the same large-scale change. For instance, in the absence of such a relationship ($\Psi_j \equiv \Psi$) even an extreme change of the large-scale circulation results in no local response. Therefore, a system of CP types having as much information on the specific climate element as possible has to be found. This problem is addressed in Section 2 including the choice of optimal number of CP types, too.

The proposed methodology is applied to daily mean temperature and daily precipitation amount in Section 3. Finally, a section is provided for discussion.

2. Methodology

A large number of initial circulation pattern types is developed using an objective classification method as a first step. The k-means clustering technique is applied and say 100 clusters are developed. These clusters are then aggregated into a fixed number of types such that the types have as large information on the specific climate element as possible. Finally, the optimal number of types is estimated.

Let Y be a normal random variable with expected value m representing a climate element at a fixed site. Let X be a discrete random variable such that $X=k$ corresponds to the occurrence of k th type with $r_k=P(X=k)$. Having an independent sample (x_i, y_i) , $i=1, \dots, n$ for (X, Y) the task is to find the best system of CP types for a fixed number of types K . Having conditional means

$$\hat{m}_k = \frac{1}{n_k} \sum_{i: x_i=k} y_i, \quad k=1, \dots, K, \quad (2)$$

where n_k is the observed number of k th CP type, the quantity

$$\sum_{k=1}^K n_k (\hat{m}_k - \hat{m})^2 \quad (3)$$

has to be maximized, where

$$\hat{m} = \frac{1}{n} \sum_{i=1}^n y_i \quad (4)$$

is the estimate of expected value $E[Y]$. Then, after *Akaike* (1971), the optimal number of CP types is estimated by minimizing

$$AIC(K) = n \ln \left(\hat{d}^2 - \sum_{k=1}^K \hat{r}_k (\hat{m}_k - \hat{m})^2 \right) + 2K \quad (5)$$

with respect to K , where

$$\hat{d}^2 = \frac{1}{n} \sum_{i=1}^n (y_i - \hat{m})^2, \quad \hat{r}_k = \frac{n_k}{n}, \quad k=1, \dots, K. \quad (6)$$

Since daily climate data are statistically dependent, the above formulation, valid for independent sequences, has to be modified. A first order autoregressive approximation to y_i is

$$y_i - m = a(y_{i-1} - m) + e_i, \quad (7)$$

where a is the autoregressive parameter and $\{e_i\}$ is a sequence of independent normally distributed random variables with variance s^2 . Having an estimate

$$\hat{a} = \frac{\sum_{i=2}^n (y_i - \hat{m})(y_{i-1} - \hat{m})}{\sum_{i=2}^n (y_{i-1} - \hat{m})^2}, \quad (8)$$

data

$$e_i = (y_i - \hat{m}) - \hat{a}(y_{i-1} - \hat{m}), \quad i = 2, \dots, n \quad (9)$$

are treated as $\{y_i\}$ in the previous case resulting in

$$AIC(K) = (n-1) \ln \left(\hat{s}^2 - \sum_{k=1}^K \hat{r}_k \hat{\mu}_k^2 \right) + 2K \quad (10)$$

with

$$\hat{\mu}_k = \frac{1}{n_k} \sum_{i; x_i=k}^n e_i, \quad k = 1, \dots, K. \quad (11)$$

A climate element in question at L locations is represented by a normal random vector $\mathbf{Y} = (Y_1, \dots, Y_L)$, where superscript T denotes transpose. Then

$$AIC(K) = (n-1) \ln \left(\left| \mathbf{S}_0 - \sum_{k=1}^K \hat{r}_k \hat{\mathbf{m}}_k \hat{\mathbf{m}}_k^T \right| \right) + 2KL \quad (12)$$

has to be minimized for every possible system of CP types and with respect to K , where

$$\hat{\mathbf{m}}_k = \frac{1}{n_k} \sum_{i; x_i=k} \mathbf{e}_i, \quad k = 1, \dots, K, \quad (13)$$

while symbol $||$ represents determinant, and \mathbf{e}_i are defined by

$$(\mathbf{y}_i - \hat{\mathbf{m}}) = \hat{\mathbf{A}}(\mathbf{y}_{i-1} - \hat{\mathbf{m}}) + \mathbf{e}_i, \quad \hat{\mathbf{A}} = \hat{\mathbf{S}}_1 \hat{\mathbf{S}}_0^{-1}, \quad (14)$$

where \mathbf{S}_0 and \mathbf{S}_1 are covariance matrices of \mathbf{Y} for lag 0 and 1, respectively.

The idea discussed above can be used for Gaussian processes, because the present model selection criteria based on maximizing the log-likelihood function penalized with model parameters are valid for such processes. For

many climate elements there exist appropriate transformations resulting in normal distributions, and thus the problem can be treated as in the previous paragraphs. For instance, when wind speed is in question, the random variable Y^c with a suitable $c > 0$ is distributed approximately normally due to a property of Weibull distributions used for wind speed. Similar simple transformations can be established for several other climate elements. However, daily precipitation having a crucial role in climate change studies cannot be treated such a simple way due to its spatio-temporal intermittence. Therefore, a two-step procedure is proposed for daily precipitation. In the first step only the sequence of wet and dry days are examined, then precipitation amounts on wet days are analyzed.

The observed sequence of wet and dry days can be modeled with a first order Markov chain (Matyasovszky and Dobi, 1989). Therefore, an indicator series is defined as $I_i = 0$ if $y_i = 0$, and as $I_i = 1$ if $y_i > 0$ for daily precipitation data $\{y_i\}$. The conditional probabilities

$$p_{uv} = P(I_i = v | I_{i-1} = u), \quad u, v = 0, \dots, 1 \quad (15)$$

and the probability $P = p_{01}/(p_{01} + p_{10})$ of having a wet day depend on CP types, and the task is to estimate these conditional probabilities with corresponding relative frequencies according to the CP types. Then

$$AIC(K) = n \sum_{k=1}^K \hat{r}_k \left[\left(1 - \hat{P}^{(k)}\right) \sum_{v=0}^1 \hat{p}_{0v}^{(k)} \ln \hat{p}_{0v}^{(k)} + \hat{P}^{(k)} \sum_{v=0}^1 \hat{p}_{1v}^{(k)} \ln \hat{p}_{1v}^{(k)} \right] + 2K \quad (16)$$

has to be minimized for every possible system of CP types, and with respect to K , where superscripts (k) refer to k th CP type.

Positive precipitation data are transformed into normally distributed data. Transformation is done by

$$z_i = \hat{d} \Phi^1(F_N(y_i | y_i > 0)) + \hat{m}, \quad (17)$$

where N is the number of positive precipitation data, F_N is the empirical probability distribution function of these data, Φ is the standard normal distribution function, and m and d are the expected value and standard deviation of these data. Data $\{z_i\}$ can be handled as they come from a time series broken by several non-observable periods corresponding to the sequence of dry days. Time series is modeled with a first order autoregressive process

with the autoregressive parameter a . When a data z_i follows a $(j-1)$ -day length dry period, the optimal prediction for z_i is $a^j(z_{i-j} - m) + m$ having a prediction error variance $(1 - a^{2j})d^2$. The log-likelihood function corresponding to prediction errors is then

$$-N \ln d - \sum_{j=1}^{J+1} N_j \ln \left[(1 - a^{2j})^{1/2} \right] - \frac{1}{2d^2} \sum_{j=1}^{J+1} Q_j(a) \quad (18)$$

with

$$Q_j(a) = \sum_i \left[(z_i - \bar{z}) - a^j(z_{i-j} - \bar{z}) \right]^2 / (1 - a^{2j}), \quad j = 1, \dots, J+1, \quad (19)$$

where summation extends for i ; $y_i > 0$, $y_{i-1} = 0, \dots, y_{i-j+1} = 0$, $y_{i-j} > 0$. J is the length of the longest dry period and N_j is the number of $(j-1)$ -day length dry periods. Maximizing Eq. (18) with respect to d gives

$$\hat{d}^2 = \frac{1}{N} \sum_{j=1}^{J+1} Q_j(\hat{a}). \quad (20)$$

Substituting this estimate into Eq. (18),

$$-N \ln d^2 - \sum_{j=1}^{J+1} N_j \ln (1 - a^{2j}) \quad (21)$$

has to be maximized with respect to a . Also, the maximum likelihood estimate of expectation of prediction errors under k th CP type is

$$\hat{\mu}_k = \left[\sum_{j=1}^{J+1} \bar{e}_j^{(k)} / (1 - \hat{a}^{2j}) \right] / \left[\sum_{j=1}^{J+1} 1 / (1 - \hat{a}^{2j}) \right], \quad (22)$$

where $\bar{e}_j^{(k)}$ is the mean of the prediction errors following $(j-1)$ -day dry spells under k th CP type. Finally,

$$AIC(K) = \sum_{j=1}^{J+1} N_j \ln \left(\hat{d}^2 [1 - \hat{a}^{2j}] - \sum_{k=1}^K \hat{r}_j^{(k)} \hat{\mu}_k^2 \right) + 2K \quad (23)$$

has to be minimized for every possible system of CP types and with respect to K . Now, $\hat{r}_j^{(k)}$ is the relative frequency of k th CP type conditioned on days following $(j-1)$ -day dry spells.

3. Application

The methodology discussed above is applied to daily mean temperature and daily precipitation amount. Circulation pattern types are developed using the 700-hPa geopotential field defined on a diamond grid covering the European Atlantic region and obtained from NCAR data bases.

Temperature data for five Hungarian locations, namely Budapest, Kalocsa, Kecskemét, Debrecen, and Szeged cover a 30-year period from 1961 to 1990. Results are discussed for summer and winter. The optimal number of types according to the criterion Eq. (12) is 12 and 10 in summer and winter, respectively. *Tables 1* and *2* show the means of daily mean temperatures in summer and winter for the five locations in a descending order of relative frequencies of CP types. *Figs. 1* and *2* demonstrate differences among probability distributions corresponding to different CP types. Normal density functions fitted to data under different CP types are shown here. Note that a warm and a cold type having large relative frequencies are illustrated in these figures. For instance, Type 8 is the coldest in winter but with a small relative frequency, thus Type 3 having a large relative frequency is presented in *Fig. 2*.

Table 1. Summer mean temperatures under different CP types

Type Relative frequency	Mean temperatures (°C)				
	Budapest	Kalocsa	Kecskemét	Debrecen	Szeged
0.155	21.79	21.31	21.34	20.71	21.50
0.124	20.14	19.51	19.41	18.75	19.61
0.118	18.48	18.15	18.28	17.62	18.22
0.099	20.38	20.01	19.95	19.22	20.11
0.098	21.13	20.63	20.47	19.92	20.69
0.093	22.49	22.00	21.92	21.33	22.09
0.076	22.33	21.37	21.39	21.09	21.55
0.076	18.59	18.22	18.19	17.90	18.44
0.055	22.46	21.61	21.48	20.92	21.76
0.043	20.38	19.73	19.75	19.09	20.08
0.036	17.94	17.38	17.30	17.26	17.66
0.027	20.86	20.27	20.25	19.44	20.38

Table 2. Winter mean temperatures under different CP types

Type Relative frequency	Mean temperatures (°C)				
	Budapest	Kalocsa	Keckskemét	Debrecen	Szeged
0.162	0.31	-0.83	-1.11	-1.90	-1.29
0.137	0.91	-0.07	-0.27	-0.86	-0.31
0.122	0.64	-0.52	-0.96	-1.91	-0.81
0.120	1.88	1.36	1.20	0.24	0.94
0.113	2.69	1.88	1.57	0.36	1.56
0.106	-2.18	-3.19	-3.17	-4.05	-3.40
0.099	3.21	2.30	2.37	1.75	2.02
0.073	-0.91	-1.98	-1.91	-2.14	-2.03
0.055	0.43	-0.66	-1.03	-1.71	-1.13
0.011	-4.70	-4.82	-4.97	-7.45	-5.26

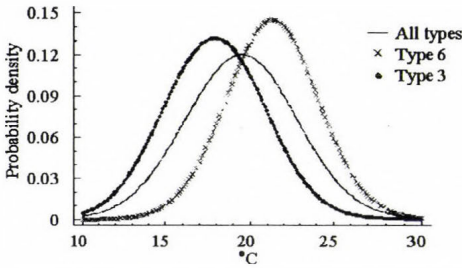


Fig. 1. Probability density function of summer temperatures under different circulation pattern types for Debrecen.

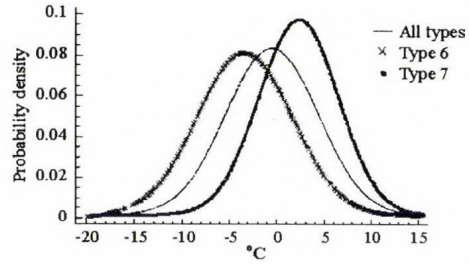


Fig. 2. Probability density function of winter temperatures under different circulation pattern types for Debrecen.

Daily precipitation amount for Budapest is analyzed also for summer and winter separately using a 30-year period of data from 1955 to 1984. In summer, the optimal number of types is 10 and 8 for sequences of wet and dry days (Eq. (16)) and for precipitation amount on wet days (Eq. (23)). Winter requires more types, namely a choice of 12 types is optimal for both the sequences of wet and dry days and for precipitation amount on wet days. It may be concluded, that the number of types is governed principally by the variance of the underlying variable, because periods accompanied with smaller variances require fewer types. Large variances decrease sharply when adding a further type, and thus fewer types are required as compared to small variances. The probability of wet days is 0.336 in summer, while this probability conditioned on CP types varies between 0.190 and 0.527. The probability of precipitation occurrence is 0.356 in winter but extends from 0.071 to 0.523 according to CP types. The mean

precipitation amount on wet days equals to 5.670 mm and 3.152 mm in summer and winter, respectively. Similar means corresponding to the CP types vary from 3.051 to 8.988 mm, and from 1.060 to 4.708 mm, for the two seasons. *Figs. 3 and 4* demonstrate differences among probability distributions of precipitation amount on wet days by fitting gamma distributions to data under different CP types. CP types having large relative frequencies and accompanied with small and large amounts are shown here.

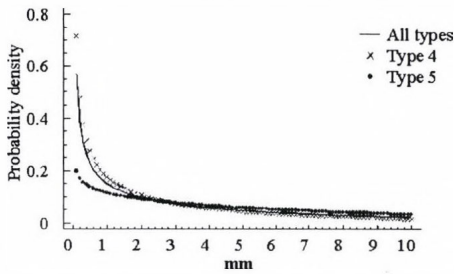


Fig. 3. Probability density function of summer daily precipitation amounts on wet days under different circulation pattern types for Budapest.

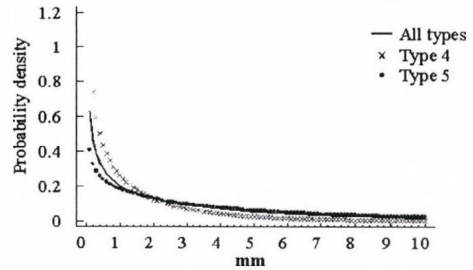


Fig. 4. Probability density function of winter daily precipitation amounts on wet days under different circulation pattern types for Budapest.

4. Discussion

A methodology to develop optimal systems of circulation pattern types for downscaling purposes has been introduced and applied to daily mean temperature and daily precipitation. An optimal system of CP types with a fixed number of possible types has as much information on the specific climate element as possible. The number of types is chosen such that the gain of introducing a further type is significant as compared to the gain of fewer types.

In order to check the performance of the method discussed above, these optimal systems of CP types are compared to Hess-Brezowski (HB) types. This latter classification having 30 types is widely used for the Central European region. A likelihood-ratio test defined as twofold difference between log-likelihood functions corresponding to HB types and the proposed types is used for the purpose. The twofold log-likelihood values are the same as the corresponding AIC values without penalty terms (second terms). Under the null hypothesis, that the proposed systems of types are optimal (HB types have no improvement over the proposed types), the test statistic follows a chi square distribution with $30-K$ degrees of freedom. A unanimous result for both the temperature and precipitation is that the null hypothesis is not rejected at even a 10% significance level in winter and at a 5% significance level in summer.

Note that 5% significance levels are very common in hypothesis testing, while 10% significance levels deliver even narrower acceptance intervals for null hypotheses. Thus, it may be concluded that the proposed methodology resulting in 8–12 types performs at least as good as HB classification with 30 types.

CP types obtained by the procedure discussed above can be used to reproduce space-time statistical structure of climate elements under a changed climate. For this purpose, for elements modeled by Gaussian processes, the multivariate AR(1) model (Eq. (14)) depends on CP types. Thus, time series simulated by type dependent AR(1) models reflect the properties of local climate via the sequence of CP types obtained from a GCM under changed climate. Local precipitation can be analyzed by a similar way using GCM-generated CP types. First, a sequence of dry and wet days is simulated with the type dependent Markov chain model. Then transformed precipitation amounts (Eq. (17)) on wet days are simulated, according to the type dependent AR(1) model. Finally, precipitation amounts are obtained by inverting Eq. (17). Simulating multisite precipitation cannot be accomplished by the procedure outlined above, because an other transformation of precipitation amounts is needed (Bartholy *et al.*, 2001). Here the optimal system of CP types should be the same for both the precipitation events and amounts. These CP types can be determined by minimizing a weighted sum of Eqs. (16) and (23) applied with areal mean precipitation. The weights can be chosen as reciprocals of Eqs. (16) and (23) under one type.

Acknowledgement—Research leading to this paper has been supported by grants from Hungarian Research and Development Foundation NKFP 3A/2002 and Hungarian Science Foundation OTKA T38038.

References

- Akaike, H., 1974: A new look at the Statistical Model Identification. *IEEE T. Autom. Contr.* 19, 716-723.
- Bartholy, J., Matyasovszky, I., and Weidinger, T., 2001: Regional climate change in Hungary: a survey and a stochastic downscaling method. *Időjárás* 105, 1-17.
- Bardossy, A. and Plate, E., 1992: Space-time model for daily rainfall using atmospheric circulation patterns. *Water Resour. Res.* 28, 1247-1260.
- Giorgi, F., and Mearns, L.O., 1991: Approaches to the simulation of regional climate change: a review. *Rev. Geophys.* 29, 191-216.
- Matyasovszky, I. and Dobi, I., 1989: Methods for the analysis of precipitation time series with Markov chains (in Hungarian). *Időjárás* 93, 276-287.
- Hughes, J.P., Lettenmaier, D.P., and Guttorp, P., 1993: A stochastic approach for assessing the effect of changes in synoptic circulation patterns on gauge precipitation. *Water Resour. Res.* 2, 3305-3315.
- Wilson, L.L., Lettenmaier, D.P., and Skyllingsta, E., 1992: A hierarchical stochastic model of large scale atmospheric circulation patterns and multiple station daily precipitation. *J. Geophys. Res.* 97, 2791-2809.

IDŐJÁRÁS

Quarterly Journal of the Hungarian Meteorological Service
Vol. 110, No. 2, April–June 2006, pp. 135–153

Relationship between soil texture and near surface climate in Hungary

Miklós Drucza and Ferenc Ács

*Department of Meteorology, Eötvös Loránd University,
P.O. Box 32, H-1518 Budapest, Hungary; E-mail: acs@elte.hu*

(Manuscript received in final form March 6, 2006)

Abstract—The near surface climate of Hungary in the period 1901–1950 is analyzed using a Thornthwaite-based model. Annual and monthly mean values of energy- and water balance components are determined for each Thornthwaite's climatic region. The analysis is performed for both constant and texture-dependent soil water holding capacity. The main purpose of this study is to evaluate the effect of soil texture on the near surface climate of Hungary. The main findings are as follows: (1) The Thornthwaite-based model is suitable for reproducing the pattern of climate on mesoscale in Hungary; (2) The effect of soil textural characteristics on the mesoscale pattern of climate in Hungary is pronounced. This effect is commensurable with the effects of relief and atmosphere.

The results suggest that Thornthwaite-based models can be applied not only for climate classification purposes but also for purposes of physical and ecological climatology.

Key-words: soil texture, soil water holding capacity, Thornthwaite, Hungary, hydroclimatic regions, water balance components, energy balance components, evapotranspiration, sensible heat flux, mesoscale

1. Introduction

In all land-surface climate analyses, one of the main concerns is to select the appropriate space/time up-scaling strategy. There are two main approaches. The first approach uses many variables, which are measured in high space/time resolution. The second one uses only a limited number of variables, which have not been determined on as great space/time resolution as the variables from the former case. In the first case the up-scaling algorithm is

very complex (*Running et al.*, 1999). It is based on the use of flux tower measurements, SVAT (Soil-Vegetation-Atmosphere Transfer schemes) model calculations, remote sensing observations, and complex interpolation and extrapolation techniques. In this case, the surface heterogeneity and time resolution is taken into account as detailed as possible.

The second approach is much simpler than the former one. In an extremely simple case, the second approach operates only with monthly mean values of precipitation P and air temperature T . These “classical” approaches are too simple and inappropriate for estimating turbulent heat fluxes. In most cases they use only atmospheric inputs, inputs from other parts of terrestrial climate system (lithosphere, biosphere, hydrosphere, and pedosphere) are rarely used. Some of them serve exclusively for climate classification purposes (*Köppen*, 1900). In some other cases, vegetation is treated only implicitly (*Thornthwaite*, 1948). It should be noted, that in Thornthwaite’s climate classification the soil is also represented. The effect of soil can be explicitly expressed by using soil textural data for determining the soil water holding capacity. Annual and monthly mean values of turbulent heat fluxes can also be estimated knowing the net radiation flux. It has to be mentioned, that temperature and precipitation themselves are poor descriptors of climate, regarding vegetation, the active climatic factors are the water balance components (water surplus, water deficit, potential evapotranspiration, actual evapotranspiration, and soil water storage).

The application of *Thornthwaite* (1948) is common today. So, for instance, *Mintz and Serafini* (1981) and *Mintz and Walker* (1993) used Thornthwaite’s method for estimating the global pattern of monthly mean values of available root zone soil water content and evapotranspiration, respectively. Thornthwaite’s potential evapotranspiration and water balance model is also used for practical purposes: in USA (jointly by the US Weather Bureau (NOAA) and U. S. Department of Agriculture (USDA)) for calculating weekly maps of the crop moisture index, and in Canada (Canadian Climate Center) for calculating weekly maps of soil moisture (see *Mintz and Walker*, 1993).

In Hungary, Thornthwaite’s method was firstly applied by *Bacsó* (1943). It was applied also by *Kakas* (1960). Some other applications of Thornthwaite’s method referred to some smaller catchment areas (*Szesztay*, 1958). Applications on special sites and daily time scale were also done (*Szepesiné*, 1959). A Carpathian Basin application was demonstrated by *Szepesiné* (1966). She also roughly evaluated the energy balance components of some stations. In these calculations, a 300 mm soil water holding capacity of a 1 m deep soil layer was assumed. Thornthwaite’s method in Hungary was applied by *Szász* (1963), too. In contrast to *Szepesiné* (1966), he investigated the effect of soil water holding capacity on water balance components, but only

for some chosen soil types. Today there is no analysis on the subject of soil/climate relationship in Hungary. Moreover, there is no analysis on the effect of the areal distribution of soil texture upon near surface climate. A diagnostic study on soil/climate relationship enables us (1) to improve the classification of near surface climate and (2) to understand and quantify the sensitivity of climate to soil characteristics.

To this end, the aim of this study is threefold: (1) to determine Thornthwaite's hydroclimatic regions in Hungary and to estimate the annual and monthly mean values of energy- and water balance components taking into consideration the soil texture, (2) to analyze the correspondence between Thornthwaite's hydroclimate types and energy- and water balance components, and (3) to evaluate the effect of soil texture on the near surface climate in Hungary. The analysis is performed using a Thornthwaite-based model and climatic data series derived from the period 1901–1950.

2. Method

A water- and energy balance model based on Thornthwaite's climate classification method is used. It is process oriented and as simple as possible. Its advanced feature is that it uses not only atmospheric, but also soil characteristic inputs.

2.1 Input data

Soil water balance calculations are performed for 125 climatic stations. Monthly values of precipitation P and air temperature T are taken from the Climate Atlas of Hungary (Kakas, 1960). These data refer to the period 1901–1950. It has to be noted, that P and T climatic fields (Kakas, 1960) agree well with the newest P and T fields presented in the *Climate Atlas of Hungary* (2000). The energy balance calculations are performed for 40 meteorological stations, where the sunshine duration S_h data were also available. These data refer also to the period 1901–1950 (Dobosi and Takács, 1959). There were two motivations to chose the period 1901–1950: firstly, the consistency between P , T , and S_h data is corresponding, secondly, the most previous studies based on Thornthwaite's method referred to this period (there is a possibility for comparison). Soil texture is determined using high-resolution soil texture map of GIS laboratory of the Research Institute for Soil Science and Agricultural Chemistry of the Hungarian Academy of Sciences. According to the map, there are five main textural classes (in addition to rocky and moor soils). Soil water holding capacity is calculated after Nemes (2003), where the

fitting parameters of *van Genuchten's* (1980) pF curves ($pF = \log_{10}(|\Psi|)$, where Ψ is the soil water potential in cm H₂O) are given for Hungarian soils using the 11 soil textures of the USDA soil classification. The correspondence between the Hungarian and USDA texture classifications is determined by *Filep and Ferencz* (1999), see Eq. (8). The wilting point soil water content is calculated for $pF=4.2$, while the field capacity soil water content is determined for $pF=2.5$. Soil water holding capacity values of rocky (4 stations) and moor (3 stations) soils are taken to be 100 mm (as given in *Thornthwaite*, 1948), because textural effects are fairly site specific on these soils. The wilting point and field capacity soil moisture contents together with soil water holding capacity are presented in *Table 1*.

Table 1. Water holding capacity, wilting point and field capacity soil moisture content of the 5 main textures as determined by *Nemes* (2003)

Main textural classes	Wilting point (mm/m)	Field capacity (mm/m)	Water holding capacity (mm/m)
Sand	15	80	65
Sandy loam	105	274	169
Loam	136	332	196
Clay loam	175	387	212
Clay	272	485	213

2.2 Water balance calculation

Water balance components (potential (PET) and actual (ET) evapotranspiration, water surplus (S), water deficiency (D), and available soil water content relative to water holding capacity (θ)) are estimated by the method of *Thornthwaite* (1948). Calculation procedure, climate classification, and climate symbols are presented in Appendix A.

2.3 Energy balance calculation

Global radiation is parameterized by the method of *Takács* (1971). Net shortwave radiation is estimated using albedo values presented in *Borhidi and Dobosi* (1967). Net long-wave radiation is approximated by its annual mean value for Hungary as given in *Major et al.* (2002). Soil heat flux is parameterized after *Ács et al.* (1986). Sensible heat flux is calculated as the residual term of energy balance equation. Other energy balance components, like the energy of melting and freezing, as well as the energy consumed by assimilation are neglected. Parameterizations used in our calculations are presented in Appendix A.

3. Results

Areal distribution of Thornthwaite's hydroclimate regions (hereafter briefly regions) in Hungary is presented in *Fig. 1*. The regions are obtained assuming texture-dependent soil water holding capacity. In Thornthwaite's climate formulae (representing the hydroclimate regions), only the first and third symbols are indicated. These symbols characterize the humidity or aridity of the climate, briefly the hydroclimate. The map shows the well-known hydroclimate pattern on mesoscale (*Péczely, 1979*): the moderately moist Trans-Danubia and North Hungarian Mountains, as well as the arid lowlands. The humid regions are located in the southwest parts of the country, in the vicinity of Sopron, in the Bakony region, and in the higher lands of Pilis, Börzsöny, Mátra. and Bükk mountains. The greatest part of the Great Hungarian Plane is dry subhumid with little or no water surplus. Moderate winter water surplus prevails in the upper 1 m soil layer at sandy regions also in lowlands (Kiskunság, Nyírség).

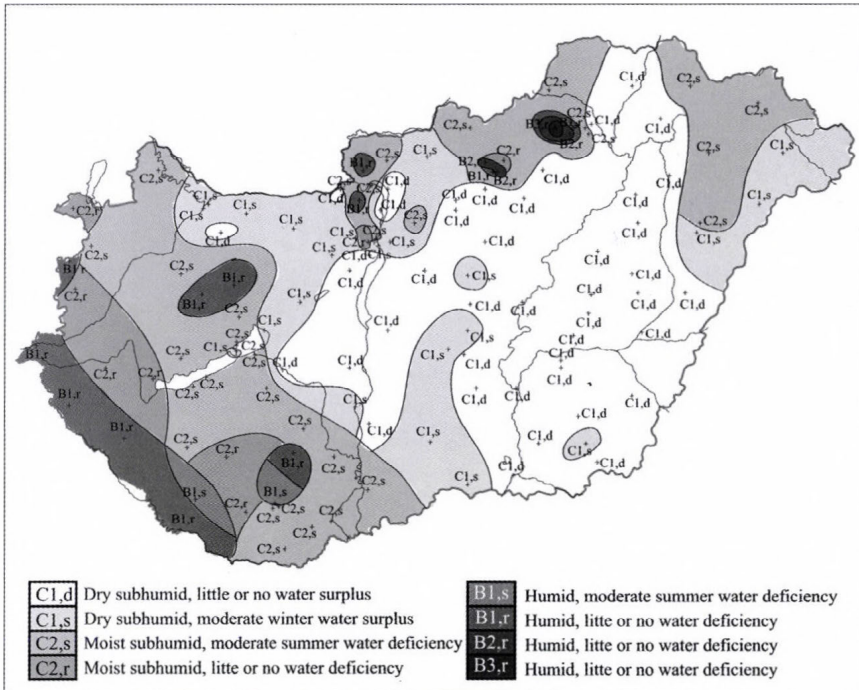


Fig. 1. Areal distribution of Thornthwaite's climate regions in Hungary assuming texture-dependent soil water holding capacity.

The hydroclimate pattern presented is much more detailed as the one presented in *Bacsó* (1943). It has to be noted, that there are also regions, which are climatically different, though their hydroclimate are the same. For instance C1,d hydroclimate exists both in the Szeged region and just below the Mátra and Bükk mountains, although the real climate is different. Similarly, C2,s hydroclimate in the southwest part of the country somewhat differs from the same C2,s hydroclimate in the northeast part of the country. This is, in one respect, caused by the resolution used in the Thonhwaite's method. Namely, the method is constructed for global scale and not for mesoscale applications. Nevertheless, it has to be underlined, that other global scale climate classification methods, as for instance the *Köppen* (1900) method, are less appropriate for Hungarian applications (*Péczely*, 1979). On the other hand, the C2,s identity in the southwest and northeast part of the country is derived from the similar hydroclimate bases.

3.1 Energy and water balance of Hungary

The energy balance components are calculated for 40 stations. The areal distribution of the radiation-, heat-, and water fluxes is illustrated using spline interpolation technique. The areal distribution of global radiation in January, April, July, and October is presented in *Fig. 2*. It is hard to say, whether the results obtained are well enough, but the basic characteristics of the areal distribution of global radiation in July are in accordance with those obtained by *Rimóczi-Paál* (2004). The actual evapotranspiration together with the global radiation is climatically the most important energy balance component. The annual sum of *ET* is presented in *Fig. 3*. *ET* is between 400–600 mm yr⁻¹. The areal distribution of *ET* is similar to that of hydroclimate regions. *ET* is the largest in B1 hydroclimate regions and on the hilly areas, where C2,s hydroclimate is prevailing. In these cases, *ET* is partly determined by the relief. Note, that the model observes relief in terms of temperature (thus, *PET*) and precipitation. The water surplus including runoff is obtained as only the result of these factors.

ET is determined not only by the relief but also by the soil texture. This can be seen comparing areal distributions of *ET* and soil texture (*Várallyay et al.*, 1980). The *ET* distribution is strongly influenced by sandy soils via its low water holding capacity values. The high water permeability combined with low water holding capacity values causes pronounced infiltration in these regions. *ET* is the smallest in regions with sandy soils for example Somogy, Kiskunság, and Nyírség, it amounts only to 400 mm year⁻¹ many times. This effect of sand can also be seen in climatic regions. Namely, in these cases the third symbol is mainly 's', which means temperate winter water surplus for C1 hydroclimates, or temperate summer water deficiency for C2 hydroclimates.

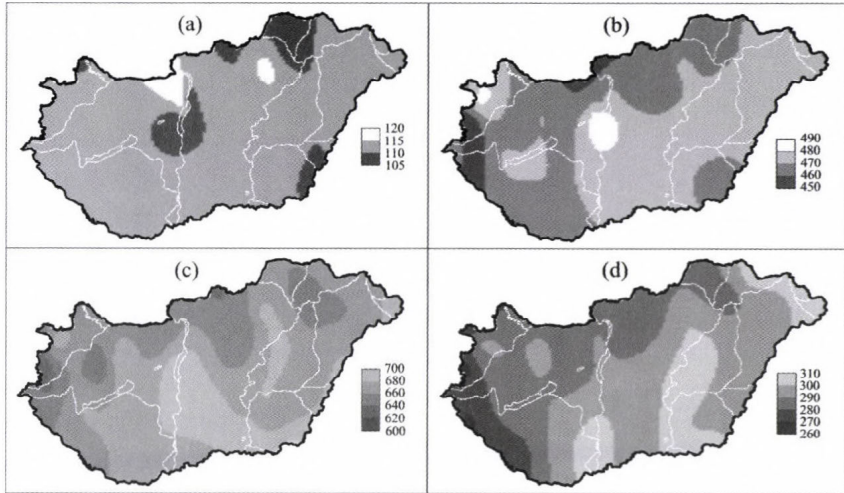


Fig. 2. Areal distribution of global radiation ($\text{MJ m}^{-2} \text{month}^{-1}$) in (a) January, (b) April, (c) July, and (d) October.

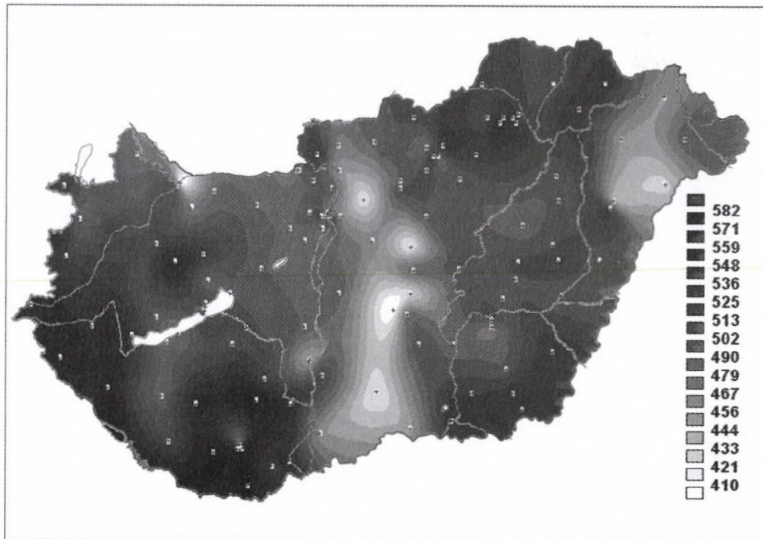


Fig. 3. Areal distribution of annual actual evapotranspiration (mm yr^{-1}).

The areal distribution of *ET* in April, July, and October is presented in Fig. 4. The effect of the relief on *ET* can also be identified in April and October, while in July *ET* is governed mostly by the soil texture. The range of obtained *ET* values is in accordance with those presented in *Climate Atlas of Hungary* (2000) (hereafter briefly *Climate Atlas*), except for the stations with driest sandy soils, where our *ET*-values are much lower. Nevertheless, the areal distributions of *ET* are quite different. In *Climate Atlas*, the effect of relief on *ET* is observable (note that no calculation procedure is presented), but the effect of soil texture on *ET* cannot be seen. For instance, in July there are no *ET* minima in sandy regions of Somogy, Kiskunság, or Nyírség. These *ET* minima regions above sandy areas should be obtained, if soil texture effects were taken into account (e.g., *Irannejad and Shao, 1998*). In spite of this, *ET* in July in Fig. 4 is governed by both the effect of relief and the effect of soil texture. According to our results, *ET* distributions in July and in the year show similarities to the pattern of the soil texture. This is in accordance with many results referring to soil-vegetation-climate interactions (*Pitman, 1994; Pielke, 1998*). It has to be noted, that the results of *Kakas (1960)* obtained by the Thornthwaite's method also differ from our ones, because the effect of soil texture was not taken into account.

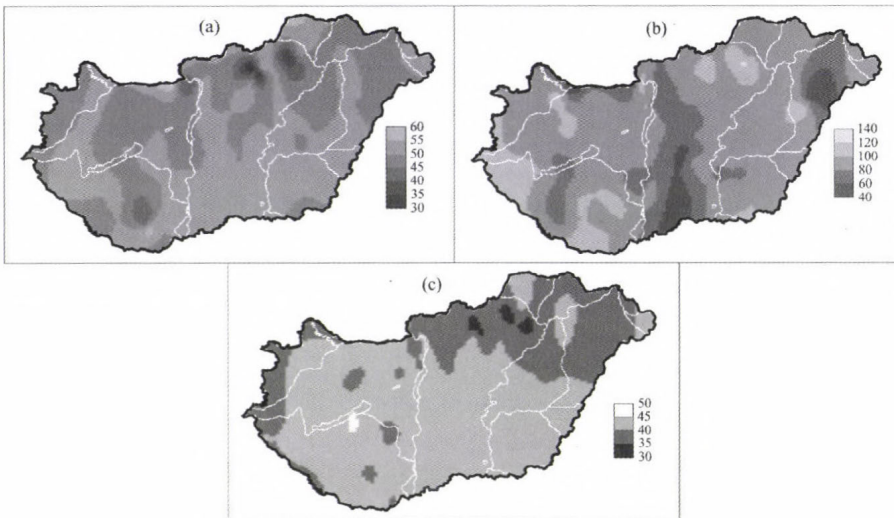


Fig. 4. Areal distribution of actual evapotranspiration (mm month^{-1}) in (a) April, (b) July, and (c) October.

The areal distribution of the relative soil water content available for vegetation (θ , percent of soil water holding capacity in the upper 1 m soil layer) in January, April, July, and October are shown in Fig. 5. In January the most arid regions — the valley of the Tisza and Kőrös rivers show unsaturated soils. In July, θ is about 30 percent in the regions with driest sandy soils. The importance of the soil textural differences can be clearly observed in summer. So, for instance, in summer the sandy regions (Pesti-síkság, Kiskunság, Paks, Külső-Somogy, Nyírség) are dryer than the surrounding areas (e.g., in Debrecen Pallagpuszta, on sand $\theta=44\%$, while in Debrecen, on loam soil $\theta=51\%$, even if there are almost no differences in temperature and precipitation values). In October, the areal distribution of θ is quite uniform in flatlands, only the humid-subhumid part of the country (in SW) and the mountains show high θ values.

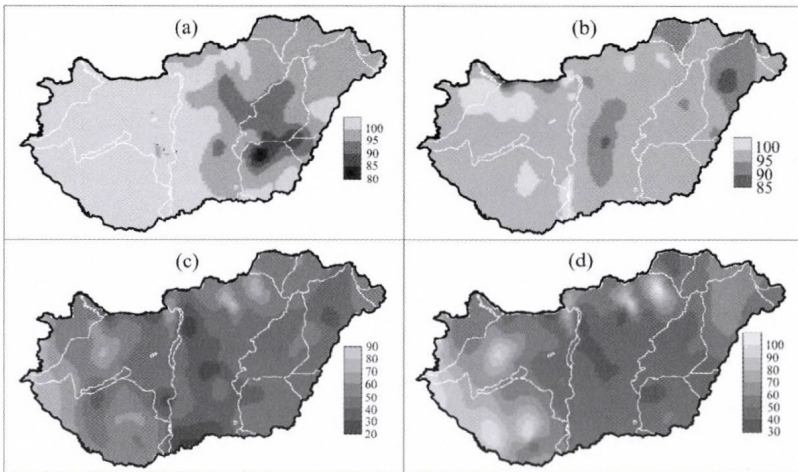


Fig. 5. Areal distribution of the available soil water in percent of soil water holding capacity in (a) January, (b) April, (c) July and (d) October.

The areal distribution of the sensible heat flux H in January, April, July, and October is shown in Fig. 6. The effect of soil texture is most pronounced in the case of H , especially in summer. In July, the sandy areas stand out well with their large H values. In winter, H is negative. In spring and autumn, the largest H values are obtained for elevated areas, mainly due to the inconsistencies in the parameterization of PET and R_g . R_g is parameterized via sunshine duration, while PET is estimated from temperature data. The rate of the temperature change and sunshine duration change is not the same due to growing elevation. Therefore, the difference between R_g and PET increases with elevation causing large H values in spring and autumn.

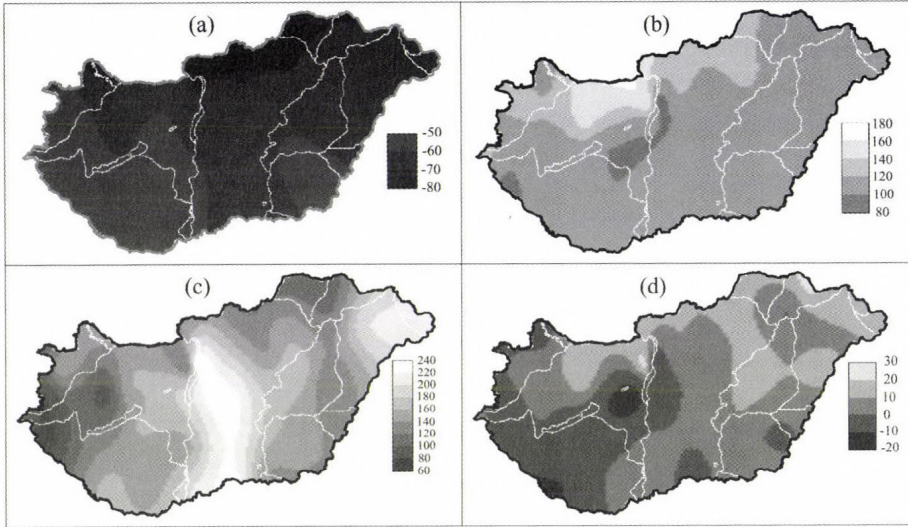


Fig. 6. Areal distribution of sensible heat flux (MJ m^{-2}) in (a) January, (b) April, (c) July, and (d) October.

3.2 Correspondence between Thornthwaite's hydroclimate regions and energy balance components

To understand Thornthwaite's climate classification for Hungary, the correspondence between hydroclimate regions and energy balance components must be known. Thornthwaite's hydroclimate regions for Hungary and the corresponding typical annual values of global radiation, sensible heat flux, actual evapotranspiration, and relative soil water content are presented in Table 2. The values of energy- and water balance components are overlapping, but the average values show definite trends. R_g is somewhat growing towards dry hydroclimates; dryer hydroclimates have larger H . 's' hydroclimates (usually above sand) have larger H than 'd' hydroclimates. The actual evapotranspiration is the largest for 'B1' hydroclimate regions because of the abundant precipitation, and θ is the largest for 'B3' hydroclimate regions due to the low temperature and relatively high amount of precipitation.

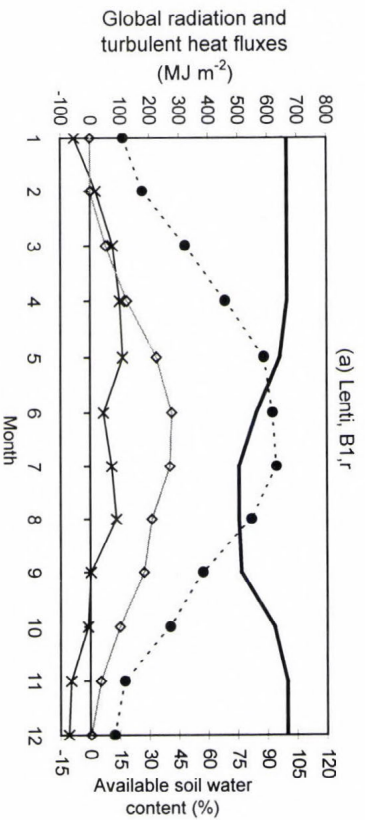
The annual course of energy- and water balance components for each hydroclimate region is shown in Fig. 7. Let us briefly take a look at the figures. The main difference between 'B1, r' and 'B1, s' hydroclimate regions (see Fig. 7a, b) can be noticed in the summer and autumn values of θ . In 'B1, s' hydroclimate, the θ values are lower, while the corresponding H values are larger than in 'B1, r' hydroclimate.

Table 2. Correspondence between the typical annual values of global radiation, sensible heat flux, actual evapotranspiration, and relative soil water in the root zone available for vegetation and the Thornthwaite's climatic regions (1st and 3rd symbols of the climate formula) for Hungary

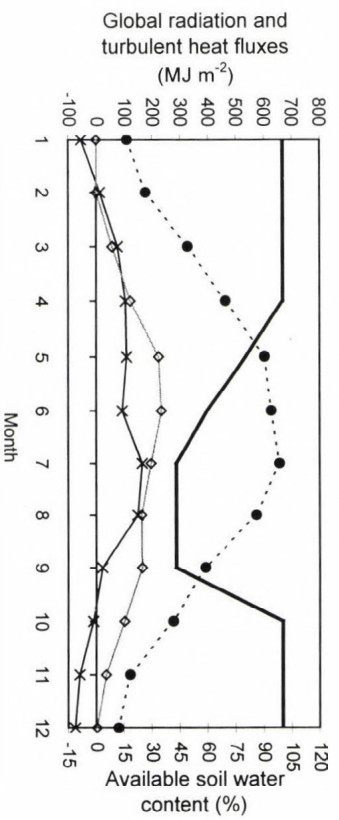
	Global radiation, Gr (MJ m ⁻² yr ⁻¹)	Sensible heat flux, H (MJ m ⁻² yr ⁻¹)	Actual evapotranspiration, ET (mm)	Relative soil water in the root zone, SM (%)	Number of stations for Gr and H	Number of stations for ET and SM
B3, r	-	-	506	95	-	1
B2, r	-	-	518 (497-540)	93 (91-95)	-	2
B1, r	4383 (4294-4516)	465 (316-637)	553 (486-596)	89 (86-96)	4	13
B1, s	4405	543	508 (494-522)	81 (81-82)	1	2
C2, r	4404 (4247-4506)	510 (405-701)	554 (508-580)	85 (82-89)	4	8
C2, s	4472 (4368-4562)	631 (543-764)	507 (426-551)	78 (69-82)	12	34
C1, s	4482 (4433-4524)	692 (575-833)	478 (411-536)	73 (66-78)	6	22
C1, d	4516 (4417-4604)	620 (519-708)	499 (464-524)	72 (66-78)	13	43
Average/ sum	4470	606	507	77	40	125

In humid 'B1, r' and moist subhumid 'C2, r' (Fig. 7c) hydroclimate regions, the annual course of energy- and water balance components are quite similar. However, the latter one is obviously dryer. In 'C2, s' hydroclimate (Fig. 7d), H is already larger than LE in July.

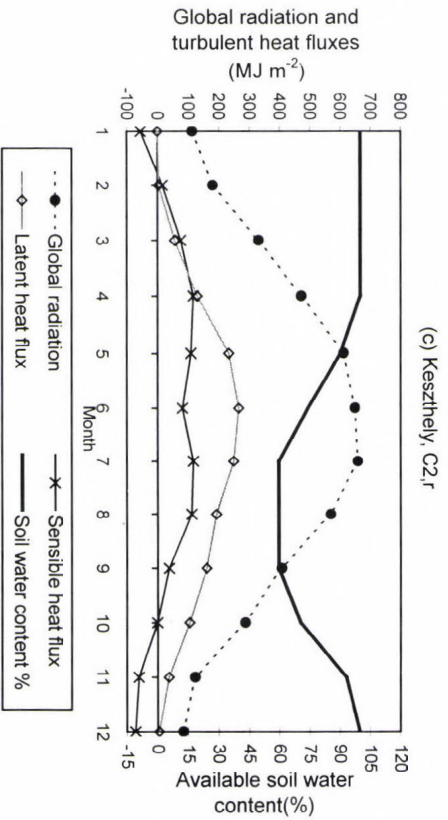
In dry subhumid (C1, Fig. 7e, f) hydroclimates, relative soil water content available for vegetation is small in summer and autumn. In summer, H is quite large exceeding LE in some months. Note, that 'r' and 's' hydroclimates are quite different in terms of annual courses of some variables. This is especially valid for θ . In 's' hydroclimates (usually sandy stations), the changes of θ are quite abrupt in spring and autumn. Also, the summer drought is more pronounced above 's' hydroclimate regions by prevailing larger H values and smaller θ and LE values than in 'r' hydroclimate regions.



(a) Lenti, B1,r



(b) Homokszennygyörgy, B1,s



(c) Keszthely, C2,r

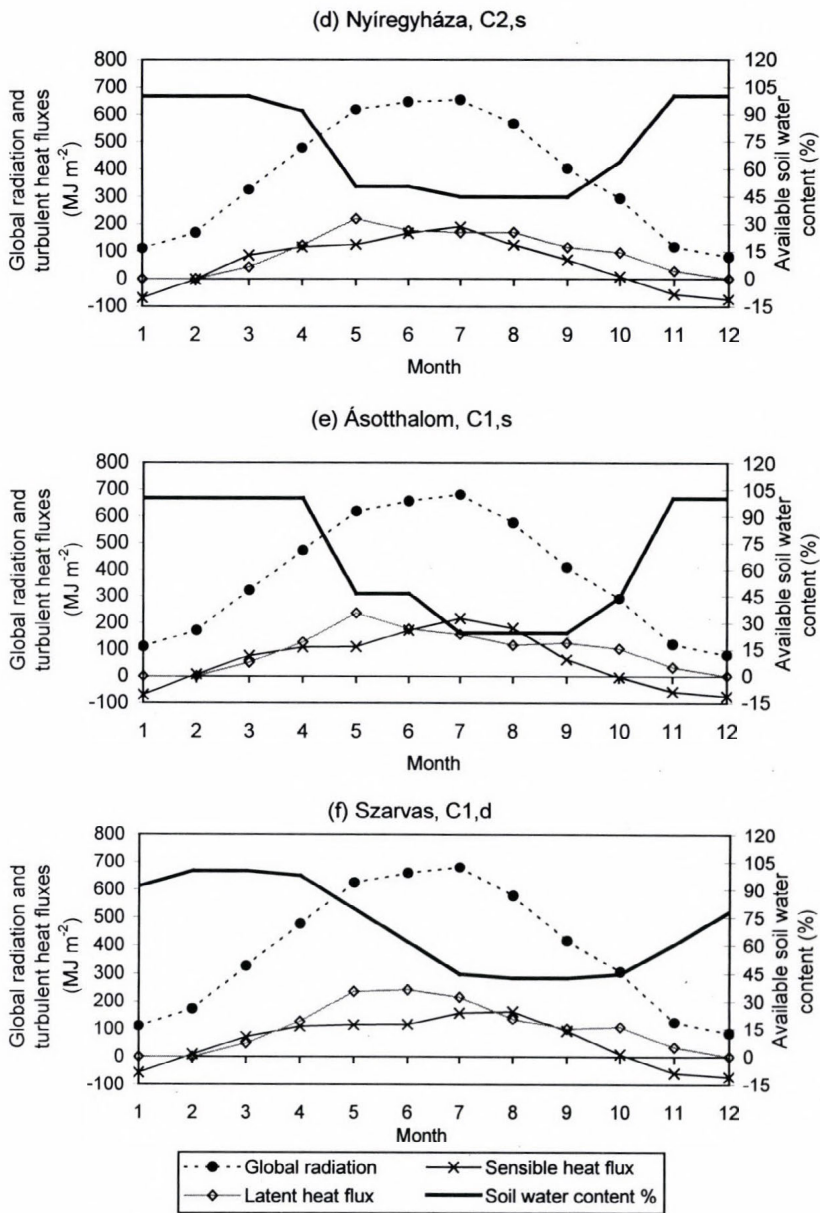


Fig. 7. The annual course of global radiation (MJ m^{-2}), sensible heat flux (MJ m^{-2}), actual evapotranspiration (mm), and available soil water content (percent of soil water holding capacity); (a) Lenti (B1, r); (b) Homokszentgyörgy (B1, s); (c) Keszthely (C2, r); (d) Nyíregyháza (C2, s); (e) Ásotthalom (C1, s); (f) Szarvas (C1, d).

3.3 Effect of soil texture on near surface climate

The effect of soil texture on near surface climate is analyzed comparing Thornthwaite's hydroclimate regions as well as water- and energy balance components obtained by constant and texture-dependent soil water holding capacity. Constant soil water holding capacity is taken to be 100 mm as it is originally made in Thornthwaite's study. The areal distribution of Thornthwaite's hydroclimate regions for 100 mm soil water holding capacity is shown in Fig. 8. Comparing Fig. 1 and Fig. 8, it is striking that the Great Plane is dryer for the texture-dependent case than for the 100 mm case. Soil water holding capacity for the texture-dependent case is generally (except sands) greater than 100 mm; consequently, the winter water surplus for the texture-dependent case is less than the winter water surplus for the 100 mm case. For sandy soils (in this case, water holding capacity is less than 100 mm), the 3rd symbol is unchanged, that is, it remains 's' in both cases.

The effect of soil on near surface climate in terms of energy- and water balance components is illustrated in Fig. 9. The areal distribution of annual differences of ET , θ , and H obtained from texture-dependent and 100 mm soil water holding capacity cases are very similar to the areal distribution of soil texture. The ET - and θ -differences are large for soils of great water holding capacity (loam, clay-loam, and clay). In these cases, the H -differences are small or negative. For sandy soils, which have smaller water holding capacity than 100 mm in the 1 m soil layer, the opposite is true. This is especially obvious for H (see Fig. 9c) in regions of Kiskunság, Nyírség, and Külső-Somogy.

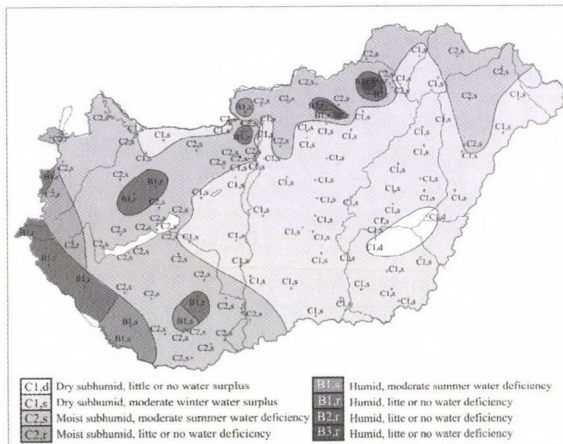


Fig. 8. Areal distribution of Thornthwaite's climate regions in Hungary for constant soil water holding capacity of 100 mm.

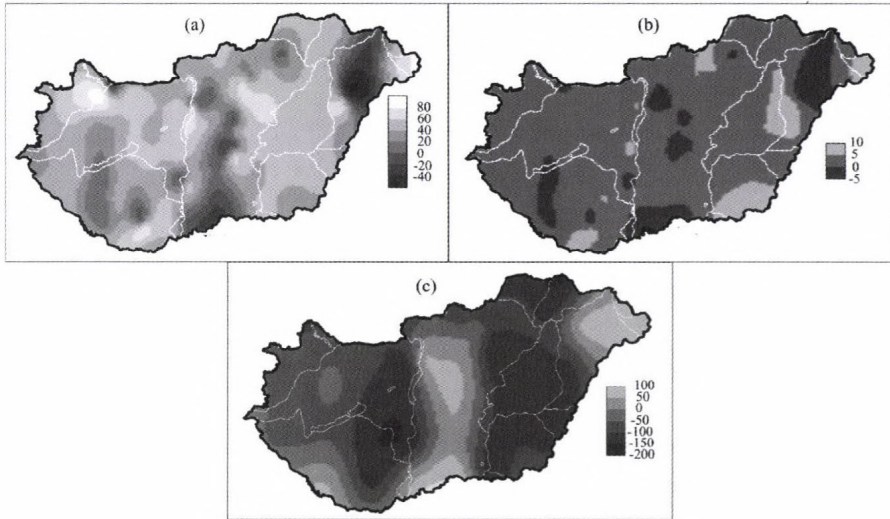


Fig. 9. The annual mean difference between the texture dependent (variable water holding capacity) and texture-independent (constant water holding capacity of 100 mm) (a) actual evapotranspiration (mm), (b) available soil water content (in percent of the soil water holding capacity), (c) sensible heat flux (MJ m^{-2}). Positive values mean that texture-dependent values are greater than constant ones.

4. Conclusions

A Thornthwaite-based water- and energy balance model is constructed to analyze the near surface climate of Hungary and the effect of soil texture on climate. The analysis refers to the period 1901–1950. For each Thornthwaite’s formula the corresponding annual and monthly mean values of energy- and water balance components are determined. The analysis is performed for constant and texture-dependent soil water holding capacities.

The main purpose of this study was to evaluate the effect of soil texture on the near surface climate of Hungary. Our purpose was not to create a new climate classification for Hungary. The only reason for obtaining different areal distribution of Thornthwaite’s hydroclimate regions than in the former studies for Hungary is, that the soil water holding capacity values are estimated on more realistic base considering the soil textural characteristics.

The main results are as follows:

- The method of *Thornthwaite* (1948) is suitable to characterize the areal distribution of the hydroclimate on mesoscale in Hungary. It has to be noted, that other global climate classification methods, as for instance *Köppen’s* method (*Köppen*, 1900), are less appropriate for Hungarian applications.

- The correspondence between the Thornthwaite's climate classification and the climate regions classified with the energy balance components is determined. Dryer hydroclimates (C1) show larger H and lower LE - and θ values than the moist (C2, B) ones. R_g is somewhat growing towards dry hydroclimates.
- The effect of soil texture on the near surface climate of Hungary is analyzed in terms of both the Thornthwaite's climate classification and the energy- and water balance components. The most pronounced effect on the areal distribution of energy- and water balance components is caused by sandy soils, where extreme large H and small ET - and θ values prevail in summer. The effect of soil texture on the near surface climate is proved to be commensurable with the effects of relief and atmosphere.

It is obvious that the Thornthwaite-based model is suitable to characterize the pattern of climate not only on the global scale but also on the mesoscale. Further, it can be easily extended with diagnostic modules based on empirical models for calculating carbon balance components including both vegetation and soil. This extension is one of the goals in our future research work.

Acknowledgements—We express our grateful thanks to the personnel of GIS Laboratory of Research Institute for Soil Science and Agricultural Chemistry of the Hungarian Academy of Sciences for supplying a high resolution soil textural map. We thank also to *Hajnalka Breuer*, who helped in figure presentations.

This study was subsidized by the PhD School Foundation of Earth Sciences of Eötvös Loránd University, by NKFP Foundation, project number NKFP-3A/0006/2002, and by the OTKA Foundation, project number T043695.

APPENDIX A

Parameterization of water balance components

Potential evapotranspiration PET is obtained by

$$PET = 1.6 \left(\frac{L}{12} \right) \left(\frac{N}{30} \right) \left(\frac{10T_a}{I} \right)^a, \quad (\text{A.1})$$

where L is the mean monthly day length in hours, N is the number of days in a month, T_a is the mean monthly air temperature ($^{\circ}\text{C}$), while I is the heat index calculated as

$$I = \sum_{j=1}^{12} \left(\frac{T_a}{.5} \right)^{1.514} \quad (\text{A.2})$$

and

$$a = 6.75 \cdot 10^{-7} I^3 - 7.71 \cdot 10^{-5} I^2 + 1.792 \cdot 10^{-2} I + 0.49239. \quad (\text{A.3})$$

Water balance calculations are performed according to *Mintz and Walker (1993)*. Actual evapotranspiration ET is proportional to PET and soil water in the root zone θ (for climatic tasks root zone is usually taken to be equal to the 1 m deep soil layer).

$$ET_i = \beta_i PET_i, \quad (\text{A.4})$$

where

$$\beta_i = \frac{\theta_{i-1} - \theta_w}{\theta_f - \theta_w}. \quad (\text{A5})$$

θ_{i-1} is the soil moisture content at the end of the previous month $i-1$ (note, that monthly θ values are represented by θ_i values obtained at the end of the actual month), θ_f is the soil moisture content at the field capacity (mm), and θ_w is the soil moisture content at the wilting point (mm). In the dry period ($P < PET$ and $ET < PET$), when ET is less than P , ET is set to be equal to P . Soil water available to vegetation (water supply for vegetation) (θ , mm), water surplus (S , mm) and water deficiency (D , mm) at the i th time step are obtained by

$$\begin{aligned} \theta_i &= \theta_{i-1} + P_i - ET_i, \\ S_i &= \begin{cases} P_i - E_i, & \text{if } \theta_i = \theta_f - \theta_w \\ 0, & \text{if } \theta_i < \theta_f - \theta_w \end{cases}, \\ D_i &= PET_i - ET_i. \end{aligned} \quad (\text{A.6})$$

Climate symbol definitions

Thornthwaite's climate classification method consists of 4 symbols. The 1st and the 3rd symbols are defined by the moisture index (I_m), the 2nd and the 4th symbols are defined by PET . The moisture index is obtained by the annual amounts of S , D , and PET :

$$I_m = I_h - 0.6I_a, \quad (\text{A.7})$$

where

$$I_a = \frac{100D_{year}}{PET_{year}}, \quad I_h = \frac{100S_{year}}{PET_{year}}, \quad (\text{A.8})$$

where I_h is the humidity index and I_a is the aridity index.

Definitions of the 1st and the 3rd symbols of Thornthwaite's climate classification are presented in *Table A 1-2*.

Table A1

Thornthwaite's first symbol	Climate type	I _m
A	Perhumid	> 100
B ₄	Humid	80–100
B ₃	Humid	60–80
B ₂	Humid	40–60
B ₁	Humid	20–40
C ₂	Moist subhumid	0–20
C ₁	Dry subhumid	–20–0
D	Semiarid	–40 – –20
E	Arid	–60 – –40

Table A2

Thornthwaite's third symbol	Moist climates (A, B, C ₂)	Aridity index
r	r: little or no water deficiency	0–16.7
s	s: moderate summer water deficiency	16.7–33.3
w	w: moderate winter water deficiency	16.7–33.3
s ₂	s ₂ : large summer water deficiency	> 33.3
w ₂	w ₂ : large winter water deficiency	> 33.3
	Dry climates (C ₁ , D, E)	Humidity index
d	d: little or no water surplus	0–10
s	s: moderate winter water surplus	10–20
w	w: moderate summer water surplus	10–20
s ₂	s ₂ : large winter water surplus	> 20
w ₂	w ₂ : large summer water surplus	> 20

Parameterization of energy balance components

The monthly amount of global radiation (R_g) is calculated after *Takács* (1971):

$$Rg = A_i S_h + B_i, \quad (\text{A.9})$$

where S_h is the monthly amount of sunshine duration in hours, A_i and B_i are empirical constants given for each month. Soil heat flux is approached by the *Budyko's* formula (see, e.g., *Ács* and *Mihailovic*, 1986):

$$\begin{aligned} G_i &= E_i G_{amp}, \\ G_{amp} &= C T_{amp} + D, \end{aligned} \quad (\text{A.10})$$

where G_i (MJ m^{-2}) is the monthly sum of the soil heat flux in the i th month, G_{amp} (J m^{-2}) and T_{amp} ($^{\circ}\text{C}$) are the annual amplitude of the soil heat flux and monthly mean air temperature, E_i , C , and D are empirical constants.

References

- Ács, F. and Mihailovic, D.T., 1986: The annual course of heat exchange in the soil in Novi Sad (in Hungarian). *Időjárás* 90, 359-364.
- Bacsó, N., 1943: Climate classification of Hungary by Thornthwaite and vegetation geography aspects of climate maps (in Hungarian). *Időjárás* XLVII, 81-91.
- Borhidi, A. and Dobosi, Z., 1967: Areal distribution of surface albedo values in Hungary (in Hungarian). *Időjárás* 71, 150-157.
- Climate Atlas of Hungary*, 2000: Hungarian Meteorological Service, Budapest. ISBN 963 7702 830.
- Dobosi, Z. and Takács, L., 1959: The areal distribution of global radiation in Hungary (in Hungarian). *Időjárás* 63, 82-84.
- Filep, Gy. and Ferencz, G., 1999: Recommendation for improving the accuracy of soil classification on the basis of particle composition (in Hungarian). *Agrokem. Talajtan* 48, 305-317.
- Irannejad, P. and Shao, Y., 1998: Description and validation of the atmosphere-land-surface interaction scheme (ALSIS) with HAPEX and Cabauw data. *Global Planet Change* 19, 87-114.
- Kakas, J., 1960: Yearly amount of potential evapotranspiration, water surplus and water deficit. *Climate Atlas of Hungary*. Akadémiai Kiadó, Budapest. 46/2-4 maps.
- Köppen, W., 1900: Versuch einer Klassifikation der Klimate, vorzugsweise nach ihren Beziehungen zur Pflanzen Geograph. *Zeitschr.* 6, 593-611, 657-679.
- Major, Gy., Nagy, Z., and Tóth, Z., 2002: Climate-energetic studies for Hungary (in Hungarian). *A Budapesti Közgazdaságtudományi és Államgazgatási Egyetem Környezettudományi Intézetének tanulmányai*. 9. 52pp.
- Mintz, Y. and Serafini, Y.V., 1981: Global fields of soil moisture and surface evapotranspiration. *NASA Goddard Flight Center Tech. Memo. 83907, Research Review 1980/1981*, 178-180.
- Mintz, Y. and Walker, G.K., 1993. Global fields of soil moisture and land surface evapotranspiration derived from observed precipitation and surface air temperature. *J. Appl. Meteorol.* 32, 1305-1334.
- Nemes, A., 2003: Multi-scale hydraulic pedotransfer functions for Hungarian soils. *PhD. Dissertation*. Wageningen Universiteit. ISBN 90-5808-804-9. 143 p.
- Péczely, Gy., 1979: Climatology (in Hungarian). Nemzeti Tankönyvkiadó, Budapest. 336 pp.
- Pielke, R.A., 1998: Climate prediction as an initial value problem. *B. Am. Meteorol. Soc.* 79, 2743-2746.
- Pitman, A.J., 1994: Assessing the sensitivity of a land-surface scheme to the parameter values using a single column model. *J. Climate* 7, 1856-1869.
- Rimóczi-Paál, A., 2004: Radiation maps of Hungary. *Időjárás* 108, 195-208.
- Running, S.W., Baldocchi, D.P., Turner, S.T. Gower S.T. Bakwin, P.S., and Hibbard, K.A., 1999: A global terrestrial monitoring network integrating tower fluxes, flask sampling, ecosystem modeling and EOS satellite data. *Remote Sens. Environ.* 70, 108-127.
- Szász, G., 1963: Analysis of the climatic values of water balance components in Hungary (in Hungarian). *Debreceni Agrártudományi Főiskola Tudományos Közleményei*, 49-71.
- Szesztay, K., 1958: Estimation of water balance of catchment areas in Hungary. *Időjárás* 62, 313-328.
- Szepesiné, L.A., 1959: Estimating diurnal values of soil water content using climatic data series (in Hungarian). *Időjárás* 63, 7-18.
- Szepesiné, L.A., 1966: Characteristics of the hydro-climate of the Carpathian-Basin (in Hungarian). *Beszámoló az 1965-ben végzett tudományos kutatásokról*. Országos Meteorológiai Intézet, Budapest, 86-114.
- Takács, M., 1971: Radiation climate of Hungary (in Hungarian). *Szakdolgozat*. ELTE Meteorológiai Tanszék, Budapest.
- Thornthwaite, C.W., 1948. An approach toward a rational classification of climate. *Geogr. Rev.*, XXXVIII., 55-93.
- Várallyay, G., Szűcs, L., Rajkai, K, Zilahy, P. and Murányi, A., 1980: Hydro-physical classification and 1:100 000 scale maps of Hungarian soils (in Hungarian). *Agrokem. Talajtan* 29, 77-112.
- van Genuchten, M.T., 1980. A closed-form equation for predicting the hydraulic conductivity of unsaturated soils. *Soil Sci. Soc. Am. J.* 44, 892-898.

IDŐJÁRÁS

Quarterly Journal of the Hungarian Meteorological Service
Vol. 110, No. 2, April–June 2006, pp. 155–173

Characteristics and synoptic classification of heavy snowfall events in Budapest for the period 1953–2003 **Part II**

Tamás Hirsch and György Babolcsai

Hungarian Meteorological Service
P.O. Box 38, H-1525 Budapest, Hungary; E-mail: hirsch.t@met.hu

(Manuscript received in final form May 31, 2006)

Abstract—In this research, heavy snowfall events (HSEs) in Budapest have been investigated based on a 50-year period. Following the results connected with the main characteristics of HSEs presented in Part I of the paper, the synoptic classification of the cases has been addressed in Part II. Because of the well-known deficiencies of previous synoptic classifications, it was necessary to define our own weather type system. For this purpose, temporally averaged fields of selected meteorological parameters have been used to characterize processes during the whole event, rather than only reflecting the instantaneous state of the atmosphere. In this way, 8 weather types have been defined with quite different characteristics in many aspects. Not surprisingly, most of the HSEs in Budapest have been caused by different types of Mediterranean cyclones. Our classification has also been tested with the help of case studies taken from an independent winter period (2005/2006). Our results show that synoptic-scale processes are strongly connected to heavy precipitation in winter, and that synoptic climatological investigations covering long periods are very useful for operational weather prediction.

Key-words: synoptic climatology, heavy snowfall events, synoptic classification, weather types

1. Introduction

Subjective classification of the weather on synoptical scales dates back to 1944, when *Baur et al.* (1944) created the first classification for Europe and introduced the phrase “Grosswetterlage” (macrosynoptic weather situation). Their 21 weather types described periods, usually lasting for several days, when the spatial distribution of mean sea level pressure remained more or less the same over a large area, e.g. Europe.

Inspired by the development of synoptic meteorology, this first classification was completely renewed by *Hess and Brezowsky* (1952). When defining their macrosynoptic weather types – also known as “HB types” –, they used characteristics of the upper layer of the atmosphere (500 hPa level) as well as the mean sea level pressure field. In the following years, this classification was continually improved (*Hess and Brezowsky*, 1969, 1977; *Gerstengarbe et al.*, 1993), and by now it consists of 29 weather types including the zonal, meridional, and mixed main circulation forms and a clear distinction between cyclonic and anticyclonic situations. Although HB types have been defined focusing on Central Europe (in other words, the location of synoptic-scale weather systems has been considered in relation to this part of the continent), this classification cannot be regarded as very useful for the Carpathian Basin in many cases. The reason for this is that the authors have considered the area of Germany as Central Europe rather than the Carpathian Basin. In this way, some weather situations, which are very important for Hungary, are not included in the HB types. Mediterranean cyclones are good examples of this as they play essential role in developing heavy precipitation events in Hungary, mainly in the winter season.

Another synoptic classification designed specifically for the Carpathian Basin, has been defined by *Péczy* (1957, 1983). This classification has been widely used for many purposes including long-range weather prediction. Like the HB types, it is based on the mean sea level pressure and 500 hPa geopotential height fields. For investigations for the area of Hungary, *Péczy*'s weather types have proved to be much more appropriate than HB types. There are, however, also some deficiencies in this classification. Probably the main problem is that it reveals only a snapshot of the instantaneous state of the atmosphere. Consequently, a situation of a Mediterranean cyclone moving quickly over Hungary can be classified as one of three possible weather types (forward side of a Mediterranean cyclone, cyclone centre over Hungary, or rearward side of a Mediterranean cyclone) depending on the instantaneous location of the cyclone at the time of classification. Another problem is the distinction between anticyclonic and cyclonic types depending on whether the mean sea level pressure is above or below 1015 hPa over the major part of Hungary. Considering the relative value of mean sea level pressure compared to surrounding areas or the curvature of isobars would be a much better choice than using a given absolute value to separate cases.

When investigating heavy precipitation events, the use of the weather types suggested by *Bodolainé* (1983) may be beneficial. The author classified cases that led to considerable flooding on the basin of the river Danube and Tisza. Her 7 weather types were determined using the fields of 4 meteorological parameters, namely mean sea level pressure, 500 hPa

geopotential height, 500/1000 hPa thickness, and precipitable water. Based on these fields, it is possible to consider the surface location of weather systems, the steering flow, the temperature conditions of the lower half of the troposphere, and the location of the warm conveyor belt. The author tried to describe processes usually lasting for several days, rather than giving an instantaneous state of the atmosphere as in former classifications. In spite of this, these weather types describe only those situations when considerable flooding is likely in the basin of the rivers Danube and Tisza. Consequently, these do not include all the heavy precipitation events. Not surprisingly, 25% of our heavy snowfall cases could not be classified as any of the weather types of Bodolainé. *Hirsch* (2001) also faced this problem, and in addition to the 7 existing categories, he introduced a new weather type, which is responsible for most of the heavy snowfall events in Hungary.

Given our experience with other classifications, in this research we have decided to define a new weather type system by classifying only those cases that led to heavy snowfall in Budapest. There are two main methods of synoptic classification: subjective and objective. In the former case, classification is done by comparing fields of selected meteorological parameters and manually determining groups of similar synoptic patterns. In case of objective classification, an algorithm is used to separate cases into different groups, which can be done fully automatically. An example of an automated objective weather type classification was prepared by *Bissoli and Dittmann* (2001), who used advection of air masses at 700 hPa together with cyclonicity and humidity characteristics of the atmosphere to define their types. This method is used operationally at the German Weather Service. Cluster analysis methods have also been used to set up objective weather classification for many purposes. Climate research is one area, where these methods are often used. As an example of the numerous investigations, *Busch and Heimann* (2001) used cluster analysis based weather-type classification to extrapolate results of a regional climate model in time. *Hirsch* (2005) also applied cluster analysis technique to classify weather types causing heavy precipitation events in winter in Hungary.

In this research, however, we have decided to use subjective classification, with the possibility of applying objective methods to the same data set and comparing results of both investigations in the future.

2. Database and method

Research has been carried out on exactly those cases defined in Part I of the paper (*Babolcsai and Hirsch, 2006*). Heavy snowfall events (HSEs) were defined as cases of continuous snowfall producing a snow cover increase exceeding 8 cm at

the station Budapest/Lőrinc. 71 HSEs meeting this definition were found in the 50 winter periods (November to March) between 1953/54 and 2002/03.

Using the NCEP/NCAR Reanalysis dataset available online at <http://www.cdc.noaa.gov/cdc/data.ncep.reanalysis.html>, temporally averaged fields of selected meteorological parameters were produced for the full duration of each event. Data was used in GRIB format; and grid-time averages were calculated for the following parameters:

- mean sea level pressure (MSLP),
- geopotential height at 500 hPa (H500),
- temperature at 850 hPa (T850),
- temperature at 925 hPa (T925),
- relative humidity at 700 hPa (RH700),
- total precipitable water (PW).

These parameters are widely used in operational weather forecasting. MSLP fields provide information about the weather systems near the surface, upper-level processes have been investigated using H500, while temperature conditions of the lower troposphere have been studied based on T850 and T925. Finally, RH700 fields are useful to learn about the main cloud level, while PW fields are essential to identify areas with high water content of the whole atmosphere. Due to temporal averaging, each field contains the whole process during the heavy snowfall event, rather than referring to only one instantaneous state. According to our results presented in Part I, most HSEs lasted for less than 1.5 days, and the highest duration reached 53 hours. Due to these relatively short time intervals, important features will not be filtered out from temporally averaged fields, and these fields are still characteristic of the whole duration of the events. Consequently, it is much more suitable to use time averages than only one field (e.g., the centre time of the event), which obviously does not describe all the processes that occurred during the event and might lead us to draw inappropriate conclusions.

3. Synoptic classification of heavy snowfall events in Budapest

Average fields of all the mentioned parameters for the area of Europe have been considered together in order to divide HSEs into different types. In our subjective classification, most emphasis has been placed on mean sea level pressure, but we have also attempted to find similarities among all the other fields. Using the opportunities provided by subjective classification, the similarities in the structure of the fields were regarded as most important, instead of concentrating on actual grid point values. For two parameters, mean

sea level pressure and 500 hPa height (which are directly linked to synoptic weather systems), the whole European area has been considered. The other meteorological parameters were mainly used to refine the classification, so in these cases we only focused on the region of Central Europe.

In the first step, HSEs were separated based on the mean sea level pressure pattern. Even using only this main parameter, it was possible to make clearly different groups. In the following, the classification has been made finer by analyzing the fields of other selected parameters. Our aim was to find the groups of events with similar patterns for as many parameters as possible. This is obviously not a definitive task, but the use of subjective classification makes it possible to consider different types of separation and to select the best classification among these in a complex way, which would be rather difficult or even impossible to solve using objective methods.

During this process, several sets of weather types were defined manually. Within each set, the difference of the mean characteristics of the weather types was determined. Eventually, the weather-type system was selected, for which the difference between the defined weather types was found to be the largest. The number of weather types was limited by our intention to define groups of HSEs, which are *significantly different* at synoptic and sub-synoptic scales. The following 8 weather types have been separated:

- Secondary low in the forward side of a Northwest European cyclone (NWp),
- Secondary low/frontal wave on the cold front of a cyclone with centre over Denmark (Dp),
- Warm front with frontal waves of a West European cyclone (Wwf),
- Forward side of a West European cyclone (Ww),
- Forward side of a Mediterranean cyclone (Mw),
- Passing Mediterranean cyclone (M),
- Cyclonic curvature on the southern edge of an anticyclone (Nc),
- Cold advection type (C).

Four of the 71 HSEs could not be classified. These were usually a mixture of some of the defined weather types, and it was decided not to include these in any of the categories. The frequency of each type in case of heavy snowfall events and their mean characteristics for Budapest are shown in *Table 1*. The cold advection type (C) is not included in this table, because it led to heavy snowfall only three times during the investigated 50 years, and the macrosynoptic situation was very different in each case. The reason for defining this group in spite of this large difference is the presence of continuous cold advection in all of the three cases, which makes these unique among other HSEs.

According to *Table 1*, the two weather types directly connected to Mediterranean cyclones (M and Mw) had the highest frequency and caused nearly 50% of all HSEs in the investigated 50 years. The number of cases related to the types Dp and Nc was also quite large, whereas the other types led to heavy snowfall in Budapest/Lőrinc less frequently. Clear differences can be seen in the mean characteristics of the defined weather types. When investigating HSEs classified as Pécely's macrosynoptic types, much smaller differences were determined, which shows that our new classification provides a better separation of HSEs. This is obviously due to the fact that Pécely's weather types were defined for all synoptic situations, whereas our classification involves only those cases when heavy snowfall occurred in Budapest/Lőrinc.

Table 1. Average values of the characteristics of heavy snowfall events for each weather type (excluding the C type) and the average of all cases for Budapest/Lőrinc

Characteristics	Weather types							Mean
	NWp	Dp	Wwf	Ww	Mw	M	Nc	
Number of cases	5	9	5	5	16	16	8	71
Duration (h)	20	19	26	15	20	22	24	20
Snow depth increase (cm)	13	16	15	15	13	19	14	15
Snowfall intensity (cm/h)	0.7	1.1	0.6	1.2	0.8	0.9	0.7	0.9
Precipitation intensity (mm/h)	0.6	1.0	0.6	0.9	0.7	0.7	0.5	0.7
Ratio of snow depth incr. to its water equiv. (cm/mm)	1.2	1.1	1.0	1.3	1.2	1.3	1.6	1.3
Mean sea level pressure (hPa)	1017	1001	1011	1005	1015	1003	1012	1009
Height of 500 hPa level (gpm)	5445	5305	5440	5350	5440	5360	5375	5380
Total precipitable water (mm)	12.4	11.2	13.6	11.6	11.9	11.3	9.8	11.6
2 m temperature (°C)	-2.6	-1.4	-3.4	-2.3	-2.3	-2.7	-4.4	-2.5
Temperature at 925 hPa (°C)	-1.4	-1.2	-3.4	-1.4	-3.8	-4.3	-7.9	-3.5
Temperature at 850 hPa (°C)	-2.8	-3.7	-3.6	-2.8	-5.1	-5.8	-8.5	-4.9

In the following, a detailed description of each weather type will be presented. For each type, we show the two fields which were found to be most characteristic of the given weather type. The figures were prepared using the Metview software developed by the European Centre for Medium-Range Weather Forecasts (ECMWF).

Secondary low in the forward side of a Northwest European cyclone (NWp)

Surface: A deep cyclone of large extent with centre west of the British Isles or over the Norwegian Sea and with a secondary low moving over the Adriatic Sea. Large blocking anticyclone over the East European Plain (*Fig. 1*).

500 hPa: Southwesterly flow on the forward side of a large trough over the Atlantic.

PW: Wedge-shaped flow of moist air from the southwest over the region of Hungary. Very dry air over the Alps and northeast of Hungary (*Fig. 1*).

850 hPa: Warm advection from the southwest, warm ridge over Hungary.

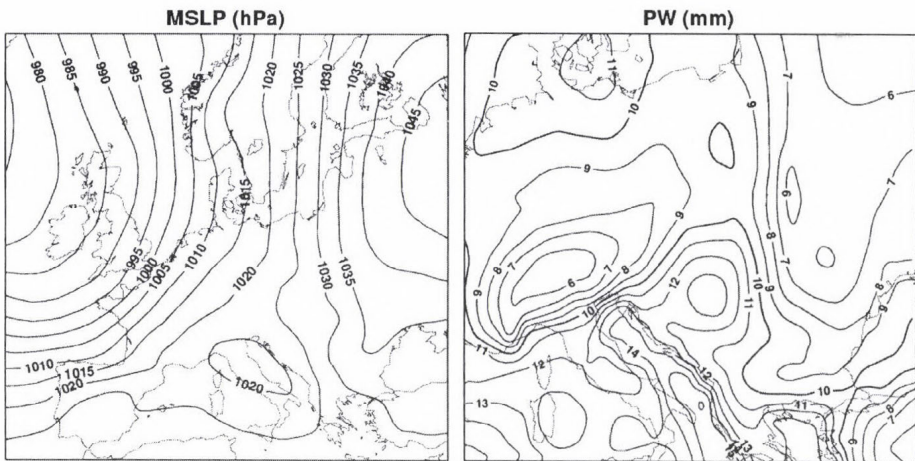


Fig. 1. Characteristic mean sea level pressure (MSLP) and precipitable water (PW) field in case of the NWp type.

Characteristics of HSEs connected to the NWp type:

- smallest snow depth increase,
- low intensity,

- significantly the highest mean sea level pressure,
- highest mean value of 500 hPa geopotential height,
- large values for total precipitable water,
- high temperatures at 925 hPa,
- highest temperatures at 850 hPa,
- characteristic of the middle of the winter period: cases occurred between December 28 and February 6.

Secondary low/frontal wave on the cold front of a cyclone with centre over Denmark (Dp)

Surface: Large low pressure area with a north-south axis reaching down to the North African coast. The cold front of the cyclone with center near Denmark generates a secondary low in the North Adriatic region, which usually moves south of Hungary towards the east, northeast (*Fig. 2*).

500 hPa: The fast propagation of the secondary low is caused by the strong south-westerly flow on the forward side of a trough west of Hungary (*Fig. 2*).

PW: Large gradient along a southwest-northeast axis crossing the northwestern part of Hungary with moist air southeast of this zone. Typical maximum PW values near the Bosphorus.

850 hPa: This field may have rather diverse configurations depending on the location and depth of the trough.

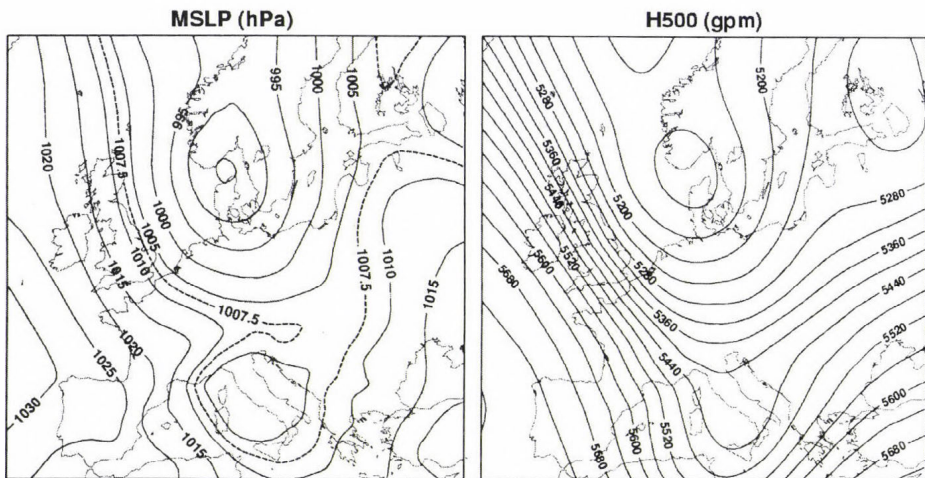


Fig. 2. Characteristic mean sea level pressure (MSLP) and 500 hPa geopotential height (H500) field in case of the Dp type.

Characteristics of HSEs connected to the Dp type:

- highest precipitation intensity (mm/h), intense snow accumulation,
- ratio of snow depth increase to its water equivalent is small,
- lowest mean sea level pressure,
- lowest mean value of 500 hPa geopotential height,
- highest temperature at 2 meter and 925 hPa level,
- often occurs at the beginning of the winter: 5 of the 9 cases were observed in the week between November 28 and December 4.

Warm front with frontal waves of a West European cyclone (Wwf)

Surface: The Carpathian Basin is situated on the forward side of a cyclone stretching from the Atlantic coast towards the middle part of the continent. Meanwhile, a strong anticyclone can be found in North and Northeast Europe, which leads to a strong pressure gradient northeast of Hungary on the border of the two systems. From Scandinavia, cold air is streaming southwards and meets mild airmasses of Atlantic origin resulting in a strong, stationary frontal zone over Central Europe (Fig. 3). Spreitzhofer (1999) also determined a similar weather type, as one of the situations causing heavy snowfall in Austria.

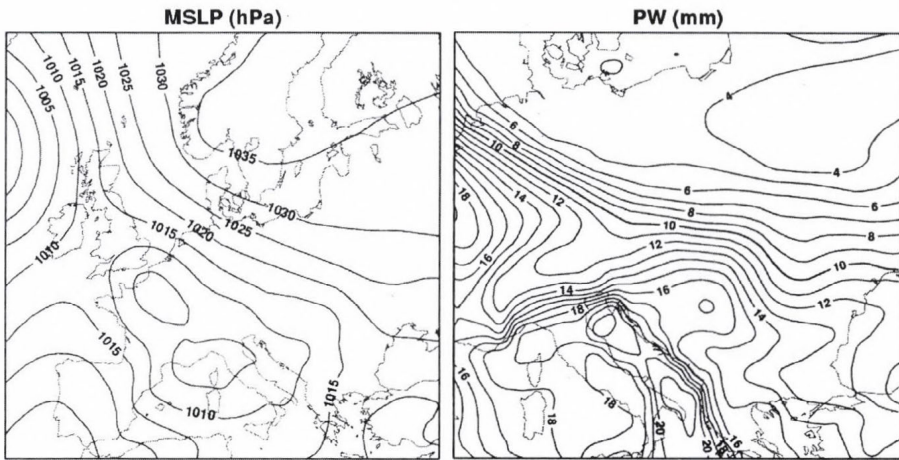


Fig. 3. Characteristic mean sea level pressure (MSLP) and precipitable water (PW) field in case of the Wwf type

500 hPa: Upper level low or trough over East or Northeast Europe.

PW: Extremely strong gradient can be observed over the Carpathian Basin with very dry air to the north and very moist air south of Hungary (Fig. 3).

700 hPa: A band of high relative humidity stretching from west to east over Hungary clearly showing the sign of the sharp frontal zone.

850 hPa: Very strong temperature gradient along the mentioned frontal zone.

Characteristics of HSEs connected to the Wwf type:

- lasts significantly longer, small variability among the cases in their duration,
- least intense snow accumulation,
- ratio of snow depth increase to its water equivalent is the smallest,
- significantly highest total precipitable water,
- temperature below average at 2m, near average at 925 hPa, above average at 850 hPa, which leads to an approximately isothermal temperature profile in the lower troposphere,
- occurred twice in March.

Forward side of a West European cyclone (Ww)

Surface: The weather over the whole of Europe is determined by a huge cyclone centred over the western part of the continent. Hungary is situated on the forward side of the cyclone (*Fig. 4*).

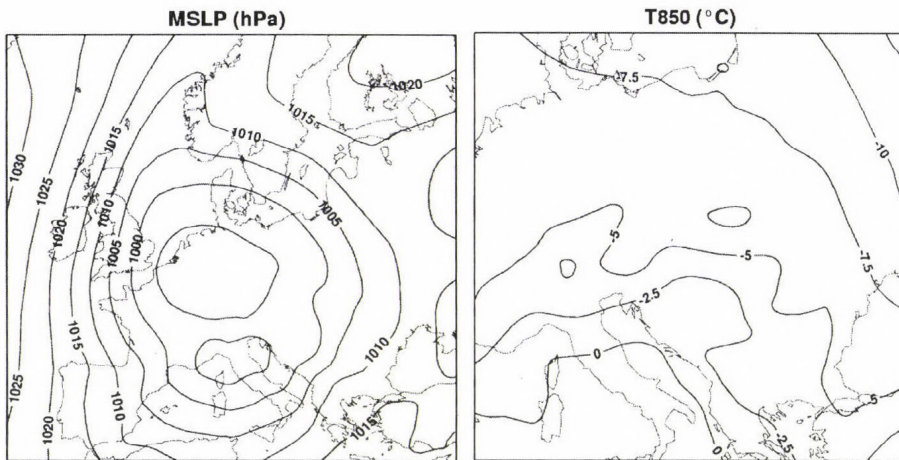


Fig. 4. Characteristic mean sea level pressure (MSLP) and 850 hPa level temperature (T850) field in case of the Ww type.

500 hPa: Strong southwesterly flow over Hungary and mostly closed isolines of geopotential height over Germany.

PW: Moist air from southwest stretching over Hungary.

850 hPa: Clear signs of strong warm air advection (*Fig. 4*).

Characteristics of HSEs connected to the *Ww* type:

- significantly the shortest duration,
- significantly the highest intensity,
- great variability in 500 hPa height,
- high temperature at 925 hPa,
- highest temperature at 850 hPa,
- obviously connected to the end of the winter period: all the 5 cases occurred in February or March.

Forward side of a Mediterranean cyclone (Mw)

Surface: Cyclone with centre over the western or central Mediterranean Sea with Hungary located in the warm sector of the cyclone during the whole event. The low pressure system hardly moves, which is caused by a blocking anticyclone over Northeast Europe or an upper level low directly above the surface cyclone (*Fig. 5*).

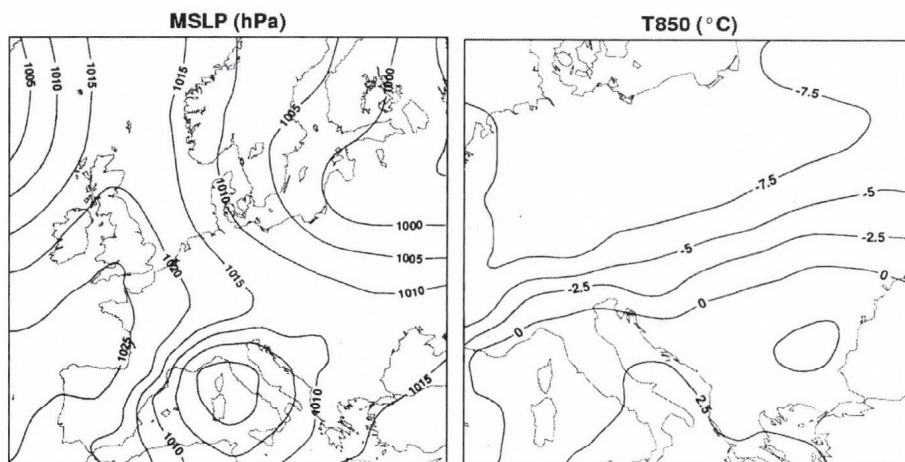


Fig. 5. Characteristic mean sea level pressure (MSLP) and 850 hPa level temperature (T850) field in case of the *Mw* type.

500 hPa: This field shows great variability. Closed isolines of geopotential height over the surface cyclone or southwesterly flow over Hungary on the forward side of a trough.

PW: This shows great variability as well. Most frequently, wedge-shaped flow of moist air from the southwest over the area of Hungary or moist air stretching much further to the northeast of the Carpathian Basin.

850 hPa: A band of strong temperature gradient usually stretching from southwest-west to northeast-east over the Carpathian Basin (Fig. 5).

Characteristics of HSEs connected to the Mw type:

- snow depth increase below average,
- high mean sea level pressure,
- geopotential height at 500 hPa is the highest,
- only 1 of the 16 cases occurred in January.

Passing Mediterranean cyclone (M)

Surface: Cyclone developed in the western part of the Mediterranean Sea moves in the Vb cyclone track over Hungary (van Bebber, 1891) or across the Balcan Peninsula. Usually anticyclone over Northwest or North Europe (Fig. 6).

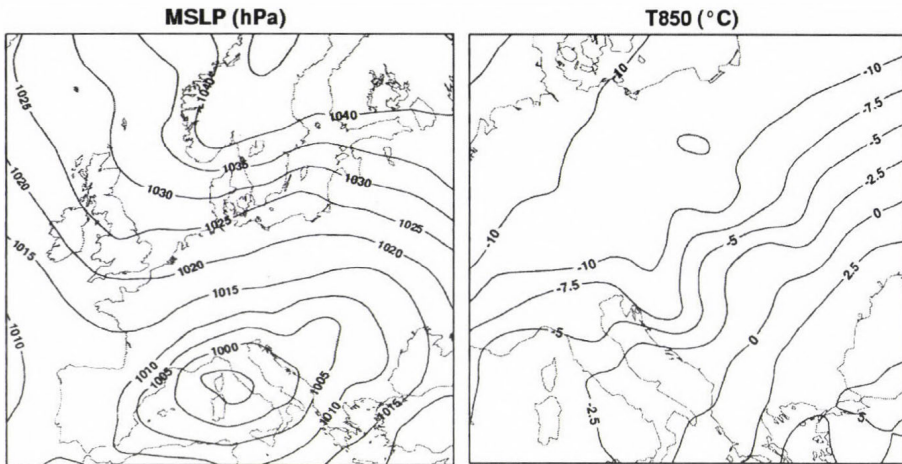


Fig. 6. Characteristic mean sea level pressure (MSLP) and 850 hPa level temperature (T850) field in case of the M type.

500 hPa: Very strong southwesterly flow on the forward side of a trough west of Hungary. Sometimes, closed isolines of geopotential height over North Italy.

PW: Flow of moist air towards the north, northeast over the Carpathian Basin.

850 hPa: Warm advection from the southwest on the forward side of the cyclone, gradually replaced by cold advection from the northeast in the rear of the low pressure system, as it moves eastwards (Fig. 6).

Characteristics of HSEs connected to the M type:

- snow depth increase significantly the largest,
- low mean sea level pressure,
- temperature below average at all levels,
- probability of its occurrence similar in all months except for March.

Cyclonic curvature on the southern edge of an anticyclone (Nc)

Surface: Anticyclone of large extent over Northeast Europe. Cyclone in the central and eastern Mediterraneans. Cyclonic curvature and easterly flow in the Carpathian Basin with convergence in the middle of Hungary, mostly along the Danube (Fig. 7).

500 hPa: Upper level low with variable location from case to case.

PW: Total precipitable water field can be quite variable depending on the distance of the mentioned Mediterranean cyclone.

850 hPa: Cold air of continental origin flows around the Carpathian Mountains and enters Hungary from northeast and northwest at the same time (Fig. 7).

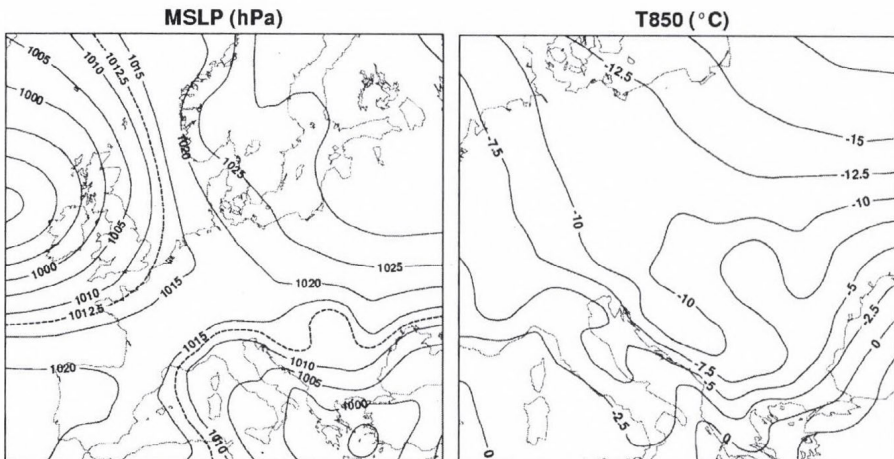


Fig. 7. Characteristic mean sea level pressure (MSLP) and 850 hPa level temperature (T850) field in case of the Nc type.

Characteristics of HSEs connected to the Nc type:

- usually lasts longer, but rather large variability in the duration of the cases,
- precipitation intensity is the smallest,
- significantly the largest ratio of snow depth increase to its water equivalent, but great variability,
- significantly the lowest total precipitable water,
- significantly the lowest temperatures at all levels,
- typical in the middle of the winter period: occurred only between December 12 and February 11.

Cold advection type (C)

There were only 3 examples of continuous cold advection during the whole HSE. Characteristic synoptic scale MSLP and 500 hPa level geopotential height field could not be determined for this type. What makes these cases similar, however, is the following. On the rearward side of a cyclone east, northeast, or southeast of Hungary, there is a cold surge in the Carpathian Basin from the north (*Fig. 8*). An upper level low or trough axis can be found near Hungary. In the averaged total precipitable water field, a pronounced back-bent configuration can be seen (*Fig. 8*). Because of the large differences and the small number of cases, mean characteristics have not been calculated for this type.

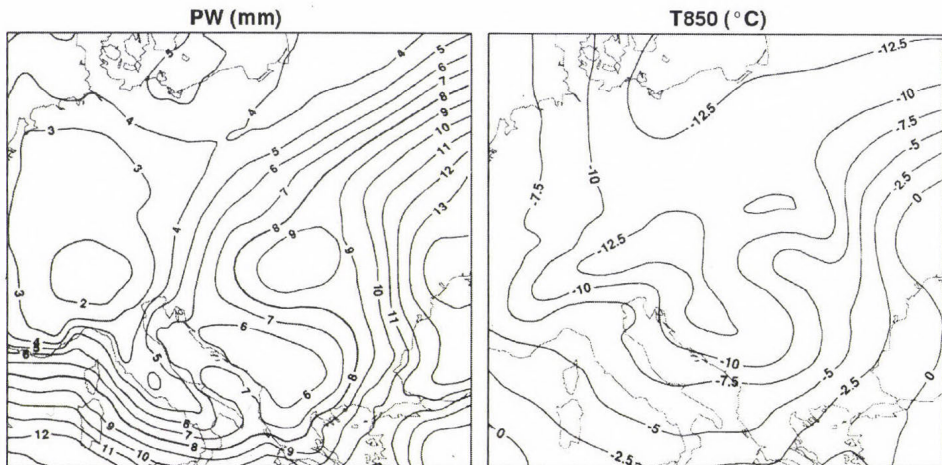


Fig. 8. Characteristic precipitable water (PW) and 850 hPa level temperature (T850) field in case of the C type.

Fig. 9 shows the mean vertical temperature profiles in the lower troposphere for the 7 weather types and for the average of all the 71 HSEs. There are 3 types with inversions (NWp, Dp, Ww). The mean temperature profile for the type Wwf is nearly isothermal. Cases occurring on the southern edge of a North European anticyclone (Nc) are by far the coldest.

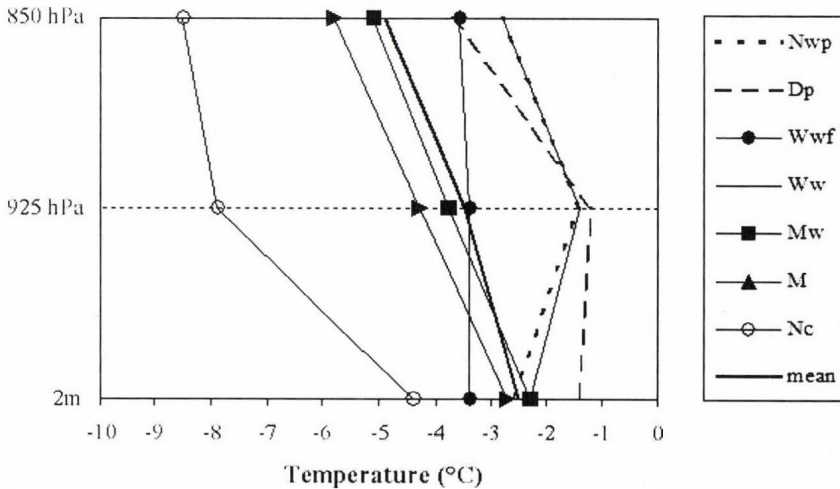


Fig. 9. Mean temperature profile of the different weather types and the average of all cases.

4. Case studies

In the following, some of the heavy snowfall events from the winter period 2005/2006 have been investigated. This winter period was not included in the 50 years (1953–2003), which served as the basis for our subjective classification. In this way, it is possible to analyze whether cases from an independent period can be classified as any of our weather types; this may also be regarded as a test of our classification.

The first case occurred on February 8, 2006 (Fig. 10). The mean sea level pressure field averaged for the duration of the event shows a cyclone with centre over Denmark and a secondary low southwest of Hungary, which clearly corresponds to our Dp type. The mean 500 hPa geopotential height field calculated for this case is also quite similar to the configuration that is characteristic of the Dp type, shown in Fig. 2. None of the HB or the Péczeley types shows this very specific pattern, which is very favorable for heavy snowfall in Budapest, as shown by our research.

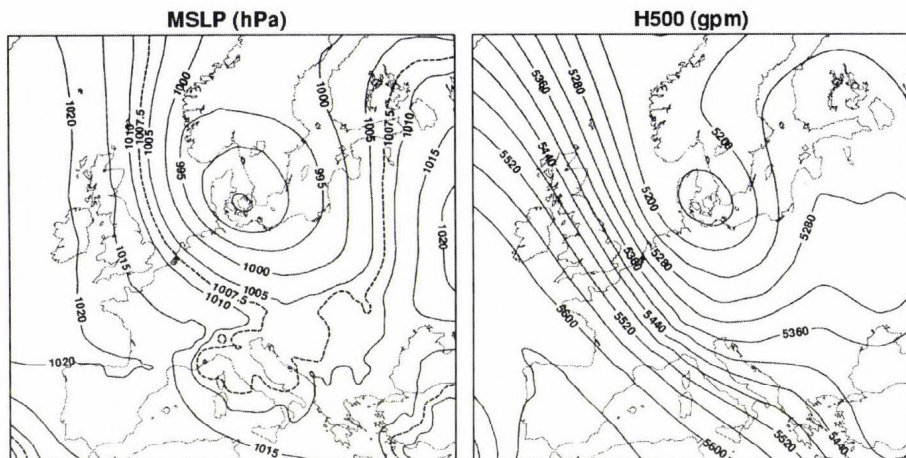


Fig. 10. Mean sea level pressure (MSLP) and 500 hPa geopotential height (H500) field averaged for the period February 8, 2006, 18:00 UTC–February 9, 2006, 06:00 UTC.

The temperature conditions in the lower troposphere were absolutely critical in terms of this heavy snowfall event. During the day, mild air had reached the line of the Danube from the northwest, whereas in eastern Hungary including Budapest, the temperature remained below freezing all day with easterly winds. A very strong temperature gradient reaching nearly 15°C had developed between the northeastern and southwestern part of country (Fig. 11). By the evening, the secondary low over North Italy had moved closer and in its pressure field the wind had turned to east over the whole country again. This stopped mild air over Transdanubia from stretching even more eastwards. Consequently, the type of heavy precipitation connected to the secondary low, was snow in the area of Budapest and eastern Hungary.

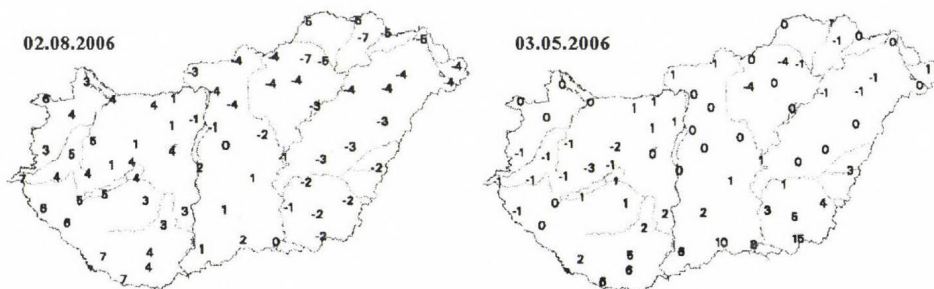


Fig. 11. Distribution of maximum temperature ($^{\circ}\text{C}$) on February 8 and March 5, 2006.

Another heavy snowfall event occurred on March 5, 2006. According to the temporally averaged fields (*Fig. 12*), a Mediterranean cyclone moved from North Italy towards the southern part of the Carpathian basin. At 850 hPa, a very strong temperature gradient of about 12°C can be observed over Hungary with an axis of west, southwest to east, northeast. This case can be obviously classified as our M type, even if the axis of the temperature gradient usually shows a more pronounced southwest-northeast direction than in this particular case. At 2 metres, the mentioned temperature gradient was even stronger than at 850 hPa (*Fig. 11*). Similarly to the earlier case, Budapest was situated on the cold side of the strong frontal zone, resulting in snow instead of rain and sleet, which were observed south of Budapest.

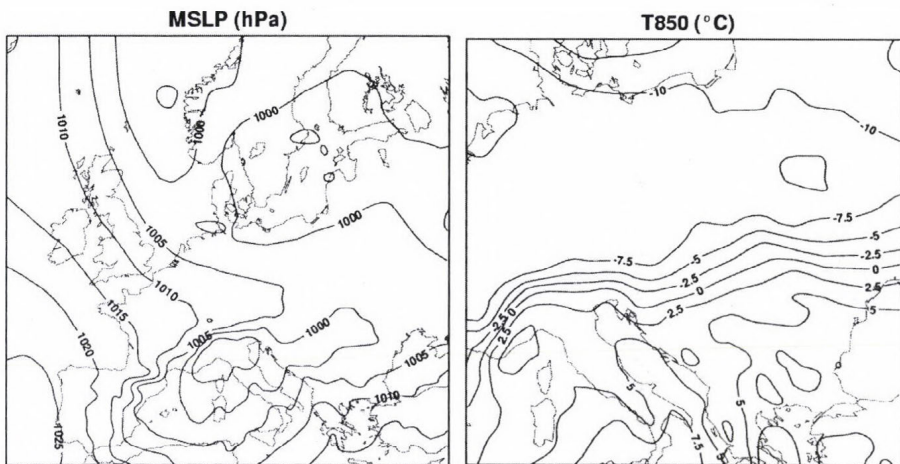


Fig. 12. Mean sea level pressure (MSLP) and 850 hPa level temperature (T850) field averaged for the period March 05, 2006, 06:00 UTC–18:00 UTC.

Mediterranean cyclones are not mentioned in any of the Hess-Brezowsky types. There are HB types where there is a possibility for the existence of Mediterranean cyclones, but these can be located in various places. As our results suggest, however, a specific location and pattern must exist for the development of HSEs in Budapest, which means that HB classification would not be appropriate. Similar statements can be made about Péczely types. Our second case could be classified as “Warm sector of a Mediterranean cyclone” using Péczely’s classification. For this Péczely type, however, very different temperature conditions might occur, most of which would not be suitable for a heavy snowfall event.

5. Conclusion

In this research, heavy snowfall events occurring between 1953 and 2003 in Budapest have been investigated. Using temporally averaged reanalysis fields of selected meteorological parameters, subjective classification of the cases has been carried out. Besides usual parameters such as mean sea level pressure and 500 hPa geopotential height, which make it possible to define the macrosynoptic situation, other parameters have also been used to take into account the temperature conditions of the lower troposphere and processes connected to heavy precipitation.

As the result of this classification, 8 weather types have been defined. Nearly 50% of the cases were caused by two types, which are directly connected to Mediterranean cyclones. Furthermore, at least 3 of our other types also include Mediterranean cyclones. Consequently, it can be stated that the number of heavy snowfall events without some sort of Mediterranean cyclones is quite small.

Our weather types have been found to have quite different mean characteristics. For example, there are types which last longer on average, occur at significantly lower temperatures, produce more intense snowfall than other types or are limited to a particular part of the winter period. The specific characteristics of each type provide much more useful information for operational weather forecasting than the overall characteristics presented in Part I of the paper. Due to the relatively large differences between the types in many aspects, the knowledge of these characteristics can be efficiently used when preparing operational weather forecast, e.g., by modifying numerical weather prediction model results.

Two heavy snowfall events from an independent winter period have also been presented as case studies. Each of these could easily be assigned to one of our weather types, showing the success of our classification. These case studies were also useful to show why other general classifications are less appropriate to apply to very specific cases like heavy snowfall events. As far as future plans are concerned, it would be worth investigating cases when one of our weather types occurred without causing heavy snowfall. This may reveal other processes which are essential to heavy snowfall, but have not so far been considered. Also, developing an objective procedure for identifying our weather types would be extremely useful and could enable a whole series of further investigations in this area.

Acknowledgements—The authors are grateful for the possibility of using NCEP Reanalysis data provided by the NOAA-CIRES ESRL/PSD Climate Diagnostics branch, Boulder, Colorado, USA, from their web site at <http://www.cdc.noaa.gov>. We would also like to thank *David Richardson* (Head of Meteorological Operations Section at ECMWF) for his linguistic revision of this paper.

References

- Babolcsai, Gy. and Hirsch, T.*, 2006: Characteristics and synoptic classification of heavy snowfall events in Budapest for the period 1953–2003. Part I. *Időjárás* 110, 1–13.
- Baur, F., Hess, P., and Nagel, H.*, 1944: *Kalender der Grosswetterlagen Europas 1881–1939*. Bad Homburg v. d. H.
- Bissoli, P. and Dittmann, E.*, 2001: The objective weather type classification of the German Weather Service and its possibilities of application to environmental and meteorological investigations. *Meteorol. Z.* 10, 253–260.
- Bodolainé, J., E.*, 1983: Synoptic conditions of flood waves on the basin of the rivers Danube and Tisza (in Hungarian). Országos Meteorológiai Szolgálat Hivatalos Kiadványai, LVI., Budapest.
- Gerstengarbe, F.W., Werner, P.C., Busold, W., Rüge, U., and Wegener, K.O.*, 1993: : Katalog der Grosswetterlagen Europas nach Paul Hess und Helmuth Brezowsky 1881–1992. 4. vollständig neu bearbeitete Auflage. Ber. Dt. Wetterd. 15 (113).
- Hess, P. and Brezowsky, H.*, 1952: Katalog der Grosswetterlagen Europas. Ber. Dt. Wetterd. in der US-Zone 33.
- Hess, P. and Brezowsky, H.*, 1969: Katalog der Grosswetterlagen Europas. 2. neu bearb. u. erg. Auflage Ber. Dt. Wetterd. 15 (113).
- Hess, P. and Brezowsky, H.*, 1977: Katalog der Grosswetterlagen Europas 1881–1976. 3. verb. u. erg. Aufl. Ber. Dt. Wetterd. 15 (113).
- Hirsch, T.*, 2000: Synoptic-climatological investigation of weather systems causing heavy precipitation in winter in Hungary. *Időjárás* 104, 173–196.
- Hirsch, T.*, 2005: Objective classification of weather systems causing heavy precipitation in winter in Hungary using ERA40 data. ECAM 2005 Conference, September 12–16, 2005, Utrecht, Netherlands.
- Péczely, Gy.*, 1957: Großwetterlagen in Ungarn. Kleinere Veröff. Zentralanst. Meteorol. Budapest.
- Péczely, Gy.*, 1983: Catalogue of the macrosynoptic types for Hungary, 1881–1983 (in Hungarian). Országos Meteorológiai Szolgálat Kisebb Kiadványai, 53, Budapest.
- Spreitzhofer, G.*, 1999: Synoptic classification of severe snowstorms over Austria. *Meteorol. Z. N. F.* 8, 3–15.
- van Bebber, W.J.*, 1891: Die Zugstraßen der barometrischen Minima nach den Bahnenkarten der Deutschen Seewarte für den Zeitraum von 1875–1890. *Meteorol. Z.* 8, 361–366.

IDŐJÁRÁS

Quarterly Journal of the Hungarian Meteorological Service
Vol. 110, No. 2, April–June 2006, pp. 175–182

Short communication

Estimating global radiation using the meteorological input data of crop models

Nándor Fodor

*Research Institute for Soil Science and Agricultural Chemistry
of the Hungarian Academy of Sciences
Herman O. út. 15, H-1022 Budapest, Hungary; E-mail: fodornandor@rissac.hu*

(Manuscript received in final form April 18, 2006)

Abstract—Although not measured at many meteorological stations, the daily global radiation at the earth's surface is a very important component of ecosystem mass and energy processes and so it is in crop modeling. The lack of radiation data is a limitation to the use of crop models. The original and an improved form — that takes precipitation data into account — of the Bristow-Campbell solar radiation estimation method were investigated regarding their performance for providing radiation estimates as crop model input. While the original method did not give acceptable radiation estimations for the used crop model, the improved method did. With an additional site specific calibration, the new method gave so good radiation estimates that the average errors of simulated yield and cumulative evapotranspiration could be decreased below 2% and 0.5%, respectively.

Key-words: radiation estimation, Bristow-Campbell method, crop model, yield prediction

1. Introduction

The primary purpose of crop models is to describe the processes of the very complex atmosphere-soil-plants system using mathematical tools and to simulate them with the help of computers. The ultimate aim of using crop models, however, is to answer questions that otherwise could only be answered by carrying out expensive and time-consuming experiments.

Although not measured at many meteorological stations, the daily global radiation at the earth's surface is a very important component of ecosystem mass and energy processes and so it is in crop modeling. The minimum dataset

for many crop models includes daily solar radiation, minimum and maximum temperature, and precipitation data. Unlike temperature and precipitation, solar radiation is recorded only at few weather stations in the United States (*Ball et al.*, 2004) and so it is in Hungary. This lack of radiation data can be a major limitation to the use of crop models. In order to use crop models, techniques are required to estimate radiation based on other commonly measured meteorological variables such as temperature and precipitation. Thus, crop modelers have a share in developing radiation estimation methods.

There are two groups of methods used to generate radiation data: stochastic generation and empirical relationships (*Liu and Scott*, 2001). Since it was found (*Hayhoe*, 1998) that empirical methods using the common meteorological input data of crop models (temperature and precipitation) provided better estimates than stochastic methods, in this paper only techniques based on empirical relationships are discussed.

There are estimation methods to calculate daily global radiation using different input data: *Angström* (1924), *Szász* (1968), *Hargreaves and Samani* (1982), *Bristow and Campbell* (1984), *Fodor et al.* (2000), *Donatelli and Bellocchi* (2001). The first two methods use the daily sum of sunshine hours, while the others use the daily thermal oscillation. In an earlier study, *Szász's* method was found to give radiation estimates good enough to substitute measured radiation for crop models (*Fodor et al.*, 2003a). However, the applicability of this method is limited, since it uses the daily sum of sunshine hours that is measured at much fewer weather stations than temperature. The focus of this study is to investigate whether the popular and widely used Bristow-Campbell method (*Bristow and Campbell*, 1984) is able to provide global radiation estimates good enough to substitute the measured global radiation in the 4M (*Fodor et al.*, 2003b) crop simulation model.

2. Materials and methods

Recent methods usually determine solar radiation (R) at the earth's surface as a product of extraterrestrial radiation (R_E) and atmospheric transmissivity (A_T):

$$R = R_E \times A_T. \quad (1)$$

Extraterrestrial radiation can be easily calculated for any given day of the year knowing the solar constant and the latitude of the site in question. The estimation methods differ in the way they determine atmospheric transmissivity. The Bristow-Campbell (BC1) method (*Bristow and Campbell*, 1984) calculates the transmissivity as follows:

$$A_T = a \times (1 - \exp(-b \times D^c)), \quad (2)$$

where

D is the smoothed temperature difference ($^{\circ}\text{C}$): $T_{max} - 0.5 \times (T_{min} + T_{min}^{tom})$,

T_{max} is the maximum daily temperature ($^{\circ}\text{C}$),

T_{min} is the minimum daily temperature ($^{\circ}\text{C}$),

T_{min}^{tom} is the minimum daily temperature for tomorrow ($^{\circ}\text{C}$),

a, b, c are parameters, determined by using an optimization method minimizing RMSE (Root Mean Square Error) between the measured and predicted radiation.

We introduce a modified Bristow-Campbell (BC2) method which takes the daily precipitation into account. This method uses the same equations (Eqs. (1)–(2)), but with different parameters for dry and wet (precipitation greater than zero) days:

$$A_T = a_p \times (1 - \exp(-b_p \times D^{cp})), \quad (3)$$

$$A_T = a_{np} \times (1 - \exp(-b_{np} \times D^{cnp})), \quad (4)$$

where $a_p, b_p, c_p, a_{np}, b_{np}, c_{np}$ are parameters, determined by using an optimization method minimizing RMSE between the measured and predicted radiation. The p index stands for days with precipitation, np index stands for days with no precipitation.

The National Weather Service of the USA provides detailed weather data for several hundred sites for the country. Data of 238 weather stations were prepared for crop models and published on the internet: <http://nowlin.css.msu.edu/indexritchie.html>. This database contains the daily global radiation, minimum and maximum temperature, precipitation and relative humidity data from 1961 to 1990. Not every record of the database was used for calibrating both Bristow-Campbell methods but only those years that were similar to the Hungarian ones in certain aspects. A set of agrometeorological characteristics was established (*Table 1*) to find ‘Hungary-like’ data in the database. The ranges in *Table 1* were slightly larger than the Hungarian averages (*Péczely, 1979*) to obtain more years for calibration. Using these conditions 81 years from 15 different sites were selected. These records were used to calibrate both BC1 and BC2 methods.

Based on Eqs. (1) and (2), the ratio of the daily global and the extraterrestrial radiation can be expressed as a 3-parameter function of the smoothed temperature difference:

$$R/R_E = a \times (1 - \exp(-b \times D^c)). \quad (5)$$

Table 1. Agrometeorological characteristics for selecting 'Hungary-like' data from the American database

Characteristic	Minimum	Maximum
Elevation (m)	0	800
Distance from larger body of water (km)	200	-
Annual average temperature (°C)	7.0	12.5
Annual cumulative solar radiation (MJ m ⁻¹ year ⁻¹)	4200	5200
Number of days with precipitation (year ⁻¹)	120	160
Annual cumulative precipitation (mm)	400	850

Three files, each containing two data columns (R/R_E as dependent variable and D as independent variable) were created using the weather data of the fifteen selected stations. One file contained data for every day, one for days with precipitation, and one for days without precipitation. The a , b , c , a_p , b_p , c_p , and a_{np} , b_{np} , c_{np} parameters were determined by nonlinear regression (Marquardt, 1963) using the corresponding data files. After defining the parameters, the BC1 and BC2 methods were validated on an independent dataset. Global radiation was estimated for Budapest/Lőrinc, Hungary, where the measured daily radiation, the minimum and maximum temperature, and precipitation data were available from 1968 to 1987. It was the only available dataset for verifying the estimation methods for Hungary. The adjusted R^2 of the regression, RMSE, bias (mean signed error, MSE), and relative error were used as measures of model performance.

Both measured and simulated radiation were then used in the 4M crop simulation model (Fodor *et al.*, 2003b). First the model was run with measured radiation, then with estimated radiation given as input. The calculated yield and cumulative evapotranspiration outputs were recorded every year between 1968 and 1987. Model results obtained by using measured and estimated radiations were compared. Since global radiation indirectly affects the water balance of the soil, three soil profiles with different water regimes were selected for the model runs. The comparison was carried out for a chernozem, a meadow soil, and a brown forest soil profile (Várallyay *et al.*, 1994), since the vast majority of the agricultural lands in Hungary are covered by these three soil types. The soil data was provided by the Research Institute of Soil Sciences and Agricultural Chemistry (Rajkai *et al.*, 1981; Várallyay, 1987). The required genetic parameters of the maize cultivar were retrieved from the DSSAT database (Tsuji *et al.*, 1994) and were used as crop specific model inputs. Each run started on March 1. The initial water content of the soil profiles was set to 80% of the field capacity.

A recent study on the sensitivity of crop models to the inaccuracies of meteorological observations (Fodor and Kovács, 2005) showed that the uncertainty caused by the systematic errors of the measured global radiation can be up to 5% for the calculated yield. This threshold (acceptance limit) was used for deciding whether the radiation estimation is acceptable for the crop model or not. If the difference between the model results obtained by using estimated radiation and the ones obtained by using measured radiation is less than 5%, the radiation estimation is said to be acceptable.

3. Results and conclusions

After calibrating the BC1 and BC2 methods, both gave fairly good estimates for the independent Hungarian dataset (Table 2). Taking the precipitation into account (BC2) made a slight improvement in radiation estimation. The expected value of error of the estimated daily global radiation is $2.52 \pm 0.078 \text{ MJ m}^{-2}$ and $2.28 \pm 0.070 \text{ MJ m}^{-2}$ ($\alpha=0.05$), for the BC1 and BC2 methods, respectively. Both methods tend to overestimate ($\text{MSE} > 0$) the measured solar radiation (Table 2).

Table 2. Performance indicators of the estimation methods, comparing the measured and estimated radiation for Budapest/Lőrinc, Hungary

Method	R ²	RMSE	MSE*	Relative error**
BC1	0.827	3.390	0.161	0.269
BC2	0.861	3.060	0.351	0.241

* Mean Signed Error – Bias

** In the summer half-year

Note that using the Budapest/Lőrinc dataset for (site specific) calibration, the bias could almost totally be eliminated from the estimation and the absolute error decreased with an additional 10 percent. In this case the expected value of the error of the estimated daily global radiation is $2.34 \pm 0.051 \text{ MJ m}^{-2}$ and $1.97 \pm 0.045 \text{ MJ m}^{-2}$ ($\alpha=0.05$), for the BC1 and BC2 methods, respectively.

The statistical evaluation of the methods can not judge whether the estimated radiation is good enough for crop models or not. Simulation results obtained by using measured and estimated radiation and their evaluation are presented in Fig. 1 and in Table 3 for BC1 and BC2 methods. The simulated cumulative evapotranspiration is not discussed here in detail, since the average error for this model output was way below the acceptance limit 0.7–2.4%, depending on the estimation method and soil type.

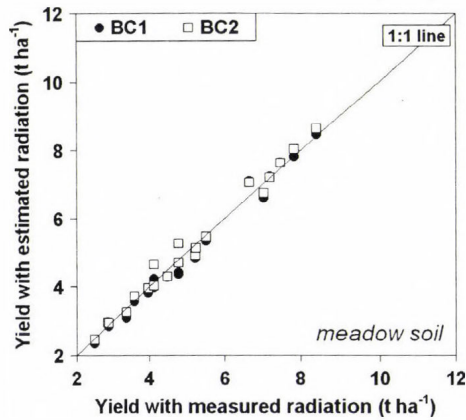
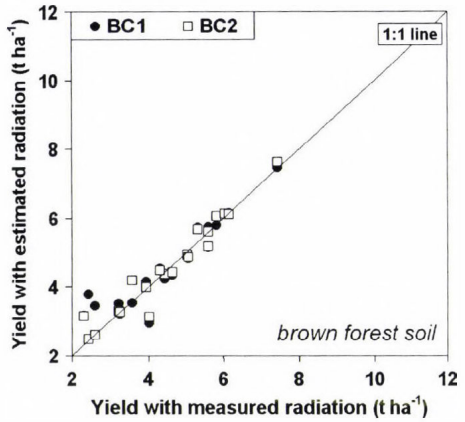
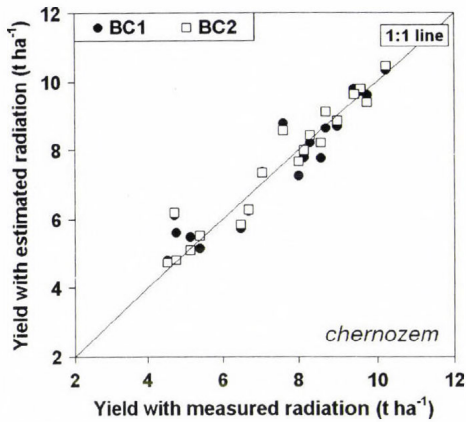


Fig. 1. Maize yields with estimated radiation vs. yields with measured radiation simulated by 4M model for three different soil types, 1968-1987. Solar radiation was estimated with BC1 and BC2 methods.

The year of 1986 is a very interesting example with an extremely high difference between the simulated yields (*Table 3*) on chernozem soil. During the early grain filling period, the (virtual) plants had severe water stress. Because of the slightly higher estimated radiation values, on the August 7 the plants getting the estimated radiation died, while the plants getting the measured radiation barely survived the day. The 23 mm of rain on the very next day (and an other 24 mm 10 days later) was enough for these plants to finish the grain filling period normally.

Apart from this, taking the precipitation data into account enhanced the quality of estimated radiation data as a crop model input (*Table 3*). The average errors of yield prediction using the estimations of the BC2 method were 10-35% smaller than those obtained by using the estimations of the BC1 method. While the BC1 method did not give acceptable radiation estimations for the 4M crop model, the BC2 method did. The average errors of yield prediction were smaller than the 5% acceptance limit for all of the investigated

soil types. With an additional site specific calibration, the new method gave so good radiation estimates that the average errors of simulated yield and cumulative evapotranspiration could be decreased below 2% and 0.5%, respectively.

Table 3. Comparison of simulated maize yields using measured and estimated solar radiation for three different soil types, for the 1968–1987 period. Radiation was estimated with BC1 and BC2 methods

Characteristic	Unit	BC1			BC2		
		Chernozem	Brown forest soil	Meadow soil	Chernozem	Brown forest soil	Meadow soil
Maximum difference	kg ha ⁻¹	4165*	1351	442	4185*	905	520
Average absolute difference	kg ha ⁻¹	655	346	201	543	227	178
SD of the differences	kg ha ⁻¹	905	383	147	922	270	147
Proportion of years with acceptably good radiation estimations	%	50	50	65	75	75	80
Expected value of the difference ($\alpha=0.05$)	%	5.7 ± 2.7	7.7 ± 2.0	4.9 ± 2.0	3.9 ± 2.0	4.5 ± 1.2	3.6 ± 1.5

*In the simulation in 1986, plants died due to severe water stress using estimated radiation

Consequently, an effective solar radiation estimation method could be developed for providing this very important crop model input by using the measured data of some meteorological stations covering Hungary. This method would enable the crop modelers to use their models on the sites where it was impossible beforehand due to a lack of measured solar radiation data. As long as the parameterization is not carried out using a larger Hungarian dataset, we suggest using the improved Bristow-Campbell method (BC2) with the following parameters for estimating radiation for crop models:

Days with precipitation

a=10.966
b= 0.01714
c= 0.34652

Days without precipitation

a=6.514
b=1.03380
c=0.40343

For further study we suggest using the data of more meteorological stations from Hungary to investigate the general applicability of the method for the whole country. Additional details on temperature (more than the daily maximum and minimum) and precipitation data (rainfall intensity, etc.) might be a point of interest in enhancing the estimation method.

Acknowledgement—This paper was supported by the János Bolyai Research Scholarship of the Hungarian Academy of Sciences and the grant of OTKA F046465.

References

- Ångström, A., 1924: Solar and terrestrial radiation. *Q. J. Roy. Meteorol. Soc.* 50, 121-125.
- Ball, R.A., Purcell, L.C., and Carey, S.K., 2004: Evaluation of solar radiation prediction models in North America. *Agron. J.* 96, 391-397.
- Bristow, R.L. and Campbell, G.S., 1984: On the relationship between incoming solar radiation and daily maximum and minimum temperature. *Agr. Forest Meteorol.* 31, 159-166.
- Donatelli, M. and Bellocchi, G., 2001: Estimate of daily global solar radiation: new developments in the software RADEST 3.00. *Proc of the. 2nd International Symposium Modelling Cropping Systems*. Florence, 16-18 July, 2001, Italy.
- Fodor, N., Kovács, G.J., and Ritchie, J.T., 2000: A new solar radiation generator for Hungary. Poster. *ASA-CSA-SSSA, Annual Meetings*. November 5-9, 2000, Minneapolis, MN., Abstract. 23 p.
- Fodor, N., Kovács, G.J., and Pokovai, K., 2003a: Reliability of estimated global radiation for crop model input. *Időjárás* 107, 273-281.
- Fodor, N., Máthéné-G., G., Pokovai, K., and Kovács, G.J., 2003b: 4M - software package for modelling cropping systems. *Eur. J. Agron.* 18, 389-393.
- Fodor, N. and Kovács, G.J., 2005: Sensitivity of crop models to the inaccuracy of meteorological observations. *Phys. Chem. Earth* 30, 165-170.
- Hargreaves, G.H. and Samani, Z.A., 1982: Estimating potential evapotranspiration. *J. Irrig. Drain. Eng.* 108, 225-230.
- Hayhoe, H.N., 1998: Relationship between weather variables in observed and WXGEN generated data series. *Agr. Forest Meteorol.* 90, 203-214.
- Liu, D.L. and Scott, B.J., 2001: Estimation of solar radiation in Australia from rainfall and temperature observations. *Agr. Forest Meteorol.* 106, 41-59.
- Marquardt, D.W., 1963: An algorithm for least-squares estimation of nonlinear parameters. *SIAM J. Appl. Math.* 11, 431-441.
- Péczely, Gy., 1979: Climatology (in Hungarian). Nemzeti Tankönyvkiadó, Budapest.
- Rajkai, K., Várallyay, Gy., Pacsepszki, J.A., and Cserbakov, R.A., 1981: Calculation of water retention data from the texture and the bulk density of soils (in Hungarian). *Agrokem. Talajtan* 30, 409-438.
- Szász, G., 1968: Determining the global radiation by means of calculation (in Hungarian). *Debreceni Agrártudományi Főiskola Tudományos Közleményei* XIV, 239-253.
- Tsuji, G.Y., Uehara, G., and Balas, S., (eds.), 1994: *Decision Support System for Agrotechnology Transfer (DSSAT) v3* Vol. 2. University of Hawaii, Honolulu, Hawaii.
- Várallyay, Gy., 1987: Water regime of soil (in Hungarian). Vol. 2. Appendix 1. *DSc Thesis*. Magyar Tudományos Akadémia, Budapest.
- Várallyay, Gy., Szabó, J., Pásztor, L., and Michéli, E., 1994: SOTER (Soil and Terrain Digital Database) 1:500,000 and its application in Hungary (in Hungarian). *Agrokem. Talajtan* 43, 87-108.

IDŐJÁRÁS

Quarterly Journal of the Hungarian Meteorological Service
Vol. 110, No. 2, April–June 2006, pp. 183–189

Short communication

Comparison of values of the chosen meteorological fields measured at the aerological stations and the values taken from NCEP/NCAR Reanalysis

Jadwiga Woyciechowska and Rafał Bąkowski

Institute of Meteorology and Water Management
61 Podlesna st., 01-673 Warszawa, Cracow Branch, Poland
E-mail: ziwoyocie@cyf-kr.edu.pl

(Manuscript received in final form December 18, 2005)

Abstract—Statistical relationship between the air temperature and the geopotential height of the pressure levels measured at the air-sounding station in Poland and taken from NCEP/NCAR Reanalysis for the same location was analyzed, based on data from the 30-year period of 1974–2003. It was shown, that NCEP/NCAR Reanalysis data is fully complementary and valuable data series, particularly in the lower and middle troposphere, and it can be used along with direct measurements (meteorological sounding of the atmosphere).

Key-words: correlation coefficient, reanalysis, sounding, air temperature, geopotential height

1. Introduction

At present, the climatology benefits more and more from the free atmosphere data when analyzing the fields of meteorological elements. The data are taken from the direct measurements, i.e., aerological soundings of the atmosphere or the mean values of the particular meteorological parameters derived from the geographical grid. These derived products are the result of interpolation. The values in the relevant grid points can vary depending on the algorithm routine used for calculation.

The directly measured radiosounding data have gaps, and it leads to the question on the possibilities of data completing by the measurements from reanalysis calculated for the grid nodes (*Marshall, 2002a,b; Gaffen et al., 2000*). In the scientific centers (e.g., NCAR, NOAA, ECMWF), the reanalysis data products are available for numerous meteorological fields on

various pressure levels in data grids with different spatial and time resolution covering the Earth. Therefore, it seems reasonable to do the comparative analysis of direct measurements and reanalysis (*Marshall, 2002a; Atkinson and Solomon, 2003*).

2. Aims and methods

The aim of the survey was to check the usefulness of the NCEP/NCAR Reanalysis data products in meteorological and climatological studies using free atmosphere data. This objective was fulfilled by the comparison of values of the chosen meteorological fields, measured at the aerological stations: Legionowo, Leba, Wroclaw (where the soundings of the atmosphere are carried out), and the values of the same fields at the same geographical locations taken from NCEP/NCAR Reanalysis. In addition, the results of such study provides an answer on compatibility of the NCAR (in US) Reanalysis and the sounding data from Polish stations. It also could indicate if NCEP/NCAR Reanalysis data are useful as complementary sounding data series.

NCEP/NCAR Reanalysis data, that becomes more and more often used in studies and analysis, the results of which are discussed and presented in numerous papers, deserve recognition. Thereby, some words about the archive should be placed here. NCEP/NCAR Reanalysis is a project to produce analysis of atmospheric fields. NCEP GTS (Global Telecommunications System) data (including pilot-balloons and aircraft) with upper-air observations is the main source of data for reanalysis. The rocket sounding data from national archives in various countries are also provided. Surface marine data from the COADS (Comprehensive Ocean-Atmosphere Data Set) with ships, fixed, drifting, pack-ice buoys, and near-surface data from ocean station are taken. Surface land synoptic data, satellite sounder data, SSM/I (Special Sensing Microwave/Imager) data, and satellite cloud drift winds are used as the source of data in the project as well.

In the preprocessing reanalysis module, data from many different sources are transformed into a BUFR (binary universal format representation) format, and the surface boundary conditions are prepared. The data assimilation module contains the system configuration, analysis scheme (a three-dimensional variational analysis scheme, spectral statistical interpolation), global spectral model, CQC (complex quality control) of rawinsonde data, OIQC (optimal interpolation quality control) of all data, BUFR observation "events" (a spectrum of processing information) files, optimal averaging and periodic forecasts from the reanalysis. The reanalysis gridded fields are the major project results. These fields, depending on the influence of the observational data and the model, are classified into four classes. Class A, the most reliable one, is the class of variables strongly influenced by observations,

B is for variables which are strongly influenced by the model as well. There are no observational data directly affecting the C class fields values. Variables, indicated with D are obtained from climatological values, do not depend on the model. More details on the NCEP/NCAR Reanalysis project can be found in *Kalnay et al. (1996)*. Temperature and geopotential height fields considered in this paper are both class A variables.

Temporal and spatial variations of the geopotential heights and temperatures at the standard WMO pressure levels (850 hPa, 700 hPa, 500 hPa, 300 hPa, 250 hPa, 200 hPa, 150 hPa, 100 hPa, 70 hPa, and 50 hPa) were taken into consideration in our study for two sets of data. One data set consisted of the aerological soundings from TEMP data and the second of the NCEP/NCAR Reanalysis range, respectively. The data covered the period from 1974 to 2003 at 00:00 UTC for both data sets. In spite of representing about 90% of observation, on account of sounding measuring techniques, direct measured sets of atmospheric data for the upper levels in particular are incomplete. NCEP/NCAR Reanalysis data (e.g., monthly means of meteorological elements fields used for the purpose of this paper) are available from the archives for the geographical regular $2.5^\circ \times 2.5^\circ$ gridded surface and represent homogeneous series. For this study needs, the data sets for geographical co-ordinates of aerological stations were interpolated from the nearest grid nodes. The values of air temperature and geopotential height for Leba, Legionowo, and Wroclaw were interpolated from the nearest grid points on the given pressure level using two methods: first order linear interpolation and inverse squared weighted interpolation. In both cases the calculations were made under the assumption that meteorological fields, as the continuous function of longitude and latitude, do not have the local extremes in the considered intervals (in longitude and latitude). In addition, the constraint was set that there is no extreme inside the given window (i.e., the convex hull created by the mentioned four points).

Since the Earth's radius a is far larger than the spatial grid resolution, and the angular distance between the station and the nearest gridpoint in longitude or latitude is less than 2.5° , the Earth's curvature can be neglected, and the linear distance from the point at the height of h over the station to the grid node at the same height can be expressed as

$$\sqrt{(a+h)^2 \sin^2(\Delta\varphi) + b^2 \sin^2(\Delta\lambda)}, \quad (1)$$

where the $(a+h)\sin(\Delta\varphi)$, $b\sin(\Delta\lambda)$ terms are for meridional and zonal distances, respectively, $\Delta\varphi$ and $\Delta\lambda$ are the angular distances (in latitude and longitude) between the station and the given grid node. a is the distance between the desired point (over the station) and axis of the Earth's, assumed the same for all relevant points (i.e., station and nearest neighbour(s)).

The sine of a small angle is (approximately) the angle itself measured in radians (e.g., $25^\circ = 0.4363\text{rad}$, $\sin(0.4363\text{rad}) = 0.4362$). Thus the interpolation can be simplified significantly. The result of the first order linear interpolation and the result of the inverse squared weighted interpolation do not vary. Finally, two series of monthly means for analysis and comparison were archived one is based on direct aerodynamical sounding at 00:00 UTC, the other is founded on interpolation (of NCEP/NCAR Reanalysis) and averaged over the days for which the data from aerodynamical/aerological soundings (at 00:00 UTC) were available.

3. Results

Analyzing statistical relationship between the direct measured air temperature in the free air and temperature based on NCEP/NCAR Reanalysis in geographical co-ordinates of the particular sounding station revealed the strong positive correlation between the series, especially below the 500 hPa pressure level (Figs. 1a, 2a, and 3a). The largest values of the linear correlation coefficient r are observed in the lower troposphere. At the 850 hPa pressure level the values of coefficient r are greater than 0.9 (values of coefficient r were obtained at standard 95% confidence level) for all months of the year except for January over Leba ($r=0.86$). Higher, at the 700 hPa isobaric surface the r values are higher than 0.9, except for May over Wroclaw ($r=0.86$).

Above, in the middle troposphere (500 hPa) the values of r are lower in general, but still greater than 0.9, except for August over Wroclaw ($r=0.86$) and August over Leba ($r=0.88$).

In the upper troposphere (at the 300 hPa and 250 hPa isobaric surfaces) the correlation decreases. The correlation coefficient r drops to 0.4 for certain months (Wroclaw in June, Leba in August and September). The seasonal dependence of correlation is obvious in this part of troposphere with the lowest values of correlation coefficient r in summer and autumn on the 250 hPa level, and in winter and spring on the 300 hPa level. However, such regularity is not observed in Wroclaw. It must be stressed, that the discussed layer is a zone of the strongest winds (highest wind speed) and jet streams (reaching 250 hPa), above Poland in early spring and summer. Furthermore, due to the significant seasonal and daily variations in the tropopause, the largest variations in values of meteorological elements are observed in the UTLS (Upper Troposphere-Lower Stratosphere).

At high altitudes in the lower stratosphere the direct measurements and NCEP/NCAR Reanalysis are more related again. Nevertheless, the obtained correlation coefficient r is as low as 0.1 (in July over Leba). Due to the technique of direct measuring at the higher levels, the results from the air soundings are more unreliable (high error), and the data are more often unavailable.

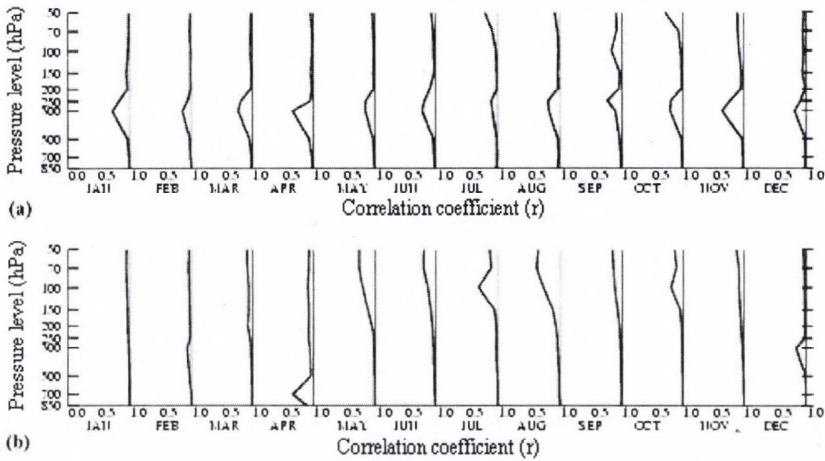


Fig. 1. Values of coefficient r of linear correlation at the standard WMO pressure levels, for each months of the year, between the air temperature (a) and geopotential height (b), measured at the aerological station in Warszawa and taken from NCEP/NCAR Reanalysis, respectively.

The relationship between the geopotential heights of the pressure levels over the air-sounding station and those at the same geographical location taken from NCEP/NCAR Reanalysis is more significant (Figs. 1b, 2b, and 3b). The values of coefficient r of linear correlation are greater than 0.9 in the lower and middle troposphere in all months of the year, except for April (Warszawa, 700 hPa, $r=0.7$) and for August (Leba, 500 hPa, $r=0.6$).

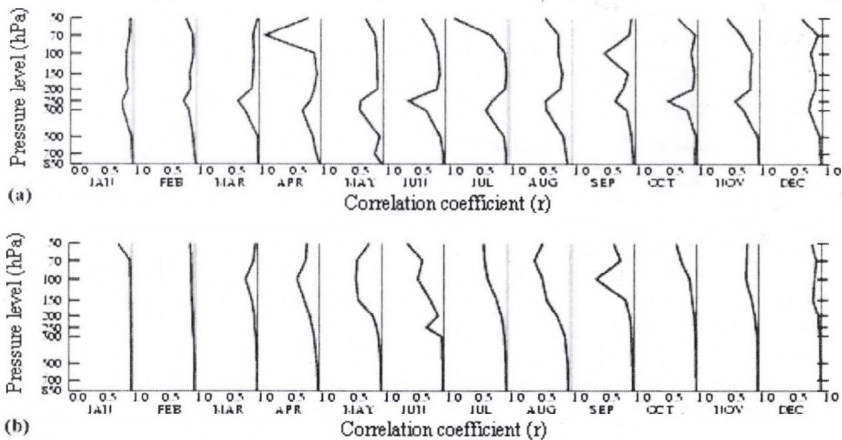


Fig. 2. Values of coefficient r of linear correlation at the standard WMO pressure levels, for each months of the year, between the air temperature (a) and geopotential height (b), measured at the aerological station in Wroclaw and taken from NCEP/NCAR Reanalysis, respectively.

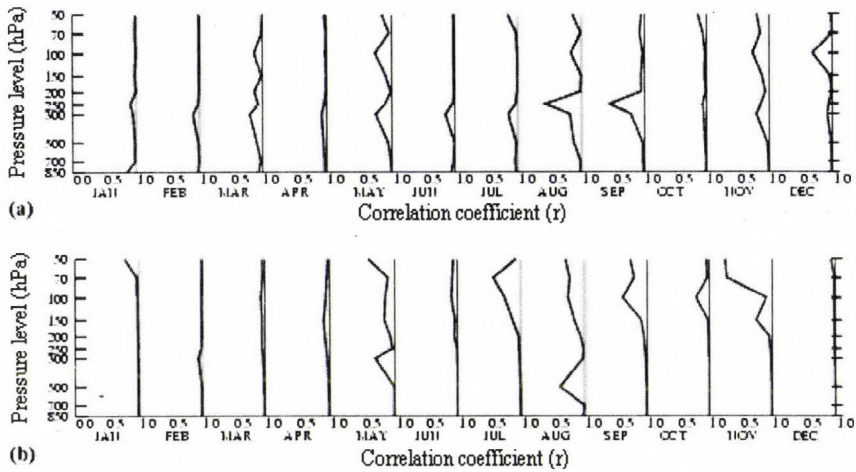


Fig. 3. Values of coefficient r of linear correlation at the standard WMO pressure levels, for each months of the year, between the air temperature (a) and geopotential height (b), measured at the aerological station in Leba and taken from NCEP/NCAR Reanalysis, respectively.

Strong positive correlation is apparent up to the 200 hPa isobaric level above which, in the lower stratosphere especially, the values of coefficient r drop into the range of 0.7–0.8, however, in November (Leba, $r=0.2$) and June (Warszawa, $r=0.4$), as it was mentioned earlier, at such high-altitude the measured data is highly unreliable.

4. Summary

Based on the results shown in the previous paragraph, the NCEP/NCAR Reanalysis and direct aerological measurements provided by Polish meteorological stations are strongly positive correlated in the lower and middle troposphere (i.e., in the region bounded by pressure levels 500 hPa at the top and 850 hPa at the bottom). This is valid for both of the air temperature and geopotential heights of isobaric surfaces.

In the zone between the 300 hPa and 250 hPa level, where strong winds (often jet streams) influenced by baric gradients are observed, distinct differences, especially in the temperature field, are noticed. Above 250 hPa, the linear correlation coefficient r reaches values again close to 1. However, due to the methodology of the direct measurements, data from aerological sounding in this part of the atmosphere (low stratosphere) are highly unreliable. Also, the frequency of correctly performed measurements decreases with height.

To examine pairs of time series (e.g., temperature or geopotential heights), simple statistical methods are usually used: the standard deviation, that is the best measure of spread or root mean square, whenever the relationship between variables is analyzed. Following other authors (e.g., Poccard *et al.*, 2000; Atkinson *et al.* 2003), for our study purpose a correlation method was involved. The simple linear correlation is not affected by systematic offset and gives a good idea of how two time series of variables are coherent. The non-linear correlation, based on polynomial approach of degree more than 1, requiring more difficult calculation, can be used in statistical examination. However, more sophisticated methods would be neither reliable nor efficient enough in our study case.

Finally, the presented analysis leads to the conclusion that NCEP/NCAR Reanalysis data is fully complementary and valuable data series, particularly in the lower and middle troposphere and can be used along with direct measurements (meteorological sounding of the atmosphere).

Analysis for the meteorological fields of humidity and u , v wind components are in preparation.

Acknowledgements—Reanalysis data was provided by the NOAA-CIRES Climate Diagnostics Center, Boulder, Colorado, USA, from their web site at <http://www.cdc.noaa.gov/>. This study was accomplished with the financial support of the Polish State Committee for Scientific Research under the Grant 618/E-217/SPB/COST/KN/DWM80/2005-2006.

References

- Atkinson, D.E. and Solomon, S.M., 2003: Comparison of NCEP/NCAR Reanalyses Data with Station Data for the Circum-Polar Coastal Regime (2003 – 7POLARCLIM). *AMS Conference on Polar Meteorology and Oceanography and Joint Symposium on High-Latitude Climate Variations*, 7 [np].
- Gaffen, D.J., Sargent, M.A., Habermann, R.E, and Lazante, J.R., 2000: Sensitivity of tropospheric and stratospheric temperature trends to radiosonde data quality. *J. Climate* 13, 1776-1796.
- Poccard, I., Janicot, S., and Camberlin, P., 2000: Comparison of rainfall structures between NCEP/NCAR reanalyses and observed data over tropical Africa. *Clim. Dynam.* 16, 897-915.
- Kalnay, E., Kanamitsu, M., Kistler, R., Collins, W., Deaven, D., Gandin, L., Iredell, M., Saha, S., White, G., Woollen, J., Zhu, Y., Chelliah, M., Ebisuzaki, W., Higgins, W., Janowiak, J., Mo, K. C., Ropelewski, C., Wang, J., Leetmaa, A., Reynolds, R., Jenne, R., and Joseph, D., 1996: The NCEP/NCAR 40-Year Reanalysis Project. *B. Am. Meteorol. Soc.* 77, 437-471.
- Marshall, G.J., 2002a: Analysis of recent circulation and thermal advection change in the northern Antarctic Peninsula. *Int. J. Climatol.* 22, 1557-1567.
- Marshall, G.J., 2002b: Trends in antarctic geopotential height and temperature: A comparison between radiosonde and NCEP-NCAR. *J. Climate* 15, 659-674.

Obituary — Kirill Kondratyev (1920–2006)

“Hereby we grievously inform you about the premature decease of Kirill Kondratyev that occurred on the 1st of May, 2006. Our friend and colleague, Kirill Kondratyev was a famous scientist, full Academician of the Russian Academy of Sciences, an acknowledged expert in the area of climate and environment. He is the author of more than one thousand papers in the most prestigious journals as well as of more than hundred monographs and textbooks published in the former USSR, Russia and abroad.

The area of scientific interests of Kirill Kondratyev was extremely broad encompassing the theory of transfer of thermal radiation through the atmosphere, greenhouse effect, natural and man-induced disasters and catastrophes, remote sensing of environment and global climate change.

Kirill Kondratyev was the honorary member of the American Meteorological Society, Royal Meteorological Society of the Great Britain, Academy of Natural Sciences “Leopoldina” (Germany), foreign member of the American Academy of Arts and Sciences, member of the International Astronautic Academy, honorary Doctor of Sciences of the Universities of Lille (France), Budapest (Hungary) and Athens (Greece). During many years he was Editor-in-Chief of the Russian Journal “Earth Observations and Remote Sensing”, he also was member of the editorial board of such journals as “Optics of the atmosphere and ocean”, “Proceedings of the Russian Geographical Society”, “Meteorology and Atmospheric Physics” (Austria), “Időjárás” (Hungary), “Il Nuovo Cimento C” (Italy), “Atmosfera” (México), “Energy and Environment” (Great Britain).

For his salient scientific attainments Kirill Kondratyev was awarded with the State Award of the USSR, and decorated with a Gold Medal by the World Meteorological Organization, the Simons Gold Medal by the Royal Meteorological Society of the Great Britain.

During first 30 years of his scientific career, Kirill Kondratyev was insolubly related to the State University of Leningrad, where he made a way from a professor assistant to the rector of the university. An important part of his activities was also related to the A. I. Voeikov Main Geophysical Observatory.

Next 30 years were tied up with his work at the Institute of Limnology and the Center for Ecological Safety, Russian Academy of Sciences. The latter

GUIDE FOR AUTHORS OF *IDŐJÁRÁS*

The purpose of the journal is to publish papers in any field of meteorology and atmosphere related scientific areas. These may be

- research papers on new results of scientific investigations,
- critical review articles summarizing the current state of art of a certain topic,
- short contributions dealing with a particular question.

Some issues contain "News" and "Book review", therefore, such contributions are also welcome. The papers must be in American English and should be checked by a native speaker if necessary.

Authors are requested to send their manuscripts to

Editor-in Chief of IDŐJÁRÁS

P.O. Box 39, H-1675 Budapest, Hungary

in three identical printed copies including all illustrations. Papers will then be reviewed normally by two independent referees, who remain unidentified for the author(s). The Editor-in-Chief will inform the author(s) whether or not the paper is acceptable for publication, and what modifications, if any, are necessary.

Please, follow the order given below when typing manuscripts.

Title part: should consist of the title, the name(s) of the author(s), their affiliation(s) including full postal and E-mail address(es). In case of more than one author, the corresponding author must be identified.

Abstract: should contain the purpose, the applied data and methods as well as the basic conclusion(s) of the paper.

Key-words: must be included (from 5 to 10) to help to classify the topic.

Text: has to be typed in double spacing with wide margins on one side of an A4 size white paper. Use of S.I. units are expected, and the use of negative exponent is preferred to fractional sign. Mathematical formulae are expected to be as simple as possible and numbered in parentheses at the right margin.

All publications cited in the text should be presented in a *list of references*,

arranged in alphabetical order. For an article: name(s) of author(s) in Italics, year, title of article, name of journal, volume, number (the latter two in Italics) and pages. E.g., *Nathan, K.K.*, 1986: A note on the relationship between photo-synthetically active radiation and cloud amount. *Időjárás* 90, 10-13. For a book: name(s) of author(s), year, title of the book (all in Italics except the year), publisher and place of publication. E.g., *Junge, C. E.*, 1963: *Air Chemistry and Radioactivity*. Academic Press, New York and London. Reference in the text should contain the name(s) of the author(s) in Italics and year of publication. E.g., in the case of one author: *Miller* (1989); in the case of two authors: *Gamov and Cleveland* (1973); and if there are more than two authors: *Smith et al.* (1990). If the name of the author cannot be fitted into the text: (*Miller*, 1989); etc. When referring papers published in the same year by the same author, letters a, b, c, etc. should follow the year of publication.

Tables should be marked by Arabic numbers and printed in separate sheets with their numbers and legends given below them. Avoid too lengthy or complicated tables, or tables duplicating results given in other form in the manuscript (e.g., graphs)

Figures should also be marked with Arabic numbers and printed in black and white in camera-ready form in separate sheets with their numbers and captions given below them. Good quality laser printings are preferred.

The text should be submitted both in manuscript and in electronic form, the latter on diskette or in E-mail. Use standard 3.5" MS-DOS formatted diskette or CD for this purpose. MS Word format is preferred.

Reprints: authors receive 30 reprints free of charge. Additional reprints may be ordered at the authors' expense when sending back the proofs to the Editorial Office.

More information for authors is available: antal.e@met.hu

Information on the last issues: http://omsz.met.hu/irodalom/firat_ido/ido_hu.html

Published by the Hungarian Meteorological Service

Budapest, Hungary

INDEX: 26 361

HU ISSN 0324-6329